FABP5-Related Signalling Pathway used as Therapeutic Target for Castration-Resistance Prostate Cancer

THESIS SUBMITTED IN ACCORDANCE WITH THE REQUESTMENTS OF

THE UNIVERSITY OF LIVERPOOL

FOR THE DEGREE OF DOCTOR IN PHILOSOPHY

By:

Waseem Hanna Al-Jameel

June, 2017

Department of Molecular and Clinical Cancer Medicine (Pathology)

Dedication

I dedicate this humble work to:

The memory of my father, a man whom I still miss every day.

My mother, for her endless love, support and encouragement.

My wife and kids, for their love and make my life so happy.

My brother, for supporting me all the way.

Abstract

Castration resistant-prostate cancer is largely impervious to feather hormonal therapy and hence the outlook for patients is grim. Increased FABP5 expression plays a crucial role in promoting castration-resistant prostate cancer. Here we use an approach to attach the recently discovered Achilles heel. The experimental treatment established in this study is based on the recent discovery that it is the FABP5-PPARγ-VEGF signalling axis, rather than the androgen receptor pathway, played a dominant role in promoting the malignant progression of castration resistant prostate cancer cells. Treatments have been established in mice by suppressing the biological activity of FABP5 using a chemical inhibitor SBFI26 and a novel bio-inhibitor, dmrFABP5. Both inhibitors significantly suppressed the proliferation, migration, invasiveness and colony formation of castration-resistant prostate cancer PC3-M cells *in vitro*. They also produced a highly significant suppression of both metastatic rates and average sizes of primary tumours developed from cancer cells implanted orthotopically into the prostate gland of the mice. Strikingly, the bio-inhibitor dmrFABP5, a mutated FABP5 incapable of binding to fatty acids, produced a much better suppression of both primary tumour growth and metastasis. Both inhibitors interfere with the FABP5-PPARγ- signalling pathway, but by different mechanisms. The inhibitor SBFI26 interferes with the FABP5-PPARγ-signalling pathway at the initial stage of the signal transduction by binding competitively to FABP5 to inhibit cellular fatty acid uptake. This avoids the fatty-acid stimulation of PPARγ and prevents it activating the down-stream regulated cancer-promoting genes. In contrast, dmrFABP5 can block the fatty-acid stimulation of PPARγ and prevent it activating the down-stream regulated cancer-promoting genes. This is an entirely novel experimental approach and completely different from current treatments that are based on androgen-blockade therapy.

Acknowledgments

I would like to take this opportunity to express my deep gratitude to my primary supervisor Professor Youqiang Ke for providing me the invaluable opportunity to undertake the PhD study in this department and for his patient guidance, endless support, enthusiastic encouragement and useful critiques of this research work. I extended my deep acknowledgment to my secondary supervisor Doctor Syed Hussain for his support and continuous encouragement. Also, I would like to take this opportunity to express my whole hearted thanks to Doctor Shiva S. Forootan for her exemplary guidance, monitoring and valuable discussions to my work throughout the PhD study. In addition, I would like to thank Mr. Majed Al Fayi for his assistant and suggestions throughout my study.

A big humble grateful to my family and friends for their love. Endless thanks to my mother for giving me the strength to overcome all the difficulties. It is the hard-working spirits and intelligence I inherited from her have enabled me to overcome all obstacles through all the way here. Special thanks must go to my beloved wife, Roaa and my kids, Sant, Steve and Selena for their love, patient, understanding, and encouragements. Appreciation should also give to my brother, Firas and his family, for their limitless love, support and understanding all the time.

I would like to thank all the technical staff in the Department of Molecular and Clinical Cancer Medicine, University of Liverpool, for helped me with their experience on many experimental skills needed for this research. In addition, I would like to thank all the colleagues in BSU and the Centre for Preclinical Imaging of Liverpool University for the technical assistance on animal work and on IVIS.

Finally, I would like to express my sincere heartfelt gratitude to my sponsors from Iraq, the Higher Committee for Education Development in Iraq (HCED) for the

generous support. In addition, I am grateful to Professor Entisar Al-Kinani, the Dean of college of Veterinary Medicine, Mosul University and Professor Salah Hassan for their concern on my work and the frequent encouragement.

Declaration

This thesis is a product of my own work which has been carried out during my PhD study in the Department of Molecular and Clinical Cancer Medicine (Pathology), University of Liverpool. All experiments presented in the result chapters were performed by me under the supervision of my supervisor, Professor Youqiang Ke and Doctor Shiva S. Forootan, senior research associate in the Molecular Pathology Laboratory.

Publications

Waseem Al-Jameel, Xiaojun Gou, Shiva S. Forootan, Majed Saad Al Fayi, Philip S. Rudland, Farzad S. Forootan, Jiacheng Zhang, Philip A. Cornford, Syed A. Hussain, Youqiang Ke. Inhibitor SBFI26 suppresses the malignant progression of castration-resistant PC3-M cells by competitively binding to oncogenic FABP5. Oncotarget 2017, **8:** 31041-31056. (Journal article). *doi: 10.18632/oncotarget.16055.*

Majed Saad Al Fayi, Xiaojun Gou, Shiva S. Forootan, **Waseem Al-Jameel**, Zheng Zheng Bao, Philip S. Rudland, Philip A. Cornford, Syed A. Hussain, Youqiang Ke. The increased expression of fatty acid-binding protein 9 in prostate cancer and its prognostic significance. Oncotarget 2016, **7:** 82783-82797. (Journal article). *doi: 10.18632/oncotarget.12635.*

Farzad S. Forootan, Shiva S. Forootan, Xiaojun Gou, Jin Yang, Bichong Liu, Danqing Chen, Majed Saad Al Fayi, **Waseem Al-Jameel**, Philip S. Rudland, Syed A. Hussain, Youqiang Ke. Fatty acid activated PPARγ promotes tumorigenicity of prostate cancer cells by up regulating VEGF via PPAR responsive elements of the promoter. Oncotarget 2016, **7:** 9322-9339. (Journal article). *doi:10.18632/oncotarget.6975*

Waseem Al-Jameel, Syed A Hussain, Philip A Cornford and Youqiang Ke. Experimental treatment of prostate cancer by suppressing the biological activity of FABP5. A Poster presented in the International Cancer Diagnostics Conference & Expo (June 13-15, 2016) in Rome, Italy. *doi: 10.4172/1948-5956.C1.067*

Waseem Al-Jameel, Shiva S. Forootan, Syed A. Hussain, Philip Cornford, Youqiang Ke. Suppressing tumorigenicity of prostate cancer by FABP5 inhibitors. A Poster presented in the NCRI conference (1-4 Nov. 2015) in Liverpool, UK.

Waseem Al-Jameel, Shiva S. Forootan, Vijay Aachi, Syed A. Hussain, Youqiang Ke. Suppression the biological activity of C-FABP as an experimental therapeutic tool in prostate cancer. A Poster presented in the NCRI conference (2-5 Nov. 2014) in Liverpool, UK.

Table of Contents

List of Figures

Chapter 1

Chapter 2

Chapter 3

Chapter 4

Chapter 5

List of Tables

Chapter 1

Chapter 2

Chapter 3

Chapter 5

List of Abbreviations

Abbreviation	Full name
5ARIs	5-α-reductase inhibitors
ADT	Androgen deprivation therapy
AF1	Activation function-1 region
ALA	Alpha-linoleic acid
APES	3-aminopropyl triethoxy-saline
AR	Androgen Receptor
AREs	Androgen response elements
AR-Vs	AR splice variants
BCL gene	B-cell lymphoma–leukemia gene
B_{max}	Maximal fluorescence intensity
BODIPY	Difluoro-5-4-bora-diaza-s-indacene-3-dodecanoic acid
BPH	Benign Prostatic Hyperplasia
BRCA	Breast Cancer
cDNA	Complementary DNA
C-FABP	Cutaneous fatty acid binding protein
Chk1	Checkpoint kinase 1
CK	Cytokeratin
CL	Cell lysate
CRPC	Castration-resistant prostate cancer
CSCs	Cancer stem cells
CZ	Central zone
DAUDA	dimethylamino-1-naphthalenyl sulfonyl amino-undecanoic acid

Abbreviation	Full name
DBD	DNA-binding domain
DHT	5-alpha-Dihydrotestostron
dmrFABP5	Double mutant recombinant FABP5
DMSO	Dimethyl sulfoxide
E coli	Escherichia coli
EDTA	Ethylene diaminetetraacetic acid
EGF	Epidermal growth factor
EMT	Epithelial-to-mesenchymal transition
EPA	Eicosapentaenoic acid
ET	Endothelin
FABP5	Fatty acid binding protein 5
FASN	Fatty Acid Synthase
FBS	Fetal bovine serum
FOX	Forkhead box
FW	Flow-through
GATA2	GATA binding protein 2
GS	Gleason scores
H/E	Haematoxylin and Eosin
HGF	Hepatocyte growth factor
HGPIN	High-grade PIN
HSL	Hormone sensitive lipase
IGF	Insulin-like Growth Factor
IL	Interleukin
IPTG	Isopropylthiogalactoside

Abbreviation	Full name
IVIS	In *vivo* image system
K_d	Dissociation constant
kDa	kilo Dalton
KGF	Keratinocyte growth factor
K_i	Inhibition constant
LB medium	Lysogeny broth medium
LBD	Ligand-binding domain
LCFAs	Long-chain fatty acids
LGPIN	Low-grade PIN
LH	Luteinizing hormone
LHRH	Luteinizing Hormone Releasing Hormone
Lipidex-1000	Hydroxyalkoxypropyl-Dextran
LSD1	Lysine-specific demethylase 1
MDM2	Murine double minute
mRNA	Messenger RNA
MTT	3-(4, 5-dimethylthiazl-2-yl)-2, 5-diphenylterazolium bromide
NBF	Neutral buffered formalin
NES	Nuclear export signal
NF-κB	Nuclear Factor-KappaB
NLS	Nuclear localization signal
NTD	N-terminal domain
OCT-1	Octamer-binding protein Oct–1
OD	Optical density
PAP	Prostatic Acid Phosphatase
PBS	Phosphate buffered saline

Abbreviation	Full name
PI-3K	Phosphatidylinositol-3 Kinase
PIA	Proliferative inflammatory atrophy
PIN	Prostatic Intraepithelial Neoplasia
PIP2	Phosphatidylinositol-diphosphate
PIP3	Phosphatidylinositol-triphosphate
PKA	Protein kinase A
PPAR	Peroxisome proliferator-activated receptors
p-PPARγ	Phosphorylated-PPARγ
PPRE	Peroxisome Proliferator Response Elements
PSA	Prostate-Specific Antigen
PSMA	Prostate surface membrane antigen
PTEN	Phosphatase and tensin homolog
PUFA	Polyunsaturated fatty acids
PZ	Peripheral Zone
RB	Retinoblastoma protein
RFU	Relative fluorescence units
RLU	Relative luminescent units
ROI	Region of interest
RSK	Ribosomal S6 kinase
SBFI26	α-truxillic acid 1-naphthyl mono-ester
SDS-PAGE	Sodium dodecyl sulphate polyacrylamide gel electrophoresis
SE	Standard error
siRNA	small interfering RNA

Abbreviation	Full name
smrFABP5	Single mutant recombinant FABP5
SOB medium	Super Optimal Broth
SOC medium	Super Optimal broth with Catabolic repressor
SRC	Steroid receptor coactivators
SREBPs	Sterol response element-binding proteins
TAU	Transcriptional activation unit
TBE buffer	Tris-Borate-EDTA buffer
TBS-T	Tris Base Salt-Tween
TURP	Transurethral Resection of Prostate
TZ	Transitional Zone
TZDs	Thiazolidinediones
VEGF	Vascular endothelial growth factor
wtrFABP5	Wild type recombinant FABP5
YB-1	Y-box binding protein-1

Chapter One:

Introduction

1.1 Epidemiology of prostate cancer

1.1.1 Epidemiology of cancer

Cancer is a serious public health problem worldwide. In 2012, there were an expected 14.1 million new cancer cases diagnosed in the world: in men 7.4 million (53%) and in women 6.7 million (47%) (1). Lung, breast, bowel and prostate cancers are the most common types of cancer. In the UK, these cancers account for more than 42% of all new cases (1,2) **(Fig.1.1)**. During the period 1979 to 2013, the European age-standardised (AS) incidence for all cancers rose by 17% in men and by 37% in women, nearly all these total increases happened before the late 1990s. Over the last decade in the UK (between 2002-2004 and 2011-2013), the AS incidence rates increased by 3% in men and 8% in women (3) **(Fig.1.2)**. In the future, if the trend in cancer incidence and population growth continue with the current rates, it is expected there will be 23.6 million new cancer cases diagnosed globally each year by 2030 (1,4).

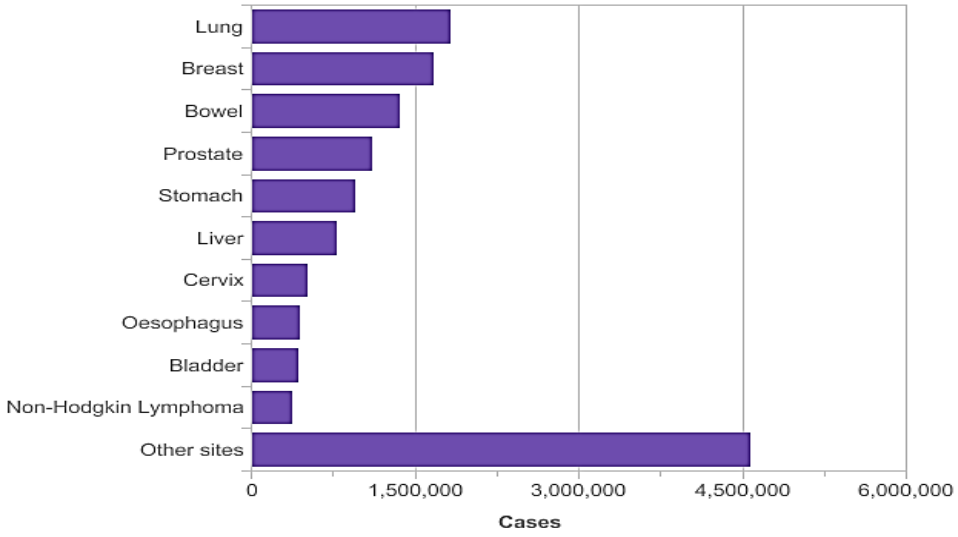

Figure 1.1 The 10 most commonly diagnosed cancers in the world; 2012 estimates (5).

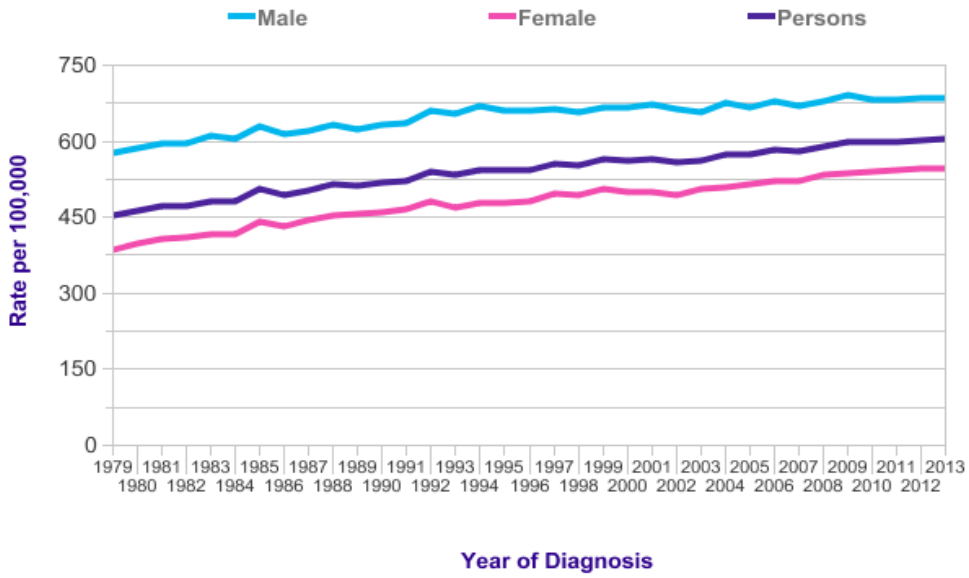

Figure 1.2 All cancer excluding non-melanoma skin cancer, European age-standardised incidence rates, Great Britain, 1979-2013 (6).

1.1.2 Epidemiology of prostate cancer

1.1.2.1 Prostate cancer incidence

Prostate cancer is the most common cancer amongst men in the developed world, with more than 1,111,000 new cases identified in 2012 (1,2,7). Increases in incidence rates of prostate cancer were seen for all nations. Prostate cancer incidences were more pronounced in the USA, Canada, Australia, France, while the incidences in medium-risk countries were moderate. Increases in incidence ranged from 25%-114%, 24%-55% and 15%-104% in high (USA, Canada, Australia, France, Sweden)-, medium (Denmark, England, Italy, Spain, Israel)- and low (Singapore, Japan, India, China)-risk countries, respectively. In high risk countries, the increased incidence may not truly mean the risk elevation, but simply due to the improvement of diagnosis by the widely use of prostate-specific antigen (PSA) tests and transurethral resection of the

prostate (TURP). Whereas rises in the low risk countries are possibly associated with westernization in these Asian populations (7,8). In Europe, prostate cancer is the most frequent cancer for males; with around 417,000 new cases diagnosed in 2012. Norway, Sweden, Finland and Netherlands are the highest incidence countries for prostate cancer; the lowest is in Albania (7,9,10). In the UK, prostate cancer incidence rate is assessed to be the 17th in Europe (7). In 2014, prostate cancer was the most common cancer in men in Great Britain, accounting a quarter of all new cancer cases diagnosed in men. There were 46,690 new prostate cancer cases diagnosed each year in the UK (147 new cases for every 100,000 males) (11).

Prostate cancer incidence is closely correlated with age; thus, a higher incidence rate is usually seen in older men. In the UK in 2012-2014, each year an average more than half (54%) of cases were identified in aged 70 years and over and only 1% were diagnosed in the under 50 years. The incidence rates were sharply increased from around age 50-54, reached to maximum in the 75-79 age group, and then dropped in the 80-84 age group, before increased steadily to the 90+ age group (11,12) **(Fig.1.3)**.

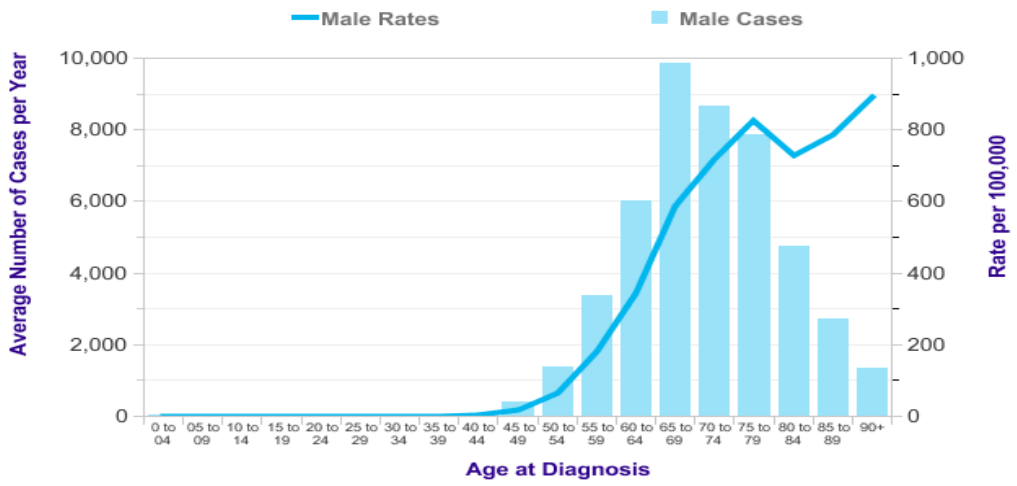

Figure 1.3 Prostate cancer: Average number of new cases per year and age-specific incidence rates, UK, 2012-2014 (13).

Prostate cancer incidence trends have increased since the mid-1970s in many countries including the UK (12). In the UK, the largest increase has been happened in men aged 25-49, with more than 8-fold (767% increase) between1979-1981 and 2011-2013, though averages to a relatively low at around 4/100,000. The rapid incidence rates have constantly increased during the early 1990s (due to the frequently use of PSA test) for the 50-59 and 60-69 age groups, with rises of 76% and 58%, respectively, between 1989-1991 and 1994-1996. Incidence rates have continued to increase for the 50-59, 60-69 and 70-79 age groups, but for males aged 75-84 and 85+, rates have declined since the early 2000s, dropping by 6% and 22% respectively between 2002-2004 and 2009-2013. PSA testing has fundamentally brought forward the age issue at diagnosis, meaning fewer men are diagnosed in older age (9) **(Fig.1.4)**.

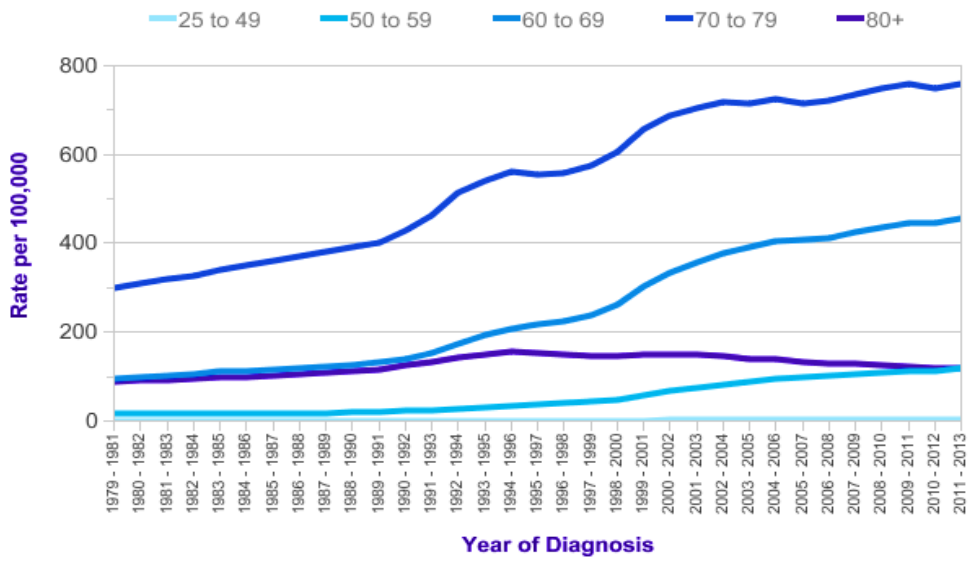

Figure 1.4 Prostate cancer: European age-standardised incidence rate by age in males, Great Britain, 1979-2013 (14).

1.1.2.2 Prostate cancer mortality and survival

Prostate cancer is the 5th most common cause of cancer death international for men, with around 307,000 deaths in 2012. Mortality rates rose more rapidly in less developed regions of the world including parts of South America, the Caribbean, Asia, and sub-Saharan Africa than in high risk countries (1,7,8). In Europe, prostate cancer is the 6th most common cause of cancer death, with around 92,300 deaths in 2012; UK prostate cancer mortality rates are assessed to be the 15th amongst the Europe countries (7-10).

In the UK in 2014, prostate cancer is the second most common cause of cancer death with 36 cancer deaths for each 100,000 men (15). Age is strongly linked to prostate cancer mortality. Between 2012 and 2014, around 57% of prostate cancer mortalities were in men aged over 80. Mortality rates increase sharply from around age 55-59, with the maximum rates in aged over 90 **(Fig.1.5)**. Prostate cancer mortality trends reminded to be stable in most age groups since the early 1970s, but dropped in men aged 70-79. In addition, a big rise was shown in men aged over 85, with an increasing by 47% from 1971-73 to 2012-14 (15-17) **(Fig.1.6)**.

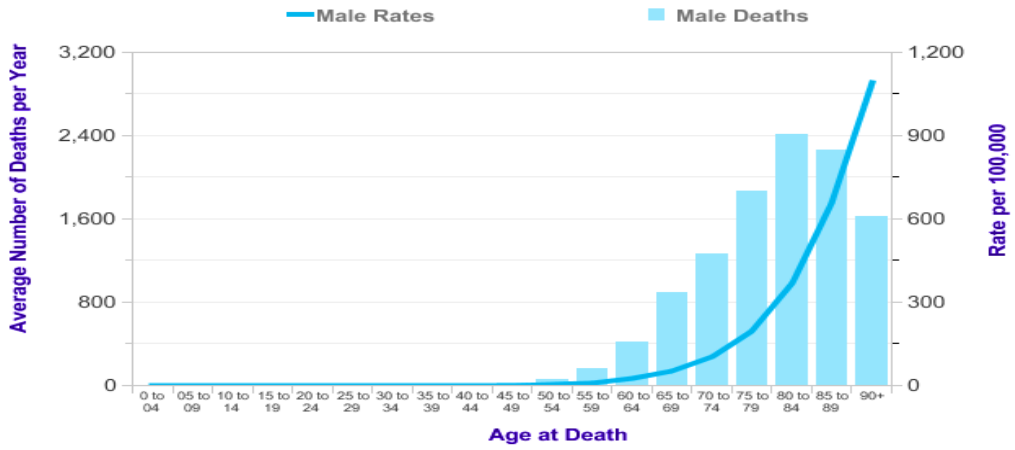

Figure 1.5 Prostate cancer: Average number of deaths per year and age-specific mortality rates in males, UK, 2012-2014 (16).

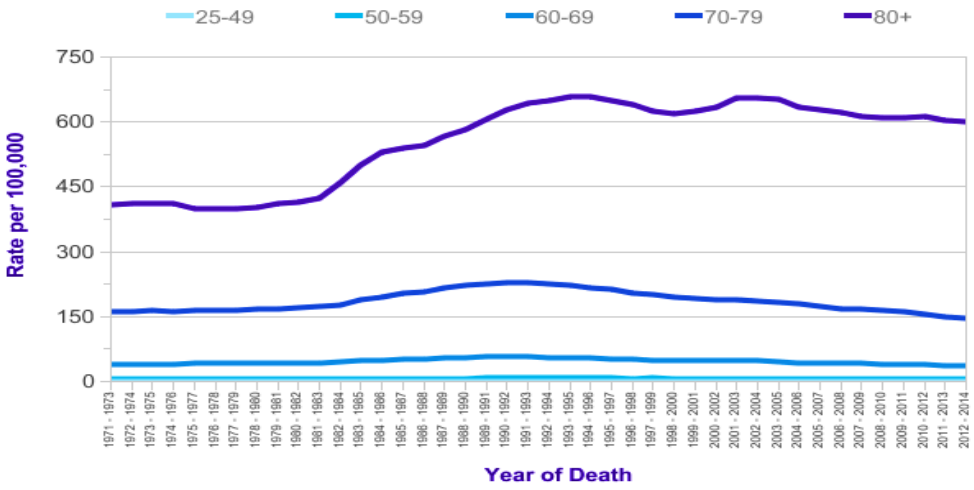

Figure 1.6 Prostate cancer: European age-standardised mortality rates by age in males, UK, 1971-2014 (18).

The survival rate of prostate cancer increased between 1970 and 2012; in 1970s nearly 2 in 10 men survived their prostate cancer ten years after the diagnosis, whereas in 2012 more than 8 in 10 survived. Nevertheless, the survival increase can be caused by the better early diagnosis via the widespread use of PSA testing in the UK (19,20). Prostate cancer survival rate is correlated with age and stage of the disease at the time of diagnosis, the relative survival for men with metastatic and advanced tumours is obviously worse than for localised diseases. Younger men are more probable to be treated effectively with prostatectomy than older men. Generally, they may have a lower grade cancer, and as a group, they have a much better 10-year survival rate. However, once the young men are diagnosed with high grade advanced prostate cancer, their survival rate is much worse than the older men (21) **(Fig.1.7, 8)**.

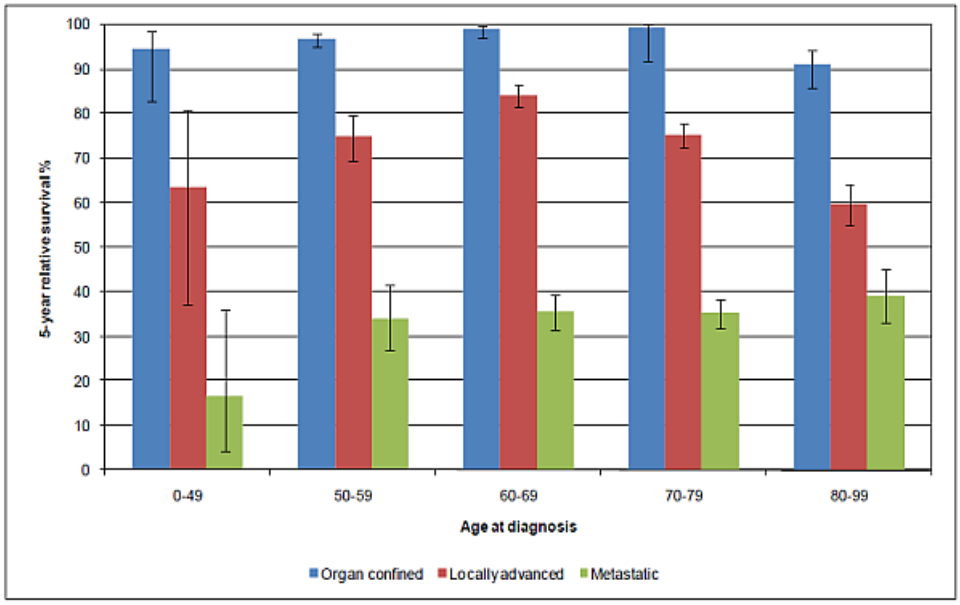

Figure 1.7 Relative survival for prostate cancer, by age and stage, in England 1999-2002 (22).

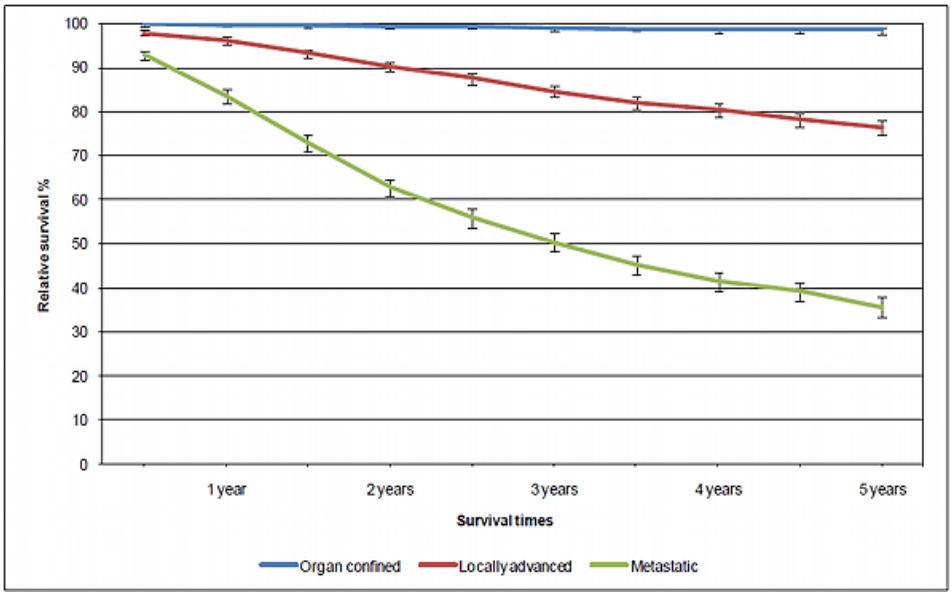

Figure 1.8 Relative survival for prostate cancer, by time and stage, in England 1999-2002 (22).

1.1.2.3 Predisposing factors of prostate cancer

1.1.2.3.1 Ethnicity/ Race

Worldwide, it is recognised that the prostate cancer risk is higher in black men than in white men. African Americans have the highest risk rates of prostate cancer in the world (275.3 per 100,000 men) (23). The risk factor in African Americans is approximately 60% higher than that in Caucasian or Asian/Pacific Islanders. In addition, mortality rate for African Americans is approximately two times of that of Caucasian. The effect of race/ethnicity in prostate cancer incidence and mortality is unclear. However, the incidence and mortality difference is explained by variances in socioeconomic status variables, stages at diagnosis, genetic factors, environmental factors or an interaction between them (24,25).

1.1.2.3.2 Family history/ Genetics

Familial component has long been recognized as an important risk factor for cancer (26). 5-10% of prostate cancers may be associated with hereditary factors; men with first degree relative having prostate cancer have 2-4 folds in risk of evolving prostate cancer comparing with the general population. Therefore, relatives with a stronger family prostate cancer history would be more probable to get prostate cancer, which means the more cases in a family the higher the risk for other male member to get cancer (25-29). In addition, it has been shown that family history with hormone-dependent cancers (breast, uterus and ovarian cancer) can significantly increase prostate cancer risk to other male relatives (30,31). Furthermore, specific inherited mutation in BRCA1 and BRCA2 (breast cancer genes) can increase the risk of prostate cancer in male relatives (32,33).

1.1.2.3.3 Diet/ Lifestyle

Many epidemiological studies showed that proper dietary complements and healthy lifestyle may be essential for reducing the risk of prostate cancer (34,35). High level consumption of fat and red meat has been significantly associated with the increased prostate cancer risk. In contrast, high level consumption of fatty fish has been associated with a reduced risk (34-36). The Mediterranean and Asian diets may provide some clues into the relationship between fat (it degrades to fatty acids) level in diet and prostate cancer. People in Asian countries with their high consumption of food containing relatively high level of omega-3 polyunsaturated fatty acids (PUFA), vegetables, complex carbohydrates, lean meats, and antioxidants have lower incidences of prostate cancer. This is opposite to those in countries consuming a Western-style diet with high omega-6 PUFA (37). The precise mechanism by which fat increases the risk of prostate cancer is now unclear. Nevertheless, it has been shown that high level of circulating insulin-like growth factor 1 (IGF-1) is associated with induced prostate cancer (34,38). PUFA, such as omega 3 and 6, are the most important fatty acids which can only obtained through dietary sources. Linoleic acid (LA) is an omega-6 PUFA and its high-level intake was related to increased risk of prostate cancer. Whereas the high-level intake of eicosapentaenoic acid (EPA), an omega-3 polyunsaturated fatty acid, is related to a declined risk of prostate cancer (39,40). Green tea, Soy phytoestrogens, Tomatoes and Cruciferous vegetables have been suggested to decrease the risk of prostate cancer (41).

1.1.2.3.4 Other factors

Alcohol consumption, cigarette smoking, men who have had a vasectomy, inflammation of prostate gland and sexually transmitted infections, such as chlamydia, may have a link to an increased risk of prostate cancer (42).

1.2 The pathology of prostate cancer

1.2.1 Anatomy and physiology of prostate gland

The prostate gland is the largest male reproductive system accessory gland surrounds the proximal part of urethra. It is composed of unstriped muscular, fibrous, connective, elastic, glandular, nerve, vascular, lymphatic, and a small amount of striped muscular tissue (43). It is located anterior to the rectum, posterior to the lower portion of the symphysis pubis, inferior to the urinary bladder in the sub-peritoneal compartment between the peritoneal cavity and pelvic diaphragm. A healthy human male prostate gland is slightly bigger than a walnut. The mean weight of the normal prostate gland in adult men is around 11 grams (44). Blood supply to the prostate gland is derived from the parts of the internal iliac artery, lymphatic drainage occurs mainly via the internal iliac nodes and nerve supply is originated from the prostatic plexus (43,44) **(Fig.1.9)**.

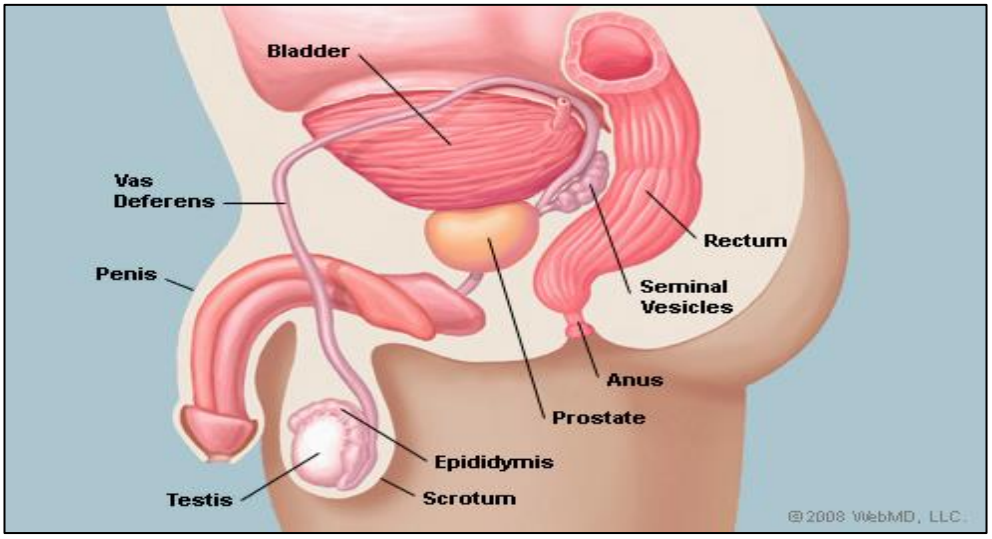

Figure 1.9 The prostate gland (45).

According to zonal anatomy, the prostate gland is divided into three zones. The peripheral zone (PZ) is the largest zone of prostate gland and forms 70% of the total gland volume. The peripheral zone, the area next to the rectum, surrounds the distal urethra at the apex of the prostate, and can be felt during a digital rectal examination. More than 64% of prostate cancer initiated from the peripheral zone. The central zone (CZ) takes up approximately 25% of the total prostate gland and covers the ejaculatory ducts. This zone accounts for only up to 2.5% of prostate cancers although these cancers tend to be more aggressive (46). The transition zone (TZ) is the central area of the prostate and compose of 5% of the total prostate gland, between the peripheral and central zones and surrounds the urethra as it passes through the prostate. In younger men, this zone is small. In some cases, as the growth of age, the transition zone starts to enlarge until it becomes the largest area of the prostate and this is called benign prostatic hyperplasia (BPH) (47-49) **(Fig.1.10)**.

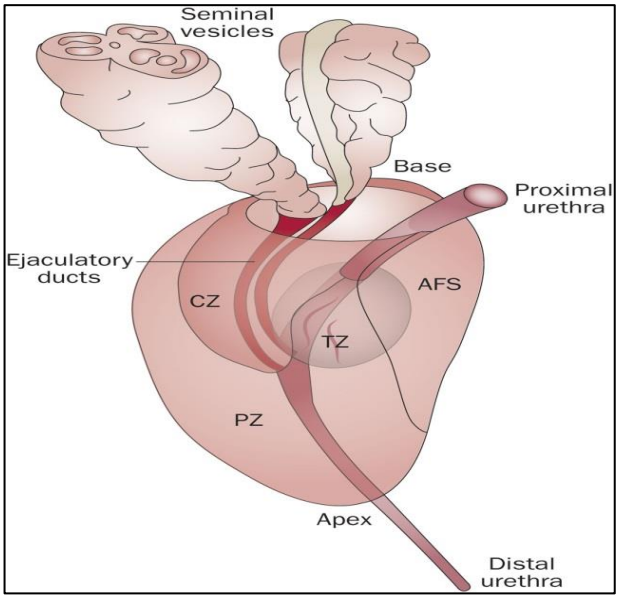

Figure 1.10 Anterior oblique view of the prostate gland and urethra (50). The urethra originates proximally from the urinary bladder and follows a course distally through the prostate. The prostate is divided into three zones: central zone (CZ), transition zone (TZ) and peripheral zone (PZ). The ejaculatory ducts and seminal

vesicles are situated at prostate base. The anterior fibromuscular stroma (AFS) is located anteriorly.

Functionally, prostate gland is an accessory sex organ, contributing to the total seminal ejaculation at the time of orgasm. The prostate gland naturally grows during adolescence under the effect of testosterone hormone, produces the fluid portion of semen volume. The prostatic secretions are slightly alkaline, milky white rich of simple sugars (fructose and glucose) which work as diet for sperm as they pass into the female body to fertilize ova. Prostate fluid also contains enzymes and PSA which break down proteins in semen to free sperm from the viscous semen. Prostate gland secretions also contains alkaline chemical and minerals (zinc, citrate) that maintain and neutralize acidic vaginal secretions to stimulate the survival of sperm (51).

1.2.2 Normal prostate cells

According to standard histology classification principles, the prostate gland has two general cell types: epithelial and stromal. Epithelial cells are composed of the luminal secretory, basal, neuroendocrine and intermediate cell types. The stromal part of prostate gland contains smooth muscle cells and fibroblasts (52,53). Peripheral nerves, blood vessels and ganglia are additional essential cell elements of the normal adult prostate gland **(Fig.1.11)**.

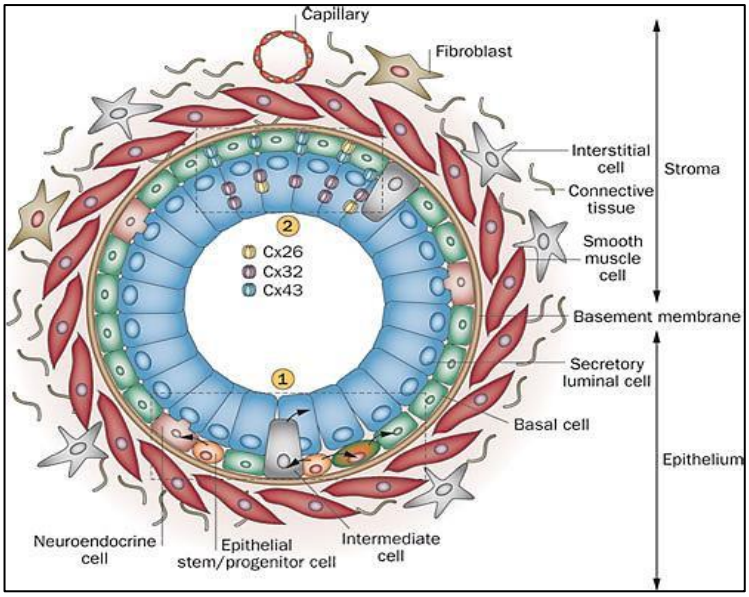

Figure 1.11 Model of the maintenance of prostate epithelial parenchyma (54). The prostate gland consists of stromal and epithelial cells. Prostate stem cells located in the basal layer of the prostate epithelium and different from basal and neuroendocrine cells, and luminal progenitors; the latter give rise to luminal secretory cells **(1)**. Another family of prostate cells is that correlates with increased expression of the connexins Cx26, Cx32 and Cx43 **(2)**.

The luminal secretory cells are columnar-shaped above the basal layer. They are the major type of prostate cells. They are exocrine compartment of prostate, secreting prostatic acid phosphatase (PAP) and PSA into the lumen (55). The secretory cells are androgen-dependant cells that need androgen for their survival. They will undergo apoptosis when androgen is removed. This cells expressing low molecular mass of cytokeratins (CK8, 18) and the cell-surface marker CD57 with high levels of AR (55-57). In addition, endothelin-1 (ET-1) and low level of prostate surface membrane antigen (PSMA) have been identified in normal luminal cells (58).

The basal cells are cuboidal to flattened shape cells above the basement membrane and believed to be the proliferative compartment of the prostate gland (59). They express

p63 (a homolog of the tumour suppressor gene p53), Bcl-2 (an anti-apoptotic factor), hepatocyte growth factor (HGF). The basal cells consist of androgen-independent cells that express the high molecular weight of CK5, 14 which marks them independent of androgen for their survival (55,60).

The neuroendocrine cells are scattered between the secretory and basal cells. They are supposed to arise from the stem cells in the basal layer, even though there is some proof to propose that they may be neuronal in origin (61,62). The neuroendocrine cells are copious in the prostate gland at birth and then disappear, only to reappear during puberty, after which their number slowly increases during adult life (63). The precise function of these cells is not totally understood, but it is supposed to that they may play a role in the growth and differentiation of the developing prostate cancer. Many studies exposed that its number increases in high grade, particularly in hormonally treated and androgen-independent prostate cancer (62,64,65).

The intermediate cells are identified with a cytokeratin phenotype intermediate between the basal and luminal epithelial cells that express high levels of CK5 and 18 as well as hepatocyte growth factor receptor C-MET. These cells are enriched in proliferative inflammatory atrophy (PIA) lesions and support that may work as favoured target cells in prostate carcinogenesis (66).

1.2.3 The initiation of prostate cancer

1.2.3.1 Benign prostate hyperplasia

BPH is a non-malignant increase in size of prostate gland observed very commonly in aging men. BPH, the actual hyperplasia of the prostate grows as gland epithelium and smooth muscle, most especially in the transition zone (67). BPH is an age-linked phenomenon in approximately all males. The histologic incidence of BPH, which has

been observed in several studies around the world, is around 10% for males in their 30s, 20% for males in their 40s, reaches 50-60% for males in their 60s, and is 80-90% for males in their 80s (68,69). There is a definitive link between BPH and prostate cancer; both have remarkable similarities with regards to age increasing and androgen-dependence, thus they are frequently found concurrently. Nevertheless, a causal relationship between these two cases has not been established (70).

In addition, in both BPH and prostate cancer the level of serum PSA is increased (71). It has been estimated that each gram of prostate cancer tissue increased PSA level by about 3.5 ng/ml, while each gram of BPH tissue elevated PSA by around 0.3 ng/ml (71). For not entirely understood reasons, the ratio of non-protein bound (free) PSA to total PSA is higher in BPH than in prostate cancer (72). Using the ratio of free PSA to total PSA improved the ability to distinguish cases of BPH and prostate carcinoma based on PSA testing of men with total PSA levels in the range 4-10 ng/ml (73). Nevertheless, the specificity of PSA testing remains to be low in men with BPH (74). Another method which has been improved the ability to differentiate BPH from prostate cancer is to use transition zone PSA density, which is the ratio of PSA level to transition zone volume measured on trans-rectal ultrasound (75).

It has been suggested that androgen/androgen receptor (AR) signalling shows key roles in development of BPH and that blockade of this signalling could be a major therapeutic method for BPH. However, the full mechanisms of this signalling, and especially the pathogenic roles of AR in BPH are still uncertain. Nevertheless, Androgen deprivation therapy (ADT) and 5-α-reductase inhibitors (5ARIs) which suppress testosterone translation into dihydrotestosterone (DHT) are used in the treatment of men with BPH (76,77).

1.2.3.2 Prostatic Intraepithelial Neoplasia

Prostatic Intraepithelial Neoplasia (PIN) is the initially accepted and morphologically recognizable stage in prostate carcinogenesis owning many of the genotypic changes of cancer. PIN is also defined by the abnormal proliferation of the secretory epithelium within prostate duct without the invasion of the basement membrane (78,79). PIN is classified in two grades: low- and high-grade PIN (LGPIN and HGPIN) with a variety of increasing severity. Pathologists now use the term PIN to designate HGPIN because LGPIN is most possibly not a precancerous lesion and the difference between LGPIN and normal epithelium is somewhat subjective (80).

In HGPIN, the degree of cellular abnormality is more pronounced than in LGPIN, including nuclear enlargement, make the lesions indistinguishable from invasive carcinomas. The presence of protuberant nucleoli within a duct structure is an easy way to identify PIN (78). Four main forms of HGPIN have been identified: tufting, cribriform, micropapillary, and flat. Although multiple forms can be found in most of the cases at the same time, the most common form found in PIN lesion is tufting (81). HGPIN is the most probable precursor of prostatic carcinoma and it is associated with progressive abnormalities of genotype and phenotype, which are middle between normal prostatic epithelium and prostate cancer. Furthermore, HGPIN and prostate cancer share many other connections, including increased incidence with age and high occurrence in the peripheral zone of the prostate gland. In contrast to peripheral, the incidence of HGPIN in transition zone of the prostate gland is much less common. It is well established that the volume of PIN has a positive correlation with both pathologic stage and Gleason score (GS) (78,82).

1.2.3.3 Grading and staging of prostate cancer by the combined Gleason scores

A commonly acknowledged method of grading the aggressiveness of adenocarcinoma of prostate was established in the 1960s and 1970s by Donald F Gleason and members of the Veterans Administration Cooperative Urological Research Group. GS system is constructed on the histologic pattern of carcinoma cells arrangement in H&E-stained sections (83,84). In this system, all prostate tumours range from Grade 1 (well differentiated and characterised by a closely packed, uniform gland, with no infiltration of the stroma) to Grade 5 (poorly differentiated and characterised by a lack of glands with sheets of cells) **(Fig.1.12)**.

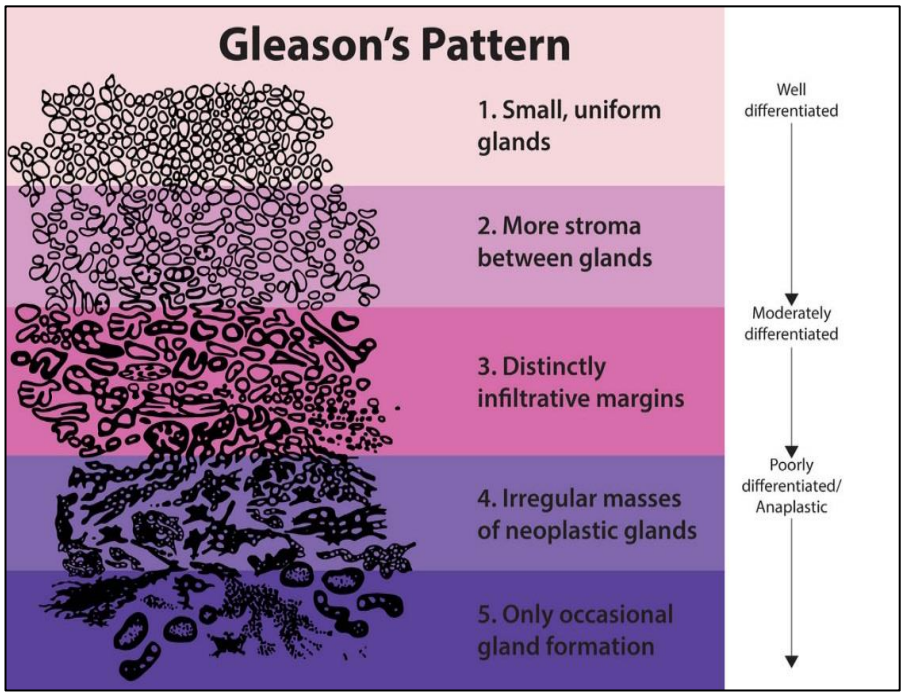

Figure 1.12 The Gleason grading system diagram (85). Grade 1, well-differentiated and slight anaplasia. Grade 2, moderately-differentiated and moderate anaplasia. Grade 3-4 poorly-differentiated and marked anaplasia.

Because of the histological variation within each tumour, two grades, the primary grade (predominant) and the secondary grade (second most prevalent) were recorded

in each case which can range from 2 to 10 by adding the primary grade pattern and the secondary grade pattern. Low GS (6 or lower) is indicative of a more indolent malignancy with a good prognosis while a high GS (8 or upper) is associated with an aggressive biological behaviour and bad prognosis (83,84,86,87).

1.2.3.4 Prostate cancer cell lines

Understanding the molecular pathogenesis and metastasis of prostate cancer is an important first step in the design of effective therapies. Consequently, cancer researchers have focused a significant amount of their energy into developing cell culture models. As a result, many cell lines have been developed in laboratory and the most common used prostate cancer cell lines are: PNT2, LNCaP, 22RV1, DU-145, PC3 and PC3-M.

1.2.3.4.1 PNT2

PNT2 cell line is obtained from a normal prostate of an old male at post mortem and has been immortalized by transfection with a vector containing SV40 genome with a defective replication origin. These cells have been cultured for more than 12 months and revealed to contain the SV40 genome (88). They express large amount of T protein and cytokeratin 8, 18 and 19 which are markers of differentiated luminal prostate cells, weakly positive for PSA and negative with a marker of epithelial basal cells (CK 14). Furthermore, these cells are non-tumorigenic in nude mice (88,89).

1.2.3.4.2 LNCaP

LNCaP cell line is derived from a needle aspiration biopsy of a metastatic lesion in the left supraclavicular lymph node of a 50-year-old Caucasian patient with human prostate adenocarcinoma in 1977 (90). Organic specific glycoproteins for example AR, PSA and PAP are expressed in LNCaP cultured cell line. LNCaP cells are

androgen sensitive, do not produce a uniform monolayer, but grow in clusters. In addition, *in vivo* LNCaP cells produced tumours at the site of injection. Male mice develop tumours at a higher frequency than in the female mice and hormonal manipulation showed that the incidence of tumour correlated to serum androgen levels (91).

1.2.3.4.3 22RVI

22RV1 cell line is an androgen-responsive human prostate carcinoma cell line obtained from a xenograft that was consecutively spread in mice after castration induced regression and relapse of the parental, androgen-dependent CWR22 xenograft (92). 22RV1 expresses PSA and AR. Its growth is weakly stimulated by DHT and the lysates are immune-detective with androgen receptor antibody by Western blot analysis. In addition, 22RV1 has a unique genotype and phenotype compared to DU-145, PC-3, and LNCaP. 22RVl has fewer chromosomes and a simpler karyotype with a low degree of variation (92,93).

1.2.3.4.4 DU-145

DU-145 cell line was isolated from a lesion in the brain of a 69-year-old Caucasian male with metastatic prostate carcinoma. These cells are androgen-independent and do not express prostate specific markers (AR, PAP and PSA) (94). These cells possess moderate metastatic potential and exhibit epithelial cell morphology (95).

1.2.3.4.5 PC3 and PC3-M

PC3 was established from a bone marrow metastasis of a GS 4 prostatic adenocarcinomas from a 62-year-old male Caucasian (96). These cells, which do not express AR and PSA, are androgen-independent and proliferate normally in androgen-deprived media. In addition, PC3 xenograft tumours proliferate rapidly with a high

incidence of tumorigenicity and metastasis in nude mice (97). Metastatic sublines of PC-3 (PC3-M) have been isolated from liver metastasis produced in nude mice subsequent to intra splenic injection of the PC3 cells. PC3-M has similar possessions with PC3 cell line but more aggressive (98).

1.3 Androgen dependent and independent prostate cancer

1.3.1 Androgen-dependent prostate cancer

Androgen has a significant influence on development, growth, maintenance and function of prostate gland. Testosterone, more than 95% produced in testes, is the most abundant circulating androgen in men. The remaining 5% of testosterone is derived from the adrenal glands (99). The hypothalamus regulates the production and secretion of androgen. It releases luteinizing Hormone Releasing Hormone (LHRH) in pulses whenever levels of testosterone are reduced in blood. The stimulation of the LHRH receptors of the pituitary gland leads to release and increased synthesis of luteinizing hormone (LH) into the blood, which persuades steroidogenesis in Leydig cells. In prostate gland, testosterone is transformed into an active form, DHT by 5-alpha-reductase enzymes, which promotes the growth and survival of prostate cells (99,100). DHT binds to the AR, causing displacement of the receptor from heat shock proteins followed by receptor dimerization and phosphorylation (101). Inside the nucleus, the stimulated receptor binds to androgen response elements (AREs) in promoter regions of different target genes such as PSA and regulates transcription (102,103).

In prostate cancer, radical prostatectomy and external radiation are the most successfully treatments when the tumour is at the localized stage (104). Androgen deprivation therapy (ADT) by medical, surgical castration, anti-androgens, and combined androgen blockade is the standard treatment for locally advanced and

metastatic prostate cancer, thereby lead to a suppression of androgen signalling (105). Although ADT is an effective treatment and able to induce clinical response in 80-90% of patients, after a median of 2–3 years, patients experience progression to androgen-independent prostate cancer (106). In most cases, the majority of androgen-independent tumour cells remain expressing AR.

1.3.2 Androgen-independent prostate cancer

Androgen-independent prostate cancer, also identified as Castration-Resistant Prostate Cancer (CRPC), is a castration-insensitive phase of disease which carries a worse prognosis and decrease in survival time from the beginning of progression (106,107). The basic for the development of new treatments in CRPC is the identification of molecular mechanisms involved in the translation of prostate cancer cells from androgen-dependent to androgen-independent status. The molecular mechanisms of prostate cancer progression from androgen-dependent to androgen-independent are still not fully understood. Nevertheless, there are several mechanisms may contribute for the development of CRPC.

1.4 Molecular mechanisms of CRPC progression

CRPC is the result of regrowth of prostate cancer cells that have adapted to the androgen deprivation environment. The molecular mechanisms of CRPC progression has been the subject of research in most laboratories that have analysed the process from different perspectives. Because the growth of prostate cancer cells depends on the presence of androgen, ADT has been the main treatment for patients with prostate cancer since the important recognition of the disease as androgen-dependent by Huggins and Hodges in 1941 (108). Nearly all patients with prostate cancer firstly respond to ADT. Nevertheless, almost every patient will relapse due to the growth of

CRPC cells. CRPC cells often continue to express androgen-responsive genes such as PSA, and often express AR.

The CRPC cells grow and proliferate at low concentrations of androgen or completely androgen-independently and show a very aggressive behaviour. At this stage, the ADT is neutralized, metastases progress and any curative treatment is no longer possible. Over the past few years, many of the molecular mechanisms during ADT were identified and they became clear that multiple AR-dependent and -independent pathways are influenced on the way to CRPC cells.

1.4.1 The role of AR-dependent signalling pathway in CRPC

AR is a member of the steroid hormone receptor family of ligand-dependant transcription factor. AR is composed of several functional domains, ligand-binding domain (LBD), a DNA-binding domain (DBD), a hinge region and a large N-terminal domain (NTD) (109). The expression of PSA occurring in the majority of CRPC cases is mediated through androgen response elements of the AR (110). In addition, it has been identified that one of the most significant mechanisms in CRPC growth is the continuous activation of AR in CRPC cells (111). Despite castration which reduces serum androgen level, tissue testosterone or DHT level in CRPC cases is similar to that in patients before ADT (112). Several molecular and cellular modifications are linked the development of CRPC, including AR amplifications, AR mutations, AR-ligand signalling, aberrant AR co-regulating factors and the AR splice-variants (113).

1.4.1.1 Overexpression of AR or AR Amplification in CRPC

AR gene amplification is a powerful mechanism that enables CRPC cells to become more sensitive to reduced level of circulating androgen which promotes progression of CRPC. It has been reported that the incidence of *AR* gene amplification was

increased by 20-30% in CRPC patients after ADT, but very few cases were reported in untreated primary prostate cancer (114). ADT may lead to amplification of AR in the cytoplasm of CRPC cells and subsequently enable the tumour cells to react to low level of androgen, permitting the prostate cancer cells to continue androgen-dependent growth even after castration (115). Amplification of *AR* gene was associated with a substantially increment in both mRNA and protein levels in CRPC tissues (116). In addition, it has been shown that AR sensitivity amplification was most likely to occur in patients who initially responded well to ADT and it was rarely seen in those who did not respond to ADT (114). Other mechanisms that has been correlated to overexpression of AR are the reduction of retinoblastoma protein (RB) and the increase of E2F activity (117). AR amplification only occurred in a proportion of CRPC patients, suggesting that it is not the only mechanism responsible for development CRPC.

1.4.1.2 Mutations of AR in CRPC

According to the report from AR Gene Mutations Database, AR has the most mutations among hormone receptors with more than 1110 different mutations, 168 of which have been associated with prostate cancer (118). AR mutations occurred very rarely in the early stages of prostate cancer, but occurred in approximately 10-30% of CRPC patients who have been treated by ADT (119). It has been suggested that ADT works as a selective pressure for the increase of mutations in the *AR* gene (120). Mutations are mainly affect the LBD (94%) or the NTD (40%), and, less frequently, the DBD (7%) and hinge region (2%). Mutations in *AR* gene may lead to support CRPC cell progression and survival even with a very low level of androgen (121). The T877A mutation has been found within the LBD and occurs in around one-third of CRPC cases (122). Mutations in the LBD reduced binding specificity to allow prostate

cells to grow in an androgen-independent manner, and to allow the AR to bind and to be activated by other ligands which are normally present in the body, including estrogens, corticosteroids and progesterone and even the androgen antagonist flutamide (123,124). Several other mutations in LBD have been identified, such as L701H, H874Y, V730M and W742C, which increased the sensitivity of AR to other steroids such as glucocorticoids at normal concentrations (125). Although most of the mutations are mainly in the LBD, mutations in the NTD and DBD were also identified (126).

1.4.1.3 Co-regulators and collaborating factors of AR in CRPC

Interaction between AR and co-regulators is another important mechanism involved in the development of CRPC. Over the past decade, around 50 AR-associated co-regulators have been identified to be aberrantly expressed in CRPC. The transcription activity of the AR can be altered by a deregulated expression of co-regulator proteins through direct interactions with the AR or components of the AR transcriptional complex. There are two types of co-regulators: co-enhancer (such as p160/SRC and CBP/p300) or repressor (such as NCoR and SMRT) (127). The co-regulators have different mechanisms to influence AR transcriptional output. These mechanisms include changes in the structure of the chromatin, facilitation of interaction with the RNA polymerase transcriptional machinery, modulation of activity of histone by enzymes and modulation of activity of AR-bound chaperones (128). The p160/steroid receptor coactivators (SRC) family mediates the transcriptional functions of nuclear receptors and other transcription factors. The SRC family, includes SRC-1, SRC-2 and SRC-3, has been demonstrated to be associated with prostate cancer progression (129). It has been identified that SRC1 plays an important role in IL-6–induced AR activation in CRPC (130). Overexpression of SRC-3, associated with poorly differentiated and

more advanced prostate cancer, is directly linked to prostate cancer progression (131). CBP/p300 has also been shown to be important for the ligand-independent transactivation of the AR in CRPC cells (132). On the other hand, co-repressors have been found at reduced levels in CRPC (133).

Collaborating factors that contribute to AR transcriptional activity have been evolved from analyses of genome-wide androgen binding sites in prostate cancer cells. Bioinformatics analysis of the androgen binding sites revealed that there is an enrichment of DNA sequences for motifs of numerous collaborating factors for example, FoxA1, GATA2, and OCT-1(134). The functions of collaborating factors were attributed not only to the ability of directly interact with AR, but also to work as a pioneer factor for AR at sites of transcriptional regulation (135). FOX proteins, specifically the FOXA1 subclass and GATA2 have been shown to play an important role in CRPC through modulation of the expression of AR (136,137)

1.4.1.4 AR splice variants in CRPC

Several AR splice variants (AR-Vs) have been identified in CRPC cells, xenografts, and tissues (138,139). It has been established that the truncated AR-Vs lacking the LBD, which is the target of androgen therapy, resulting in ligand-independent constitutive AR activation and development of CRPC (140). The mechanisms facilitating the increased expression of these AR-Vs in CRPC cells are still unknown. The possible cause of splicing is the genomic rearrangement and/or intragenic deletions of the AR gene locus (141). AR-V7 and AR^{V567ES} have been identified as the most abundant variant detected and high expression of these variants are correlated with poor prognosis in CRPC patients (142). The high expression of AR-V7 has been found in CRPC cell lines and tissue samples of CRPC patients (142,143). In mice, AR-V7 levels cannot be suppressed, and may be improved by ADT including abiraterone

acetate and enzalutamide (144). It has been suggested that AR-V7 may act as a therapeutic target in CRPC (145).

1.4.1.5 Post-translational modifications of AR in CRPC

Ligand-independent activation of AR is generally based on post-translational modifications which is related to persistent AR activity. Various post-translational modifications of AR have been known including phosphorylation, acetylation, sumoylation, methylation and ubiquitination. Amongst these, phosphorylation is the most widely studied. The majority of post-translational modifications happen in the activation function-1 region (AF1) of the AR, which includes the transcriptional activation unit 1 (TAU1) and 5 (TAU5) (146). It has been confirmed that growth factors, which include epidermal growth factor (EGF), insulin growth factor 1 (IGF-I) and keratinocyte growth factor (KGF), stimulate directly and phosphorylate AR in the absence of androgen in CRPC (147,148). In addition, it has been found that CRPC cells expressed very high level of RTK HER-2/neu receptor tyrosine kinase which can be activated by different growth factors. RTK HER-2/neu overexpression motivated the AR pathway in the absence or low levels of androgen (149). Protein kinase A (PKA) is also known to phosphorylate and activate AR (150). There are many examples of tyrosine and serine/threonine kinases involved in AR phosphorylation and the most interesting is associated tyrosine kinase (Ack1) which promoted castration-resistant growth of LNCaP cell lines (151).

1.4.1.6 Transcriptional activity of AR in CRPC

The expression of proteins, including AR, is regulated by several steps (transcription, translation, and post-translational modification) and the transcriptional step is thought to play a key role in gene expression. Throughout the progress of CRPC, AR transcriptional action is modified and abnormal regulation occurred in several genes

that promote cell proliferation and survival. It was reported that many of the AR target genes upregulated after ADT were no longer present before treatment; proposing a reactivation of the AR signalling pathway in the absence or low level of androgen (152). Moreover, it has been suggested that numerous alternative oncogenic pathways may play important roles to generate AR signalling which can enhance AR responses to low levels of androgen (153). It was clearly demonstrated that overexpression of E2F transcriptional factor with the knockdown of retinoblastoma protein (tumour suppressor) cooperatively upregulated AR transcription in LNCaP cells which may lead to androgen-independent activation of several AR stimulated genes (117).

Depending on its expression level, AR can work as a transcriptional enhancer or repressor for downstream target regulatory genes during AR signalling (154). It was found that increased level of androgen binding ARBS2 enhancer which was located within intron 2 of the *AR* gene led to a suppression of *AR* gene expression by lysine-specific demethylase 1 (LSD1) recruitment in androgen-dependent cells. However, when the level of androgen is decreased in CRPC cells, the low androgen level may lead to an increased stimulation of androgen enhancer elements and an enhanced *AR* gene transcriptional activity, but no stimulation on suppressor elements. Therefore, the deceased androgen level may cause an increased expression of AR and AR repressed genes that contribute to cellular androgen synthesis, DNA synthesis, and proliferation of CRPC cells (154).

1.4.2 The role of growth and survival signalling pathways in CRPC

Alternative growth and survival signalling pathways also play important roles during the transition of prostate cancer cells from androgen-dependence to castrate resistance state. Many of these pathways play important roles in normal growth and development

of prostate gland, but after ADT most of these pathways become oncogenic (155). Some frequently altered pathways in CRPC are summarized as the following.

1.4.2.1 PI3K/Akt pathway in CRPC

PI3K/Akt pathway is associated with several cellular procedures ranging from the growth and survival to the expansion and metastasis. PI3K/Akt pathway is activated by several receptor tyrosine kinases [EGF, IGF-I, and platelet derived growth factor (PDGF)]. After activation, PI3K phosphorylates phosphatidylinositol-diphosphate (PIP2), leading to formation of phosphatidylinositol-triphosphate (PIP3). PIP3 then activates Akt by phosphorylation and the Phosphorylated Akt normalises cellular state by phosphorylation of several molecules involved in cell survival and proliferation. These molecules include checkpoint kinase 1 (Chk1), the forkhead box O (FOXO), murine double minute (MDM2), c-myc, nuclear factor-kappa B (NF-κB) and mTOR (156,157). In prostate cancer, genetic alterations of PI3K/Akt pathway were reported in 42% of primary and 100% of metastatic cancers; suggested its importance in the progress of CRPC (155).

The genetic alterations lead to the increased activity of PI3K/Akt signalling pathway and the decreased activity of the inhibitory phosphatases PTEN. Both the increased Akt activation and the reduced PTEN activity were associated with poor clinical outcome of the patients, as well as the facilitated transition of prostate cancer from androgen dependence to CRPC (158,159). In fact, the loss of PTEN, a negative inhibitor of PI3K/AKT pathway, is observed in nearly all CRPC cases (160). It was demonstrated that PI3K activity was closely related to AR signalling during the malignant progression of CRPC. In particular, loss of PTEN in prostate epithelial cells was found to lead to a reduction in transcription of AR target genes (159,161). In PTEN-deficient preclinical mice models, it was confirmed that PI3K/Akt and AR

pathways cooperate with each other to maintain tumour cell growth and survival. The combined pharmacologic inhibition of PI3K and AR signalling axis is more effective on CRPC suppression than either single inhibiting agent to AR or Akt alone (162).

1.4.2.2 RSK/YB-1 pathway in CRPC

Y-box binding protein-1 (YB-1) performs several biological actions in both cytoplasm and nucleus. It works as a transcription factor in the nucleus to bind to the Y-box nucleotide sequence 5′-ATTGG-3′ to modulate gene specific translation (163). Upregulation of YB-1 was detected during prostate tumour progression and during ADT in a mouse model, indicating that YB-1 played a key role in the progression of prostate cancer into CRPC (164). In addition, it was suggested that YB-1 promotes castration resistance in androgen-dependent prostate cancer cells by increase expression of AR (165). It was found that YB-1 was phosphorylated by p90 ribosomal S6 kinase (RSK) and the phosphorylated YB-1 increases transcriptional activation of growth enhancing genes, such as EGFR (166). The RSK family consists of four isoforms. RSK1 and RSK2 are most expressed isoforms in prostate cancer (167). Blocking AR signalling by ADT caused the activation of RSK/YB1 pathways which can induce AR in turn. It was confirmed that RSK/YB-1 pathway contributes in CRPC and inhibition of this pathway may be a novel therapy against CRPC (168).

1.4.2.3 The apoptosis-related pathways in CRPC

The AR pathway can be completely bypassed and prostate cancer cells can improve the ability to survive independent of ligand or non-ligand-mediated AR activation. These bypass pathways are either directly or indirectly related to apoptosis. An effective bypass of the AR pathway cascade would facilitate proliferation and supress apoptosis of CRPC cells (169). Inhibition of the pro-apoptotic protein PTEN and

activation of Akt can result in CRPC cells escaping apoptosis in the absence or low level of androgen (159).

In addition, the anti-apoptotic members of the *Bcl-2* gene family, including *Bcl-2*, *Bcl-x,* and *mcl-1* are noticeable bypass candidate genes that can inhibit apoptosis. It has been identified that Bcl-2 is not expressed in normal prostate but highly expressed in all primary prostatic carcinomas and metastases tissues obtained from patients after ADT (170,171). The expression of Bcl-2 can cause prostate cancer cells to escape from apoptosis; opposites to the aim of ADT treatment which is to induce apoptosis.

1.4.3 Role of stem cells in CRPC

It was identified that CRPC develops because a small number of androgen-independent cells already exist in the carcinoma even before the ADT was initiated. These cells, which can grow and expand without androgen supply, were named cancer stem cells (CSCs). CSCs are originated from normal stem cells which are found in the basal layer of prostate gland. It was suggested that during carcinogenesis the normal stem cells accumulate mutations which make some genes more oncogenic and others less tumour-suppressive. Thus these mutations transferred the normal stem cells into the CSCs which are highly malignant and metastatic (172). In addition, it has been indicated that CSCs play key roles in epithelial-to-mesenchymal transition (EMT) during the development of CRPC. Normally, EMT is a functional procedure in which epithelial cells turn into mesenchymal cells by losing their epithelial phenotypes such as cell-cell adhesion and cell polarity and by obtaining mesenchymal functions such as high capability of migration, invasion, anti-apoptosis and disorganization of extracellular matrix (173). In prostate cancer, ADT will induce EMT which then result in cells to leave epithelium and to invade organs (174). CSCs are thought to be a subpopulation of tumour cells that express specific surface antigens, possess

mesenchymal phenotypes, and escape the ADT (169,175). It has been revealed that the tumorigenic prostate CSCs can express specific markers such as telomerase, CD44, CD133, aldehyde dehydrogenase, and low or undetectable levels of AR. Furthermore, many studies in mouse models confirmed that prostate CSCs could play critical role in metastasis and resistance to ADT (176,177). These cells became the origin of a tumour and after ADT the androgen-dependent cells would be removed but the CSCs, which have been lurking in the background all along, remain viable and become dominant (175). It is tantalizing to consider that prostate cancer resists proliferation and apoptosis by adopting structures of normal prostatic stem/progenitor cells. The putative stem/progenitor cells of the prostate, which express specific markers such as telomerase and CD44, are androgen-independent and possess the phenotype of androgen-independence as do most CRPC (178).

1.4.4 Role of fatty acids in CRPC

Dietary fat is a main contributor to obesity and specifically important for the progression of prostate cancer particularly advanced prostate cancer (179). One of the characteristics of Western diets is a high consumption of fat and several fatty acids such omega-6 PUFA. PUFA intake were related to the risk of advanced prostate cancer but not to local prostate cancer (39). On the other hand, the Western diet lacks of fish-derived omega-3 fatty acid which was shown to enhance the malignant progression of prostate cancer cells by increasing their invasiveness. But this result was disputed by studies in human (39,180). It was demonstrated that a low omega-6 to omega-3 fatty acids ratio can delay the progression of prostate cancer to CRPC after ADT (181). Fatty acids and their metabolites are involved in prostate cancer progression in different pathways with potential impact on proliferation, cell progression and apoptosis (182). It has been confirmed that high level consumption of PUFA stimulates

the progression of prostate cancer cells from androgen-dependant to castration resistant by activation the PI3K/Akt/mTOR pathway (181). A key downstream target of Akt is the transcription factor NFκB which is increased significantly in CRPC. Reduction on the ratio of omega-6 to omega-3 fatty acids in diet may lead to a greater inhibition of NFκB transcriptional activity (181,183). In addition, maintaining a low omega-6 to omega-3 ratio in diet suppresses the overexpression of cyclin D, and activates caspase-3 (181). ADT up-regulates the expression of sterol response element-binding proteins (SREBPs) as well as some of their downstream effectors involved in fatty acid biosynthesis, energy production, cholesterol synthesis and membrane production such as aceyl-CoA-binding protein, fatty acid synthase (FASN) (184). It was showed that FASN and acetyl-CoA, important enzymes involved in synthesis of fatty acids, are overexpressed in CRPC cells (185-187). Inhibition of FASN suppressed the growth of prostate cancer cells, including CRPC cells, via both androgen-dependent and -independent mechanisms (188).

A protein involved in transporting fatty acids and overexpressed in prostate cancer is fatty acid binding protein 5 (FABP5) (189). FABP5 is a cytosolic protein of the fatty acid binding protein family, which binds with a high affinity to long chain fatty acids. FABP5 is highly expressed in androgen-independent cell lines (PC3 and PC3-M), moderately expressed in androgen responsive cells (22RV1), and rarely expressed in androgen-dependent cells (LNCaP) (190,191). In LNCaP cells, low level of fatty acids is transported by FABP5 and used as a source of nutrition and energy. In CRPC cells (PC3 and PC3-M), large amount of intracellular fatty acids transported into the nucleus where they act as signalling molecules to stimulate the nuclear receptor peroxisome proliferator-activated receptor gamma (PPARγ). The stimulated PPARγ then modulates the expression of its downstream target regulatory genes, which eventually

leads to an enhanced tumour growth and aggressiveness caused by an overgrowth of cells with a decreased apoptosis and an increased angiogenesis (192) **(Fig.1.13)**.

At the cell membrane, fatty acids uptake is principally regulated by transport proteins such as CD36, plasma membrane-associated FABP, and FABP family (193,194). Nevertheless, FABPs can also be involved in this uptake, and some evidence proposes that FABPs can interact directly with CD36 in cell membrane (195). At the nuclear membrane, FABPs transfer fatty acids into nucleus for initiating nuclear receptor transcriptional activity to stimulate different signalling pathways (196). It has been found that direct and selective FABPs and PPAR interactions do occur and are functionally important (197,198).

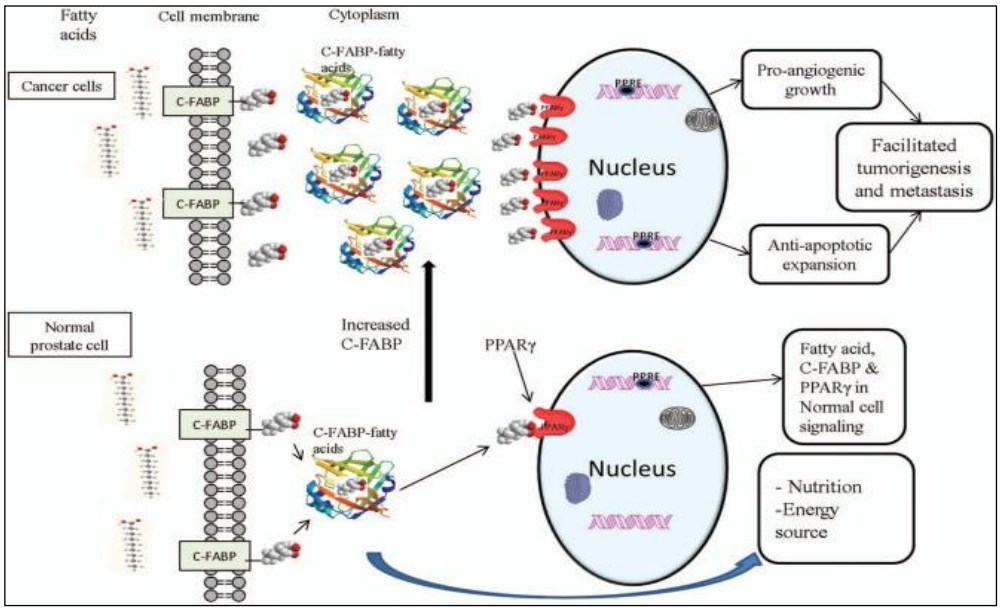

Figure 1.13 Schematic illustration of a possible C-FABP (FABP5)-related signalling pathway that lead to malignant progression in prostatic cancer cells (192). As illustrated in the above figure, in normal prostatic cells, intracellular fatty acids transported by FABP5 can be used as sources of nutrition to generate energy. In highly malignant prostatic cancer cells, high level of FABP5 transports a huge amount of fatty acids into cells. Whereas part of the fatty acids transported into cells by FABP5 is used as sources of energy, the excessive amount of fatty acids may act as signalling

molecules to activate the nuclear receptor PPARγ. The PPARγ may then initiate, through its peroxisome proliferative responsive element (PPRE), a chain of molecular events that leads to an accelerated malignant progression of the cancer cells.

1.5 Fatty acid binding proteins

1.5.1 Fatty acid binding protein family (FABPs)

Fatty acids are vital to the cell as a source of energy, as a substrate for membrane biogenesis and as a storage of metabolic energy. Recently, data show that fatty acids work as intracellular signalling molecules of many cellular processes for example membrane receptors, enzymes, and gene expression (182,199). Fatty acids are high soluble after they are generated in the cytoplasm of adipocytes. After their generation, free fatty acids may cross the plasma membrane of the cell to the extracellular environment and get into cancer cells by passive diffusion or through transporters. Fatty acids in cytoplasm can either enter a metabolic pathway or bind to intracellular fatty acid binding proteins which transport them to different organelles.

FABPs are a family of cytoplasmic proteins with similar molecular masses around 14-15-kDa that reversibly bind to saturated and unsaturated fatty acids with high affinity (200). Since the initial discovery of FABPs in 1972 (201), at least 12 members have been identified (**Table 1.1)**. All these members were named after the organs in which they were first known or commonly predominate, but their expression is not limited to that specific tissue or cell type. Some tissues express more than one FABPs, which indicates that FABPs may have exclusive functions. For example, FABP1 (liver FABP) is not only expressed in liver, but also in pancreas, intestine, lung, stomach, and kidney. While FABP5 (epidermal FABP) is one of the most expressed FABPs and it is commonly expressed in skin, tongue, adipocyte, brain, intestine, macrophage,

kidney, liver, lung, mammary gland, heart, skeletal muscle, testis, retina, lens and spleen (202). FABPs are highly expressed in adipocytes, hepatocytes, and cardiac myocytes. Wherever fatty acids are localised, they are prominent materials for lipid biosynthesis and storage. Quantities of FABPs can increase with a mass arrival of fatty acids into the cell (203).

Protein	Name	Alternative names	Tissue/cell expression
FABP1	Liver FABP	L-FABP	Liver, intestine, pancreas, kidney, lung, stomach
FABP2	Intestinal FABP	I-FABP	Intestine, liver
FABP3	Heart/muscle FABP	H-FABP	Heart, skeletal muscle, brain, kidney, lung, stomach, testis, aorta, adrenal gland, mammary gland, placenta, ovary, brown adipose tissue
FABP4	Adipocyte FABP	A-FABP	Adipocyte, macrophage, dendritic cell
FABP5	Epidermal FABP	E-FABP	Skin, tongue, adipocyte, macrophage, mammary gland, brain, intestine, kidney, liver, lung, skeletal muscle, testis, retina, lens, spleen, prostate
FABP6	Ileal FABP	Il-FABP	Ileum, ovary, adrenal gland, stomach
FABP7	Brain FABP	B-FABP	Brain, glia cell, retina, mammary gland
FABP8	Myelin FABP	M-FABP	Peripheral nervous system
FABP9	Testis FABP	T-FABP	Testis, salivary gland, mammary gland
Fabp10	Liver FABP	L-FABP	Liver of teleost fish
Fabp11	–	–	Liver, intestine, muscle, brain, heart, eye, swim bladder, gills, kidney, skin, ovary and testis of teleost fish
FABP12	–	–	Retinoblastoma cell from human. Retina, testicular germ, kidney

Table 1.1 Fatty acid-binding protein multigene family (204).

1.5.2 Structure and affinity of FABPs

Structures of FABPs have been examined by X-ray crystallography, nuclear magnetic resonance and other biochemical methods. FABPs exhibited only moderate amino acid sequence homology, varying from 20-70%. However, they have highly similar tertiary structures. In general, FABPs have a 10-stranded antiparallel β-barrel structure. The binding pocket is situated inside the β-barrel and framed on one side by an N-terminal helix-loop-helix motif that is thought to act as the major portal for fatty acids entry and exit (205). It has been showed that there are three-element fingerprints for all FABPs that provides a signature **(Fig.1.14)**.

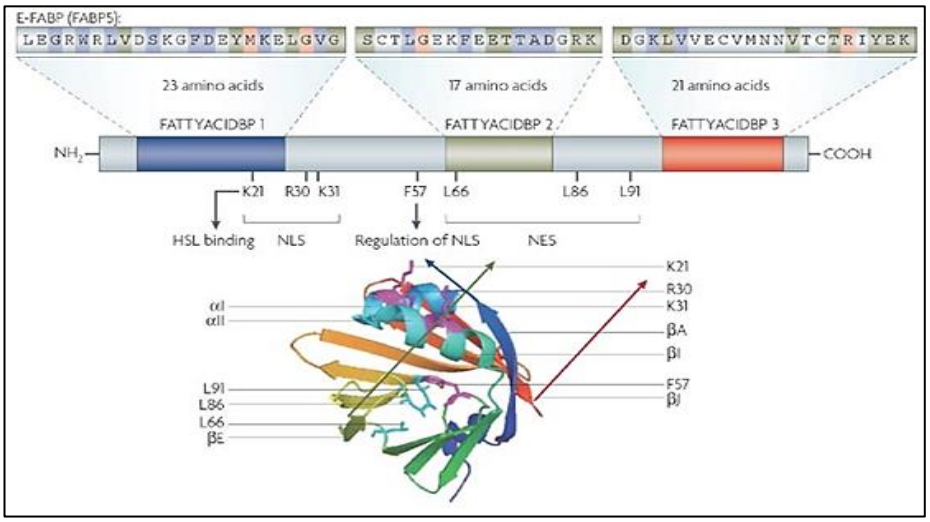

Figure 1.14 The fingerprint for FABPs (206). Three motifs are presented with this diagram. Motif 1 (blue ribbon) forms part of the first β-strand (βA). It also includes a nuclear localization signal (NLS) and a hormone sensitive lipase (HSL) binding site. The nuclear export signal (NES) domain is in Motif 2 (green ribbon) which includes strand 4 (βD) and strand 5 (βE). Motif 3 (red ribbon) encodes strands 9 (βI) and 10 (βJ).

As a result of small structural differences between FABPs, they bind fatty acids with differences in binding affinity, ligand selectivity, and binding mechanism. In general,

the more hydrophobic the ligand, the tighter the binding affinity; with the exemption of unsaturated fatty acids (205). In addition, it is possible that the needs of target cells determine the selectivity of the major FABPs present at different sites. For instance, FABP1 exhibits binding affinity for a broad range of fatty acids. In contrast, FABP7 is highly selective for very long-chain fatty acids such as eicosapentaenoic acid (207).

1.5.3 Biological function of FABPs

Different biological functions have been identified for FABPs which assist the transport of fatty acids to specific organelles in the cell, for example to the lipid droplet for storage; to the peroxisome or mitochondria for oxidation; to the endoplasmic reticulum for signalling and membrane synthesis; to cytosolic to regulate enzymes activity (206). In addition, FABPs appear to entry the nucleus, and potentially transport fatty acids to transcription regulators, such as peroxisome proliferator-activated receptors (PPARs) family, thereby permitting PPARs to perform their biological functions (208,209). Evidences suggest that FABPs deliver fatty acids from the cytosol to their receptor PPARs in the nucleus. Moreover, it has been confirmed that the expression of FABPs in cancer tissues localised in the cytoplasm and nucleus (210,211). These evidences indicated that FABPs may involve in unique signalling pathways in the nucleus to control the specific gene expression.

1.6 FABP5 and prostate cancer

1.6.1 FABP5 and CRPC

FABP5 is a 15kDa cytosolic protein of the fatty acid binding protein family (212), which binds with a high affinity to medium and long chain fatty acids (213). Previously, it was found that the gene coding for FABP5 was over-expressed in human prostate cancer cell lines and in prostate carcinoma tissue (189,190). When FABP5

gene was transfected into the benign Rama 37 model cells (214), it promoted growth of primary tumours and induced metastasis (190). In addition, it has been demonstrated that FABP5 act as a molecule involved in malignant progression of prostate and breast cancer, and its increased expression was able to induce metastasis *in vivo* through up-regulation of expression of the Vascular endothelial growth factor (VEGF) (191,215). Previously, FABP5 has been confirmed to be a potential prognostic indicator to predict patient outcome and target for malignancy suppression (189). Suppression of FABP5 by using siRNA can effectively inhibit prostate cancer in nude mice (216). It was established that the biological activity of FABP5 to promote tumorigenicity of prostate cancer cells depends on its ability of binding and transporting fatty acids which work as signalling molecules to stimulate their nuclear receptor PPARγ in CRPC cells (192). Furthermore, it was confirmed that the enhanced expression of cytoplasmic FABP5 significantly correlated with the increased nuclear PPARγ, and the increased levels of both proteins related to a shorter patient survival (211). Recently, it has been confirmed that the fatty acids activate PPARγ throw the FABP5-PPARγ-VEGF signal pathway **(Fig.1.15)** and it is important therapeutic target for angiogenesis-suppression treatment of CRPC (217).

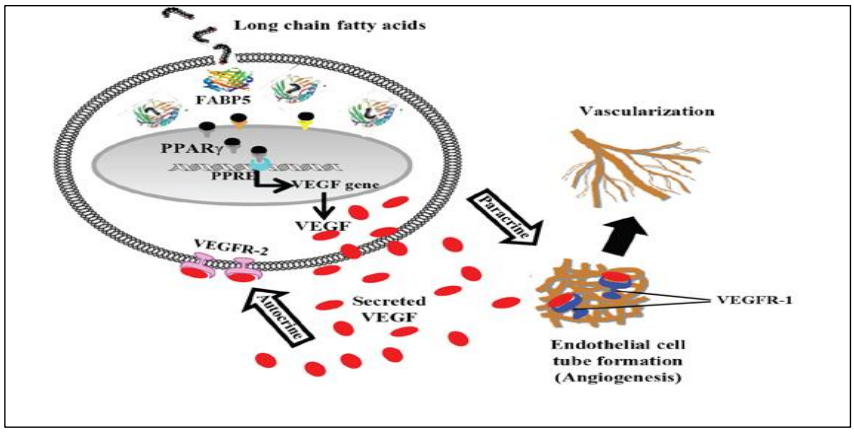

Figure 1.15 Schematic illustration of FABP5-PPARγ-VEGF transduction pathway. Through this pathway, fatty acids transported by FABP5 can activate PPARγ which

ultimately upregulate VEGF. VEGF is a potent antigenic factor which can bind to its receptor VEGFR1 to promote formation of vessel networks that are essential for growth and expansion of the cancer cells. VEGF can also promote directly malignancy of the cancer cells through an autocrine mechanism to simulate the receptor that is highly expressed on the surface of the prostate cancer cells (VEGFR-2) (217).

1.6.2 Targeting FABP5 in CRPC

When highly malignant CRPC PC3-M cells were orthotopically implanted into the mouse prostate gland, knockdown of *FABP5* gene by RNA interference produced 63-fold reduction in average tumour size; 7-fold reduction in tumour incidence, and 100% reduction in metastasis (189). These results justified our hypothesis that FABP5 is indeed a treatment target for CRPC. Although knockdown *FABP5* RNA is highly effective in inhibition of both tumourigenicity and metastasis of CRPC cells (189), siRNA molecules are not ideal agents for treatment due to their instability. Even when dissolved in a stabilizing agent (atolecollagen) and applied directly to treat prostate carcinomas already established in nude mice, it could only slow and stabilise tumour growth, but could not reverse malignant progression and reduce tumour size (216). Thus, for an effective suppression of FABP5 *in vivo*, inhibitors capable of suppressing the biological activity of FABP5, rather than completely knockdown the gene, may be more realistic tools for CRPC suppression.

Despite the extensively studies in molecular mechanisms involved in cancer-promoting activity of FABP5, it was not clear whether the FABP5-related signalling pathway can be used as an effective target for CRPC treatment. The availability of highly effective inhibitors is an essential first step. SBFI26 is the active component of a Chinese herbal medicine (Incarvillea sinensis) which was used to treat pain and rheumatism (218,219). It was shown to be effective for treatment of inflammatory and

metabolic diseases with a better effect than a group of chemically synthesized compounds, e.g. BMS309403 (206,220-222). Recently developed FABP5 inhibitors were originally effective analgesic and anti-inflammatory agents in mice (223-225). These included SBFI26 (α-truxillic acid 1-naphthyl mono-ester). In this work, we have tested treatment effect of SBFI26 for CRPC in mice.

FABP5 binds to fatty acids with its carboxylate group through a binding motif that consists of 3 key amino acids (Arg^{109}, Arg^{129}, and Tyr^{131}) (226). In the past study, we found that the tumour-promoting effect of FABP5 in prostate cancer depends entirely on the structural integrity of the fatty acid-binding motif. Enlightened by the fact that mutant tumour suppressor p53 can promote tumorigenicity (227), we have produced a mutant FABP5 (dmrFABP5) by mutating 2 of the 3 amino acids in its fatty acid-binding motif. Thus, we have also tested the potential of dmrFABP5 as a bio-inhibitor of FABP5 to treat CRPC in experimental mice.

1.7 Research scope

1.7.1 Hypothesis of this study

Based on previous long time investigations, it is reasonable to hypothesize that FABP5 (and the fatty acids transported by it) is an important pharmacological target, and modulating FABP5 biological activity may provide an attractive method for treatment of CRPC.

1.7.2 Specific Aims of this study

- Production of recombinant FABP5s and assessment their biochemical activities.
- Identification of lead inhibitor of FABP5 from a group of chemical compounds.

- ❖ Evaluation the inhibitory effect of SBFI26 and dmrFABP5 on malignant characteristics of PC3-M cells *in vitro*.
- ❖ Evaluation the effect of SBFI26 and dmrFABP5 on tumourigenicity and metastatic ability of PC3-M cells in mouse prostate gland.
- ❖ Comparing the effect of PPARγ antagonist with the effect of SBFI26 and dmrFABP5 on tumourigenicity of PC3-M cells in nude mice.
- ❖ Identification the effect of SBFI26 and dmrFABP5 on fatty acid uptake of FABP5 in PC3-M cells.
- ❖ Identification the effect of SBFI26 and dmrFABP5 on PPARγ activation.

1.7.3 Research plan

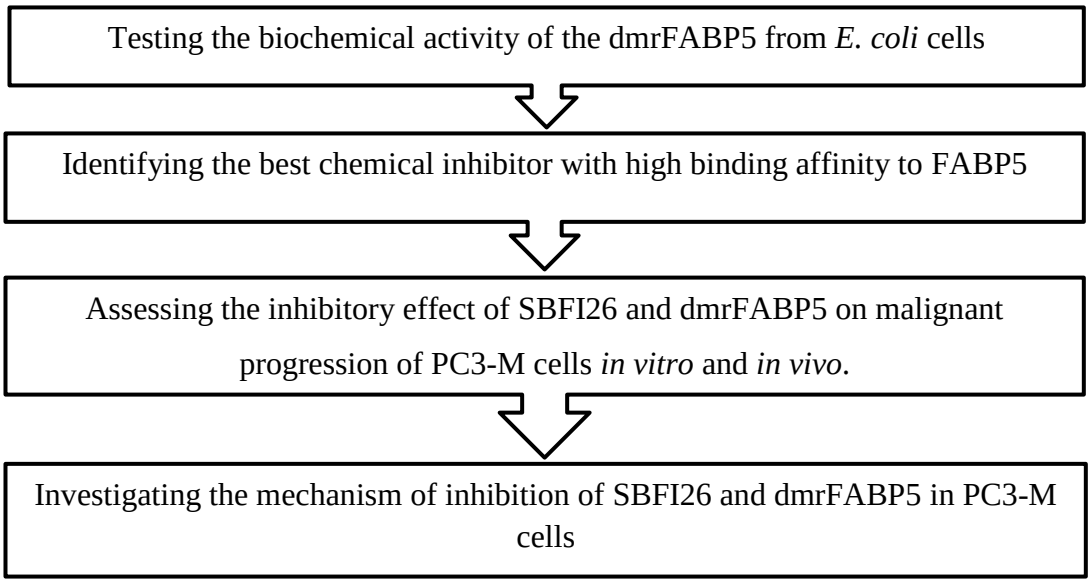

Chapter Two:

Production of recombinant FABP5s and assessment of their biochemical activities

2.1 Introduction

FABP5, a cytosolic protein of the fatty acid binding protein family (212), binds to medium and long chain fatty acids with high affinity (213). It was established that the tumour-promoting function of FABP5 on CRPC cells depends on its ability of binding and transporting fatty acids which work as signalling molecules to stimulate their nuclear receptor PPARγ (192). It was also confirmed that the expressed FABPs in the cancer tissue were localised in both the cytoplasm and the nucleus (210,211).

FABP5 binds to fatty acids with its carboxylate group through a binding motif that consists of 3 key amino acids (Arg^{109}, Arg^{129}, and Tyr^{131}) (226). In the past study, we found that the tumour-promoting effect of FABP5 in prostate cancer depends entirely on the structural integrity of the fatty acid-binding motif. Thus, changing one amino acid from $Arginine^{109}$ to $Alanine^{109}$ (single mutation) has been shown to reduce the fatty acid-binding ability significantly by 72%. Altering two of the 3 key amino acids in the fatty acid-binding motif (from $Arginine^{109}$ to $Alanine^{109}$ and $Arginine^{129}$ to $Alanine^{129}$, or double mutation) has almost completely deprived of the fatty acid-binding ability of FABP5. Whereas wild type recombinant FABP5 (wtrFABP5), fully capable of binding to fatty acids, increased tumorigenicity of the LNCaP cells significantly by 13 times, the doubly mutated recombinant FABP5 (dmrFABP5), which is incapable of binding to fatty acids, produced no increase in tumour sizes (192). Naturally, the singly mutated recombinant FABP5 (smrFABP5), which is only partially capable of binding to fatty acids, produced some increase in tumour sizes (192).

Although our previous results proved that fatty acid-binding ability is essential for the tumour-promoting ability of FABP5 and depriving the fatty acid-binding ability of FABP5 can eliminate its tumour-promoting activity, it is not known what is exact the

effect of the inactivated FABP5 on the native FABP5 inside the cancer cells. In order to investigate whether the inactivated FABP5 can be used as an effective inhibitor for the natural oncogenic FABP5, a large quantity of wtrFABP5 and dmrFABP5 is required to perform relevant experimental work. Thus, in this set of work, the recombinant protein production technique was used to produce and purify a large amount of wtrFABP5 and dmrFABP5. A large amount of smrFABP5 was also prepared for experimental control. The biological activity of the recombinant FABP5s produced from *E. coli* cells was tested by a DAUDA displacement assay.

2.2 Materials and Methods

2.2.1 Materials

Reagents are listed in Appendix A, Buffers in Appendix B and Equipment in Appendix C.

2.2.2 Methods

2.2.2.1 Molecular biology techniques

2.2.2.1.1 Construction of expression vectors by molecular cloning

2.2.2.1.1.1 Preparation of competent *E. coli* (DH5α) cells

LB medium (10mls) with *E. coli* (DH5α) was set up and incubated overnight at 37°C in shaking incubator with 150×g. One ml of overnight bacterial culture was added to the flask containing 100ml of SOB medium with 1ml of 2M Magnesium salts solution and then incubated at 37°C in a shaking incubator with 150×g. The optical density (OD) of bacterial cultured was measured at 550nm using Spectrophotometer (Jenway, Genova, UK) after the start of culture. When OD 550nm reach 0.4, bacterial culture was stopped. The culture was dispensed into 8 universal tubes (approx. 12.5ml/tube) and cooled on ice for 10 minutes. The cells were centrifuged at 2000×g for 10 minutes at 4°C and supernatant was discarded and pellets were re-suspended in a total of 16ml of RF1 buffer (8.25ml/ tube) and incubated on ice for 10 minutes. Cells were centrifuged again and the pellets were re-suspended in a total of 16ml of RF2 buffer (2ml/tube). The samples were pooled together and dispensed into 1ml aliquots in cryovials, flash frozen in liquid nitrogen and transferred immediately to -80°C.

2.2.2.1.1.2 Isolation of vector DNA (Miniprep extraction of vector DNA)

The wild type-*FABP5* DNA was isolated from cloning vector *pBluescript II SK* (192). The single and double mutant-*FABP5* DNAs were isolated from expression vector *pQE-32* (192) by using Miniprep QIAGEN extraction kit. The overnight culture of DH5α *E. coli* cells containing vectors (10ml) in LB medium plus 100µg/ml ampicillin was collected by centrifuging at 6800×g for 1min and the supernatant was discarded. The pellet was re-suspended in 250µl of suspension buffer P1 (50mM Tris-HCL PH 8.0, 10mM EDTA and 100mg/ml RNase), and 250µl of lysis buffer P2 (200mM NaOH and 1%w/v SDS) with gentle mixing and inversion of the tube for six times. 350µl of neutralization buffer N3 (4.2M GU-HCL, 0.9M potassium acetate PH 4.8) was added and mixed by inversion of tube for six times. The mixture was centrifuged at 17,900×g for 10 minutes and the supernatant was added to a Miniprep spin column. The column was centrifuged for 1 minute and the flow through was removed. The column was washed using 750µl of wash buffer PE (10mM Tris-HCL PH 7.5 and 80% ethanol) and centrifuged for 1 minute. The column was centrifuged for an additional 1 minute to remove the remaining of wash buffer. The column was placed on a clean 1.5ml tube and vector DNAs were eluted by loading 30-50µl EB buffer (10mM Tris-Cl, pH 8.5), stand for 1 minute and centrifuged for 1 minute. The DNAs concentration was examined by using the NanoDrop spectrophotometer (Labtech International, Ringmer, UK) and the vector DNAs were stored in a -20°C.

2.2.2.1.1.3 Digestion of vector DNA by restriction enzyme

The single and double mutant-*FABP5* DNAs were digested from expression vector *pQE-32* with *Kpn*I and *Pst*I to confirm the presence of insert in the vector (192). On the other hand, the wild type-*FABP5* DNA was digested from cloning vector *pBluescript II SK* with *Kpn*I and *Pst*I and the empty *pQE-32* was digested by the same

restriction endonucleases (192). Procedure of digestion was made by taking vector DNA and dilution buffer out of the freezer and thawing on ice. The mixture of restriction enzymes and vectors were prepared as shown in **Table 2.1**. The mixtures were incubated at 37°C for 1.5 hours to permit complete digesting of the vector DNA. After that, the enzymes were deactivated by heating to 65°C for 10 minutes and electrophoresis analysis in agarose gel was used to analysis the product.

reaction	***pQE-32* (single or double mutant-*FABP5* DNAs)**	***pBluescript II SK* (wild type-*FABP5* DNA)**	***pQE-32 (empty)***
DNA	**(1 µg) 15 µl**	**(3 µg) 3 µl**	**(2 µg) 20 µl**
Buffer 1	**2.5 µl**	**2.5 µl**	**2.5 µl**
***Kpn*I**	**1 µl**	**1 µl**	**1 µl**
***Pst*I**	**1 µl**	**1 µl**	**1 µl**
Water	**5.5 µl**	**17.5 µl**	**0.5 µl**
Total volume	**25 µl**	**25 µl**	**25 µl**

Table 2. 1 The restriction enzyme digestion mixture.

2.2.2.1.1.4 Electrophoresis analysis in agarose gel and the purification of gel

Agarose gel electrophoresis was performed in 1×TBE buffer (0.089M Tris-base, 0.089M Boric acid, 0.002M EDTA pH 8). The 0.8% to 2.0% (w/v) agarose was added to 200ml buffer and dissolved by boiling for 1-2 minutes and cooled down for 15 minutes. When the temperature of agarose reached 50°C, 5µl of safe view was added to the gel for visualization of DNA bands. The gel mixture was poured and placed at 4°C to solidify. Empty vectors and vectors contain the wild type, single and double mutant *FABP5* DNAs samples were prepared by adding the required amount of DNA,

sterile distilled water and 6×DNA loading buffer to get total volume of 20µl. The mixture was heated at 65°C for 5 minutes before being loaded onto gel. The gel was run for 1 hour at 90V and checked under the UV light to confirm that expression vector *pQE-32* contains the single and double mutant *FABP5* DNAs. The digested wild type *FABP5* DNA from *pBluescript II SK* vector and linearized expression vector *pQE-32* were purified from agarose gel by using Wizard® SV Gel and PCR Clean-Up System (Promega, WI, USA). The insert and linearized vector were excised under the UV light using a sterile blade. Each of the excised gel slices were weighed and same amount of the volume of QG buffer was added. The mixture was dissolved by incubating in water bath (50-65°C) for 10 minutes. The melted agarose was applied to a QIAquick spin column and centrifuged for 1 minute and the flow through was discarded. The column was washed by 750µl of PE buffer and re-centrifuged for 1 minute. The DNA was collected by adding 30µl of distilled water and the concentration was examined by using the Nano-Drop and stored at -20°C.

2.2.2.1.1.5 DNA ligation

The wild type *FABP5* DNAs were digested from cloning vector *pBluescript II SK* and ligated with linearized expression vector *pQE-32* using T4 DNA ligase. In this study the molar ratios of 10:1 insert to vector has been performed to get more clones with inserts. However, absence of clones with inserts when the molar ratios of 3:1 insert to vector has been performed. The ligation reaction mixture was shown in **Table 2.2**. After overnight incubation at 16°C, 10µl of this reaction was transformed into the competent *E. coli* (DH5α) cells as described in section 2.2.2.1.1.7 to produce sample of bacteria containing expression vector *pQE32*-wild type *FABP5* DNA.

Insert DNA(176ng/µl)	**11 µl**
Vector DNA(100ng/µl)	**1.5 µl**
Ligation buffer	**2 µl**
T4 DNA Ligase	**1 µl**
Water	**4.5 µl**
Total volume	**20 µl**

Table 2. 2 The ligation reaction mixture.

2.2.2.1.1.6 Transformation of competent bacteria with vector DNA

Competent *E. coli* (DH5α) cells were thawed on ice from -80°C. After that, 10µl of the ligation mixture for wild type *FABP5* DNAs and 50ng of expression vector *pQE-32* contains single and double mutant *FABP5* DNAs were added to 200µl of competent *E. coli* (DH5α) cells, swirled gently and incubated on ice for 30 minutes. The cells were transferred into water bath at 42°C for 90 seconds and moved on ice for a further 2 minutes. 800µl of SOC was added to the cells and DNA (0.5% w/v yeast extract, 2% w/v bactotryptone, 10mM NaCl, 10 mM MgCl, 10mM MgSO4, 2.5mM KCl, 20mM glucose) and incubated for 1 hour at 37°C in the shaking incubator at 150×g. 200µl of transformed Competent *E. coli* cells was plated onto LB plates containing 100µg/ml ampicillin and incubated at 37°C overnight. Colonies were picked from plate and grown in LB broth containing 100µg/ml ampicillin at 37°C overnight. The digestion of plasmid DNA were carried out to confirm that *E. coli* (DH5α) cells contains expression vector *pQE-32*- wild type, single and double mutant *FABP5* DNAs.

2.2.2.1.1.7 DNA sequencing

Expression vector *pQE-32*-wild type, single and double mutant *FABP5* DNAs were sent for nucleotide sequencing at Beckman Coulter (UK), 100ng/µl of plasmid was analyzed.

2.2.2.1.2 Expression and purification of wtrFABP5, smrFABP5 and dmrFABP5

2.2.2.1.2.1 Preparation of competent *E. coli* (BL21) cells

Competent bacterial (BL21) cells were prepared as described in section 2.2.2.1.1.1.

2.2.2.1.2.2 Transformation of competent bacteria with plasmid DNA

Competent *E. coli* (BL21) cells were transformed with expression vectors *pQE-32*-wild type, single and double mutant *FABP5* DNAs as described in section 2.2.2.1.1.6.

2.2.2.1.2.3 Growing *E. coli* cells and inducing expression

A single colony from LB agar plates (with ampicillin 100µg/ml) of *E. coli* (BL21) cells with expression vectors *pQE-32*-wild type, single and double mutant *FABP5* DNAs were picked and incubated in 10ml LB medium (with ampicillin 100µg/ml) at 37°C overnight in a shaking incubator 150×g. The overnight medium was added to 250ml of pre-warmed media (with ampicillin) and incubated at 37°C with vigorous shaking until an OD_{600} of 0.6 is reached. After that, the *E coli* cells were induced by adding 1mM of IPTG (Isopropylthiogalactoside) (Sigma, USA). Time course analysis was performed by collection of 0.5 ml bacterial samples before and after induction at different times of induction from 1-6 hours to find the specific time at which the highest amount of protein was produced. The cell pellets were harvested by centrifugation at 4000×g for 20 minutes and stored at -20°C. SDS-PAGE analysis was performed to check the induction of the protein.

2.2.2.1.2.4 Purification of wtrFABP5, smrFABP5 and dmrFABP5

The protein produced in *E. coli* (BL21) cells was purified by the gravity-flow chromatography on a column containing Ni-NTA agarose conjugated with an antibody against the 6xHis-tag that could bind to the 6xHis-tag FABP5 fusion proteins. The purification of the recombinant protein was conducted with a QIAGEN Ni-NTA Fast Start Kit, following the manufacturer's instructions. The cell pellets were lysed by incubating at room temperature for 1 hour in 10ml native lysis buffer (50mM NaH_2PO_4, 300 mM NaCl, 10 mM imidazole, pH 8.0). The lysate was centrifuged at 14,000×g for 30 minutes to remove the cellular debris and 5µl of supernatant was taken for SDS-PAGE analysis. The cell lysate supernatant was applied to the column and 5µl of the flow-through was collected for SDS-PAGE analysis. Then the 6×His-tagged bounding proteins were washed 2 times with 4 ml of native wash buffer (50mM NaH_2PO_4, 300 mM NaCl, 20 mM imidazole, pH 8.0) and 5µl of both wash fractions were collected for SDS-PAGE analysis. The 6×His-tagged proteins were eluted by native elution buffer (50mM NaH_2PO_4, 300 mM NaCl, 500 mM imidazole, pH 8.0) into two separate tubes and 5µl of both eluates were collected for SDS-PAGE analysis.

2.2.2.1.2.5 Dialysis of wtrFABP5, smrFABP5 and dmrFABP5

The D-Tube dialyzer (Novagen) was used to remove the high concentration of imidazole from purified recombinant proteins. First, Deionized water was added to the D-Tube and incubated upright for at least 5 minutes. Then, the water was removed using pipette and protein was added to the tube and the tube was placed in a beaker containing 1000-fold PBS using floating rack. The protein was collected after stirring gently in 4°C for at least 3 hours and stored at -80°C after flash freezing in Liquid Nitrogen.

2.2.2.1.2.6 Bradford assay

Bio-Rad protein assay (Bio-Rad Laboratories GmbH, Munchen, Germany) was used to measure the concentration of purified proteins. A standard curve established using serial concentration of BSA (from 50-500µg/µl) in 50µl PBS. Appropriate volume of protein samples was also diluted with 50µl PBS. Controls and samples were incubated with 1ml of diluted (1/5) dye reagent (Bio-Rad GmbH, Munchen, Germany), for 15 minutes before measuring the absorbance at 595nm using the MultiSkan plate reader (BioTek Instruments, USA). Standard curve was used to calculate the concentration of proteins.

2.2.2.1.2.7 Sodium dodecyl sulphate-polyacrylamide protein gel electrophoresis (SDS-PAGE)

SDS-PAGE is a very common method for separating proteins according to their molecular weight, based on their differential rates of migration through a gel under the effect of an applied electrical field. This method uses a polyacrylamide gel as a support medium and sodium dodecyl sulfate (SDS) to denature the proteins. The glass plate sandwich was performed and the resolving gel was prepared by mixing 10ml next gel, 60µl of 10% Ammonium Persulfate, 6µl of TEMED and immediately poured using a glass pipette until approximately the edge of plastic. Comb was inserted in the gel and gel was allowed to polymerize for 40 minutes. Then, comb was removed carefully and the gel was put into the tank with running buffer. The proteins were added to SDS-PAGE sample loading buffer (1M Tris PH 6.8, 40% Glycerol, 10% SDS, 2-mercaptoethanol and 1% Bromophenol Blue) and boiled at 95°C for 10 minutes and chilled on ice for 2 minutes and the samples were loaded in each well. Finally, the gel was run at 150V for 1 hour.

2.2.2.1.2.8 Coomassie staining of SDS-PAGE gels

The gel was incubated in Coomassie staining solution (Bio-Rad GmbH, Munchen, Germany) for 1 hour with gentle shaking and washed with distilled water overnight. After that the gel was photographed to show the degree of purification.

2.2.2.1.2.9 Transfer of protein from SDS gel to nitrocellulose membrane

The proteins were transferred from gel to nitrocellulose membrane by making sandwich with soaking the fiber pad, 3 sheets of Whatman paper, gel, nitrocellulose membrane, 3 sheet of Whatman filter paper and fiber pad respectively in transfer buffer (3.03g Tris, 14.4g Glycine and distilled water). The air bubbles were removed from each step using a glass roller. The transfer was performed at 100V, 4°C for 1.5 hour.

2.2.2.1.2.10 Immunodetection of 6×His-tagged proteins

The membrane was washed twice for 10 minutes with TBS-T (Tris, Sodium Chloride, distilled water). The membrane was incubated for 1 hour in blocking buffer (5% TBS-T-milk) and washed by TBS-T two times for 10 minutes. The membrane was incubated once in Penta-His antibody solution (1/12000) (QIAGEN) and then in polyclonal rabbit anti-human FABP5 antibody (1/500) (Hycult) in blocking buffer. The membrane was washed 3 times for 10 minutes with TBS-T and then incubated with secondary antibody solution [peroxidase-conjugated rabbit anti-mouse (1:1000) (Dako) and polyclonal goat anti-rabbit (1:2000) (Hycult)] for 1 hour, washed 4 times for 10 minutes with TBS-T. Finally, ECL (GE Healthcare, Buckinghamshire, UK) solution was used to detect protein expression by chemiluminescence. The membrane was exposed to X-ray (Kodak film GE Healthcare, UK).

2.2.2.2 Fluorescence displacement DAUDA assay

2.2.2.2.1 WtrFABP5 delipidation

Removal of fatty acids from wtrFABP5 was performed by delipidation using Lipidex-1000 (Hydroxyalkoxypropyl-Dextran). Lipidex-1000 (Sigma) was suspended in 10mM-Tris HCL pH 7.5 and incubated with wtrFABP5 at a ratio of 10:1(w/w) at 37°C for 1 hour with occasional mixing. The mixture was centrifuged for 4 minutes at 10,000×g and then the supernatant was collected. Finally, the protein concentration was measured by Bradford assay as described in section 2.2.2.1.2.6.

2.2.2.2.2 Fluorescence emission spectroscope for wtrFABP5

Fluorescent labelled fatty acid DAUDA 11-[5-(dimethylamino)-1-naphthalenyl sulfonyl amino]-undecanoic acid (Cayman) was used to check the emission wavelength of wtrFABP5 after binding with DAUDA. DAUDA was dissolved in methanol for a 100mM stock. Each time 0.1mM fresh stock was prepared by dilution in PBS. Fluorescence measurement spectra were recorded at 25°C using a Varioskan Flash (Thermo Electron Corporation, Waltham, MA) in white 96 well opaque tissue culture plates, flat bottom and Thermo Scientific SkanIt software for collection of data. Excitation, emission wavelengths and fluorescence intensity were measured by fixing the excitation wavelength on 345nm and emission wavelength from 450-600nm. The reactions were set as PBS, 3µM wtrFABP5 in PBS and presence or absence of 3µM wtrFABP5 in 2µM DAUDA. The reactions were incubated for 10 minutes to determine fluorescence peak emission wavelength.

2.2.2.2.3 Fatty acids binding ability of the purified recombinant FABP5s

The binding ability of all purified recombinant FABP5s (wtrFABP5, smrFABP5 and dmrFABP5) to fatty acid (linoleic acid) was examined using the fluorescent labelled

fatty acid analogue DAUDA. Fluorescence measurement spectra were recorded at 25°C using a Varioskan Flash Reader and Thermo Scientific SkanIt software for collection of data. Excitation and emission wavelengths were fixed on 345 and 530nm. Fatty acid binding ability of all purified recombinant FABP5s was measured by monitoring the changes in fluorescence intensity and wavelength after adding 2μM DAUDA in the present or absence of 2μM linoleic acid.

2.2.2.3 Statistical analysis

Student's *t*-test was carried out using GraphPad Prism software to compare the differences of the means between control and experimental groups and the data is presented with SE. The difference is regarded as significant when $p<0.05$; in the results, *p* value is represented by asterisks as follow: ***, $P < 0.0001$.

2.3 Results

2.3.1 Construction of expression vectors harboring wild type *FABP5* DNAs

2.3.1.1 Isolation of wild *FABP5* DNAs from cloning vector and cutting the expression vector

Wild type *FABP5* DNA was isolated from *E. coli* (DH5α) cells harboring cloning vector *pBluescript II SK* by using Miniprep Qiagen extraction kit. The cloning vector *pBluescript II SK* was digested by using *Kpn*I and *Pst*I to confirm that cloning vectors contain the wild type *FABP5* DNA. At the same time the expression vector *pQE-32* was linearized by using same restriction enzymes to be ready for ligation, as showing by electrophoresis analysis in agarose gel in **Fig. 2.1**.

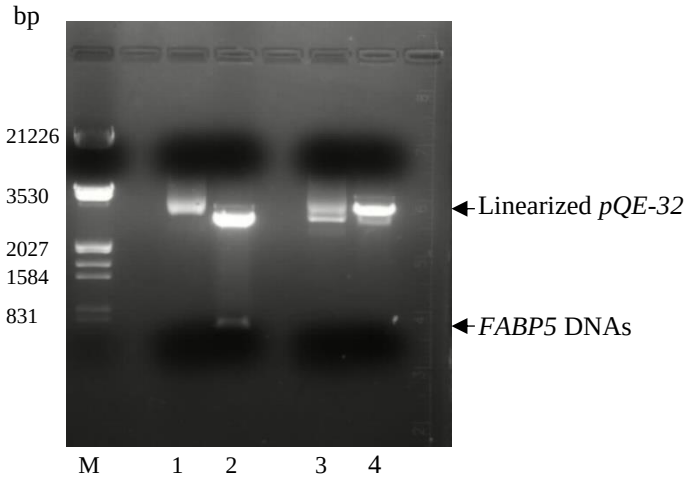

Figure 2.1 Enzymatic release of the wild type *FABP5* DNA from the cloning vector and cutting the expression vector. After digestion with two restriction enzymes. Lane 1, the control or undigested *pBluescript II SK-FABP5* DNA vector. Lanes 2, *pBluescript II SK-FABP5* DNA was digested with *Kpn*I and *Pst*I; the appearance of the small band (600bp) representing wild type *FABP5* DNA and the large band is linearized vectors. Lane 3, undigested expression vector *pQE-32*. Lane 4, linearized expression vector *pQE-32* by digestion with *Kpn*I and *Pst*I. M: Molecular markers.

2.3.1.2 Ligation of wild type *FABP5* DNA with linearized *pQE-32* vector

The wild type *FABP5* DNA was ligated with the linearized expression vector *pQE-32* using T4 DNA ligase. The reaction mixture was transformed into the competent *E. coli* (DH5α) cells to produce clones of bacteria harboring the expression vector *pQE-32-FABP5* DNA. After the mini-preparation, DNA was extracted from different colonies, the successful ligation was confirmed by electrophoresis analysis in agarose gel after digesting the expression vector with two restriction enzymes *Kpn*I and *Pst*I. A small fragment of DNAs, representing the inserted *FABP5* DNA, were existed out from the expression construct in 4 out of 5 colonies analyzed. Thus, any positive colonies containing the expression construct *pQE-32-FABP5* DNA, as shown in **Fig.2.2,** can be selected and cultured for large scale production of wtrFABP5.

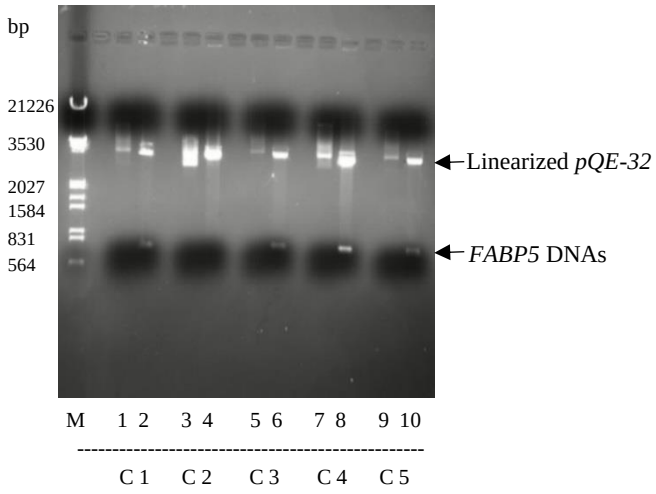

Figure 2.2 Enzymatic release of the wild type *FABP5* DNA from the expression vector *pQE-32-FABP5*. 5 *E. coli* colonies (C1-5) were cultures separately and the expression vector *pQE-32* was digested with two restriction enzymes. Lane 1, 3, 5, 7 and 9: the control or undigested *pQE-32-FABP5* DNA. Lanes 2, 4, 6, 8 and 10: the digested *pQE-32-FABP5* DNA; the appearance of the small band (600bp) representing wild type *FABP5* DNAs and the large band representing linearized vector. All the analysed colonies contained the inserted *FABP5* DNA, except clone 2 (C2). M: Molecular Markers.

2.3.2 Enzymatic digestion analysis of mutant *FABP5* DNAs

Single and double mutant *FABP5* DNAs were isolated from *E. coli* (DH5α) cells containing the expression vectors *pQE-32* by mini-DNA preparation using the Miniprep Qiagen extraction kit. Then, the expression vectors were digested by *Kpn*I and *Pst*I to confirm that the expression vectors contain the gene of interest, as showing by electrophoresis analysis in agarose gel in **Fig. 2.3**.

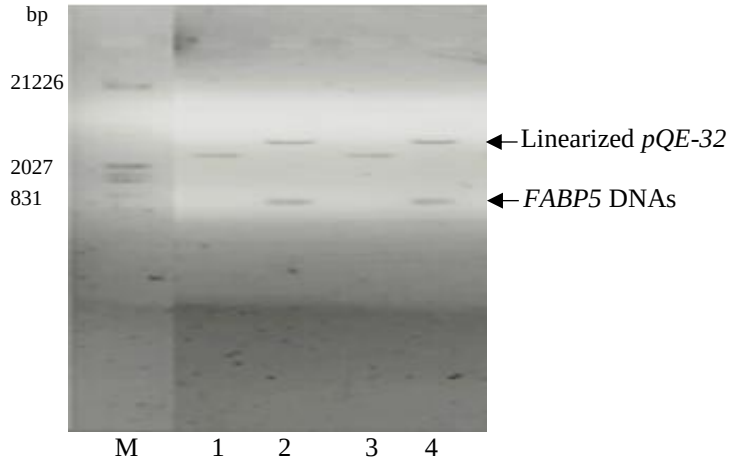

Figure 2.3 Enzymatic release of the single and double mutant *FABP5* DNAs from the expression constructs. Lane 1 and 3, the control (undigested) expression vectors *pQE-32*-mutant *FABP5* DNAs. Lanes 2 and 4, the digested expression vectors *pQE-32*-mutant *FABP5* DNAs. Expression constructs containing the properly inserted genes was confirmed by the appearance of a small band (600bp) representing single and double mutant *FABP5* DNAs, respectively. M: Molecular markers.

2.3.3 DNA sequencing analysis of *pQE-32-FABP5*

The expression constructs containing wild type and mutant types of *FABP5* DNAs were subjected to nucleotide sequence analyses. As shown in **Fig 2.4**, nucleotide sequences of all 3 expression constructs contained the genes of interest and the sequences for the wild type, single and double mutant *FABP5* DNAs were correct.

A

NNNNATATANNNNANTNACCTATAAATAGGCGTATCACGAGGCCCTTTCGTCTTCCCTCGAGAAAT
CATAAAAAATTTATTTGCTTTGTGAGCGGATAACAATTATAATAGATTCAATTGTGAGCGGATAAC
AATTTCACACAGAATTCATTAAAGAGGAGAAATTAACT**ATG**AGAGGATCT*CACCATCACCATCACCA*
*T*G**GGTACC**GGGCCCCCCCTCGAGATCTTCGAATTCGGCTTACCGCCGACGCAGACCCCTCTCTGCA
CGCCAGCCCGCCCGCACCCACCATGGCCACAGTTCAGCAGCTGGAAGGAAGATGGCGCCTGGTGG
ACAGCAAAGGCTTTGATGAATACATGAAGGAGCTAGGAGTGGGAATAGCTTTGCGAAAAATGGGC
GCAATGGCCAAGCCAGATTGTATCATCACTTGTGATGGTAAAAACCTCACCATAAAAACTGAGAGC
ACTTTGAAAACAACACAGTTTTCTTGTACCCTGGGAGAGAAGTTTGAAGAAACCACAGCTGATGGC
AGAAAAACTCAGACTGTCTGCAACTTTACAGATGGTGCATTGGTTCAGCATCAGGAGTGGGATGGG
AAGGAAAGCACAATAACAAGAAAATTGAAAGATGGGAAATTAGTGGTGGAGTGTGTCATGAACAA
TGTCACCTGTACTCGGATCTATGAAAAAGTAGAATAAAAATTCCATCATCACTTTGGACAGGAGTT
AATTAAGAGAATGACCAAGCTCAGTTCAATGAGCAAATCTCCATACTGTTTCTTTCTTTTTTTTTCA
TTACTGTGTTCAATTATCTTTATCATAAACATTTTACATGCAGCTATTTCAAAGTGTGTTGGATTAAT
TAGGATCATCCCTTTGGTTAATAAATAAATGTGTTTGTGCTAAAGCCGAATTCCGCGGCCGCAGGC
CTCTAGAGTCGAC**CTGCAG**CCAAGCTTAATTAGCTGACCTTGGACTCCTGTTGATAGATCCAGTAA
TGACCTCANAACCTCN

B

CTTTTTCTGACTTACCTATAAAATAGGCGTATCACGAGGCCCTTTCGTCTTCACCTCGAGAAATCAT
AAAATTTATTTGCTTTGTGAGCGGATAACAATTATAATAGATTCAATTGTGAGCGGATAACAATTTC
ACACAGAATTCATTAAAGAGGAGAAATTAACT**ATG**AGAGGATCT*CACCATCACCATCACCATG***GGT**
ACCGCATGCGAGCTCGGTACCGGGCCCCCCCTCGAGATCTTCGAATTCGGCTTACCGCCGACGCAG
ACCCCTCTCTGCACGCCAGCCCGCCCGCACCCACCATGGCCACAGTTCAGCAGCTGGAAGGAAGAT
GGCGCCTGGTGGACAGCAAAGGCTTTGATGAATACATGAAGGAGCTAGGAGTGGGAATAGCTTTG
CGAAAAATGGGCGCAATGGCCAAGCCAGATTGTATCATCACTTGTGATGGTAAAAACCTCACCATA
AAAACTGAGAGCACTTTGAAAACAACACAGTTTTCTTGTACCCTGGGAGAGAAGTTTGAAGAAACC
ACAGCTGATGGCAGAAAAACTCAGACTGTCTGCAACTTTACAGATGGTGCATTGGTTCAGCATCAG
GAGTGGGATGGGAAGGAAAGCACAATAACA**GC**AAAATTGAAAGATGGGAAACTAGTGGTGGAGT
GTGTCATGAACAATGTCACCTGTACTCGGATCTATGAAAAAGTAGAATAAAAATTCCATCATCACT
TTGGACAGGAGTTAATTAAGAGAATGACCAAGCTCAGTTCAATGAGCAAATCTCCATACTGTTTCT
TTCTTTTTTTTTTCATTACTGTGTTCAATTATCTTTATCATAAACATTTTACATGCAGCTATTTCAAAG
TGTGTTGGATTAATTAGGATCATCCCTTTGGTTAATAAATAAATGTGTTTGTGCTAANGCCGAATTC
CGCGGCCGCAGGCCTCTAGAGTCGAC**CTGCAG**CCNAGCTTAATTAGCTGAGCTGGGACTCCTGTTG
ATAGATCCAGTAATGACCTCAGANCTCCATCTGGATTNGTTCAGANCGCTCGGTTGCCCGCCGGGC
GTTTTTTTTGGTGAAATCCAGCTAGCTNGGCGAGATTTNNGGAGCTANGGAGCTAAATGGAAAAAA
AATCCTGGATTACCCNGTTGATTTTCCNATGGCTCGTAANA

C

CTTTTTCTGACTTACCTATAAAATAGGCGTATCACGAGGCCCTTTCGTCTTCACCTCGAGAAATCAT
AAAATTTATTTGCTTTGTGAGCGGATAACAATTATAATAGATTCAATTGTGAGCGGATAACAATTTC
ACACAGAATTCATTAAAGAGGAGAAATTAACT**ATG**AGAGGATCT*CACCATCACCATCACCATG***GGT**
ACCGCATGCGAGCTCGGTACCGGGCCCCCCCTCGAGATCTTCGAATTCGGCTTACCGCCGACGCAG
ACCCCTCTCTGCACGCCAGCCCGCCCGCACCCACCATGGCCACAGTTCAGCAGCTGGAAGGAAGAT
GGCGCCTGGTGGACAGCAAAGGCTTTGATGAATACATGAAGGAGCTAGGAGTGGGAATAGCTTTG
CGAAAAATGGGCGCAATGGCCAAGCCAGATTGTATCATCACTTGTGATGGTAAAAACCTCACCATA
AAAACTGAGAGCACTTTGAAAACAACACAGTTTTCTTGTACCCTGGGAGAGAAGTTTGAAGAAACC
ACAGCTGATGGCAGAAAAACTCAGACTGTCTGCAACTTTACAGATGGTGCATTGGTTCAGCATCAG
GAGTGGGATGGGAAGGAAAGCACAATAACA**GC**AAAATTGAAAGATGGGAAACTAGTGGTGGAGT
GTGTCATGAACAATGTCACCTGTACT**GC**GATCTATGAAAAAGTAGAATAAAAATTCCATCATCACT
TTGGACAGGAGTTAATTAAGAGAATGACCAAGCTCAGTTCAATGAGCAAATCTCCATACTGTTTCT
TTCTTTTTTTTTTCATTACTGTGTTCAATTATCTTTATCATAAACATTTTACATGCAGCTATTTCAAAG
TGTGTTGGATTAATTAGGATCATCCCTTTGGTTAATAAATAAATGTGTTTGTGCTAANGCCGAATTC
CGCGGCCGCAGGCCTCTAGAGTCGAC**CTGCAG**CCNAGCTTAATTAGCTGAGCTGGGACTCCTGTTG
ATAGATCCAGTAATGACCTCAGANCTCCATCTGGATTNGTTCAGANCGCTCGGTTGCCCGCCGGGC
GTTTTTTTTGGTGAAATCCAGCTAGCTNGGCGAGATTTNNGGAGCTANGGAGCTAAATGGAAAAAA
AATCCTGGATTACCCNGTTGATTTTCCNATGGCTCGTAANA

Figure 2.4 DNA sequencing analysis of the expression constructs. A, the vector containing wild type *FABP5* DNA. **B,** the vector containing the singly mutated *FABP5* DNA. **C,** vector containing the doubly mutated *FABP5* DNA. **D,** the sequences of human *FABP5* gene (Genbank-BLAST). The sequences alignment showed a 100% sequences match between Query (wild type *FABP5* DNA) and subject (database sequence). After the starting codon ATG, a short sequence (blue) coding for 6xHis-tag was contained in the vector. The recognition sequences for *Kpn*I (GGTACC) and for *Pst*I (CTGCAG) are bold and underlined. GC represents single mutation [the Alanine^{109} codon (GCA) was mutated from the Arginine^{109} codon (AGA)]. GC and GC represent double mutations [(the Alanine codon^{109} (GCA) was mutated from the Arginine^{109} codon (AGA) and the Alanine^{129} codon (GCG) was mutated from the Arginine^{129} codon (CGG)].

2.3.4 Expression and purification of the wild type and mutant recombinant FABP5s

2.3.4.1 Determination the optimal time of maximum amount of protein synthesis in *E. coli* cells.

All three expression vectors containing different *FABP5* DNAs (wtrFABP5, smrFABP5 and dmrFABP5) were isolated from *E. coli* (DH5α) cells respectively and transformed again into competent BL21 *E. coli* cells for protein production. Bacterial samples were removed, once per hour from culture, for up to 6 hours after 1mM IPTG induction. Expression of human recombinant FABP5s from the engineered vectors was not lethal to *E. coli* cells as demonstrated by normal growth rate of bacteria by using Western blot. After induction, the wtrFABP5 recognized by the anti-His tag antibody was gradually expressed and reached its maximum after hour 4, as shown in **Fig. 2.5**.

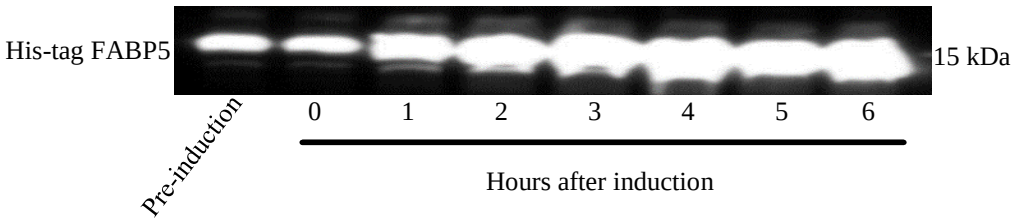

Figure 2.5 Determination the optimal experimental time point at which the maximum amount of recombinant protein was synthesized in bacterial cells. Bacterial samples were removed, once per hour from culture, for up to 6 hours after IPTG induction. 6×His-tag bound protein bands were recognized by the Penta-His antibody. The wtrFABP5 protein synthesized in bacterial cells at different time points is shown in 8 separate lanes.

2.3.4.2 Purification and Immunodetection of the 6xHis-tagged FABP5s

The protein produced in BL21 *E. coli* cells was purified by gravity-flow chromatography on a column containing Ni-NTA agarose conjugated with an antibody

against the 6xHis-tag that was able to bind to the 6xHis-tag FABP5 fusion proteins. The purification of the recombinant proteins was conducted with a Qiagen Ni-NTA Fast Start Kit, following the manufacturer's instructions. SDS-PAGE gel (Coomassie Blue staining) analysis showed that the degree of purification from other bacterial proteins and the purity of the end products in the first and the second elution are very high with only one band of approximately 15 kDa (**Fig. 2.6)**. At the final stage of the purification, immunodetection of the first and second elution with a monoclonal anti-human FABP5 showed that this protein in a single band on the blot reacted to the anti-FABP5 antibody very well. Thus, the band size plus the specific immuno-response confirmed that these 3 recombinant FABP5s eluted from the first fraction were the targets proteins wtFABP5, dmrFABP5 and smrFABP5, respectively (**Fig. 2.7)**.

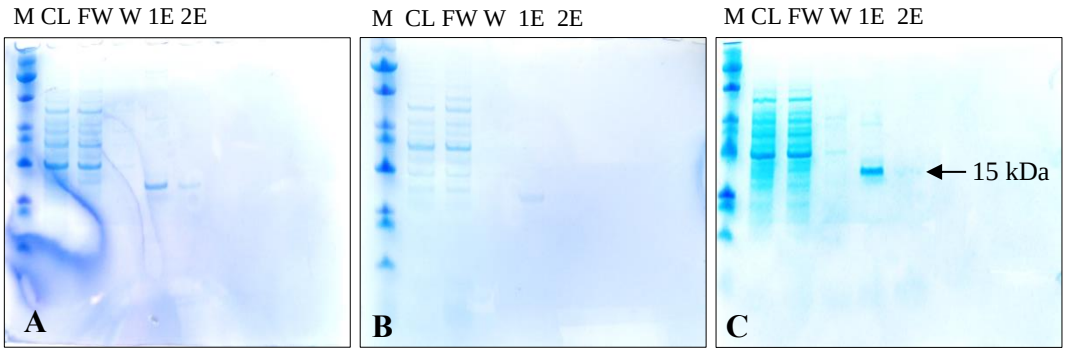

Figure 2.6 Purification of the recombinant FABP5s. After the cell pellets were lysed by native lysis buffer, the cell lysate was subjected to SDS-PAGE to separate and to visualize the bacterial proteins and the 6xHis-tagged protein. Cell lysate supernatant was applied to the column. After washing the column with the washing buffer, the 6xHis-tagged bounding protein was eluted with an elution buffer and the protein in the first 2 fractions was collected into two separate tubes (1E, 2E). **A,** purification of wtrFABP5. **B,** purification of smrFABP5. **C,** purification of dmrFABP5. M: Molecular markers. CL: the cell lysate. FW: flow-through fraction. W: wash fraction. 1E and 2E: elution fractions.

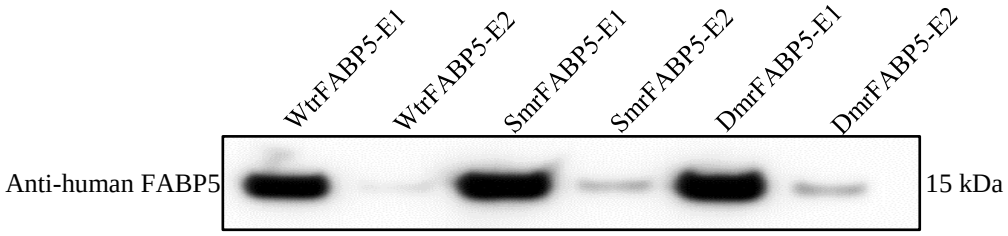

Figure 2.7 Immunodetection of the purified recombinant FABP5s. The 2 eluates (E1 and E2) collected from the chromatography were subjected to immunodetection for the purified wtrFABP5, smrFABP5 and dmrFABP5. FABP5 protein bands on the blot were recognized by a monoclonal anti-human FABP5 antibody.

2.3.5 Testing the biological activities of the recombinant FABP5s

The fatty acid-binding affinity of the recombinant FABP5s was tested by the fluorescently labelled fatty acid DAUDA [11-(Dansylamino) undecanoic Acid] displacement assay (228). The florescence measurement spectrum was recorded at 25°C using a Varioskan Flash to determine the fluorescence peak emission wavelength for wtrFABP5. After the excitation was fixed at 345nm, then the emission wavelength was fixed from 450-600nm. The fatty acid-binding affinity of wtrFABP5 for DAUDA was tested and the maximum affinity was detected at 530nm with a left shift of wavelength of emission from 560nm for DAUDA alone to 530nm upon addition of wtrFABP5 to DAUDA, accompanied by an increase in fluorescence intensity, as shown in **Fig. 2.8**.

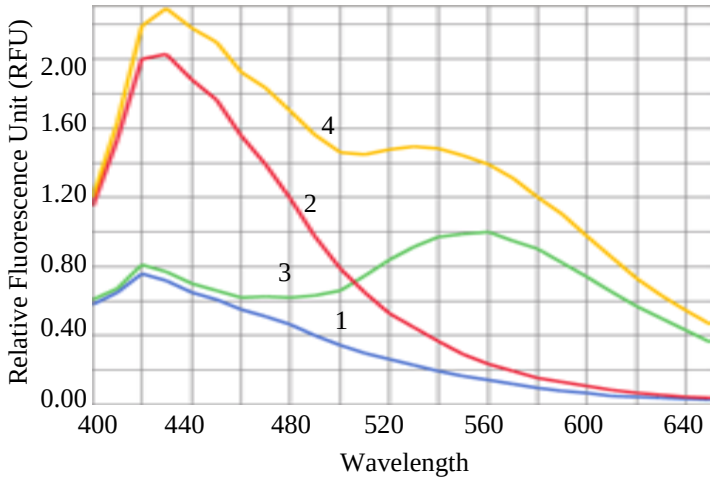

Figure 2.8 Effect of wtrFAcBP5 on the fluorescence emission spectra of DAUDA. Effect of wtrFABP5 on the fluorescence emission spectra of DAUDA ligand at the excitation wavelength of 345nm. PBS (1) and wtrFABP5 in PBS (2) did not produce any emission; whereas 2µM DAUDA produced emission at 560nm (3); 2µM DAUDA in the presence of 3µM wtrFABP5 (4) caused an increase in the fluorescence intensity and a left shift to 530nm compared to DAUDA alone.

The fluorescence intensity of displaced DAUDA from each recombinant FABP5 by a competitive unlabeled linoleic acid was used as an indication of their relative binding affinity (192). After adding wtrFABP5 to DAUDA, the complex led to an increase in fluorescence intensity and a left shift of the emission to 530nm as compared to that produced by DAUDA alone 560nm. The addition of linoleic acid to wtrFABP5-DAUDA complex created a noticeable drop in the fluorescence intensity with right shift of emission wavelength from 530 nm for the complex to 560 nm upon adding of linoleic acid (**Fig. 2.9, A)**, indicating that linoleic acid can displace DAUDA from the primary binding site of wtrFABP5. However, the fatty acid binding affinity of smrFABP5 and dmrFABP5 which is single and double mutated in fatty acid binding motif was checked by adding of linoleic acid to smrFABP5- or dmrFABP5- DAUDA complexes. This complexes were not able to decrease the fluorescence intensity (**Fig.**

2.9, B and **C)**, indicating that linoleic acid cannot displace DAUDA from the primary binding site of smrFABP5 and dmrFABP5.

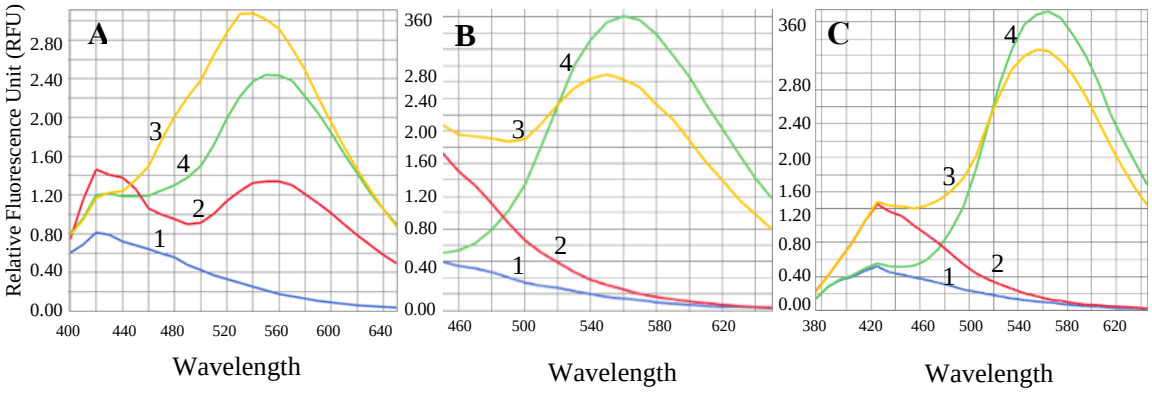

Figure 2.9 Fatty acid binding properties of the recombinant FABP5s by DAUDA. **A,** Competitive inhibition of DAUDA-wtrFABP5 binding to linoleic acid. PBS alone (1) or 2µM DAUDA alone (2) give the same results as **(Fig. 2.8)**. 3µM wtrFABP5 plus 2µM DAUDA caused an increase in fluorescence intensity and a left shift to 530nm compared to DAUDA alone (3). 3µM wtrFABP5 and 2µM DAUDA plus 2µM linoleic acid exhibited a reduced fluorescence intensity and a right shift to 560 nm; indicating an inhibition and displacement of DAUDA-wtrFABP5 binding (4). **B,** Competitive inhibition of DAUDA-smrFABP5 binding to linoleic acid. PBS alone (1) or 3µM smrFABP5 in PBS (2) did not produce any emission. 3µM smrFABP5 and 2µM DAUDA (3) caused an increase in fluorescence intensity and a left shift to 550nm compared to DAUDA alone (see A). 3µM smrFABP5 and 2µM DAUDA plus 2µM linoleic acid produced an increase in fluorescence intensity and a right shift to 560 nm; indicating no inhibition and displacement of DAUDA-smrFABP5 binding (4). **C,** Competitive inhibition of DAUDA-dmrFABP5 binding to linoleic acid. PBS alone (1), or 3µM dmrFABP5 in PBS (2) did not produce any emission. 3µM dmrFABP5 and 2µM DAUDA (3) caused an increase in fluorescence intensity, but no shift in emission spectrum compared to DAUDA alone (see A). 3µM dmrFABP5 and 2µM DAUDA plus 2µM linoleic acid produced an increase of fluorescence intensity but no shift in emission wavelength; indicating no inhibition and no displacement of DAUDA-dmrFABP5 binding (4).

In addition, the fluorescence intensities of displacement DAUDA from different FABP5s was confirmed by adding 10μM linoleic acid to each recombinant FABP5-DAUDA complex in triplicate to verify their relative binding affinity. When the level of fluorescence intensity of DAUDA (D) + Buffer (B) was set at 1 **(Fig. 2.10)**, the fluorescence intensity of the complex of wtrFABP5, D and B without linoleic acid was 3.25 ± 0.07. When linoleic acid was added to the complex, the level of fluorescence intensity was significantly reduced by 43.7% to 1.83 ± 0.6 (Student's *t* test, $p < 0.0001$). Thus, wtrFABP5 exhibited a strong ability to bind to linoleic acid and displaced 43.7% DAUDA. When linoleic acid was added to complexes of either smrFABP5 + B + D or dmrFABP5 + B +D, no displacement was observed, indicating that smrFABP5 and dmrFABP5 were not capable of binding to fatty acids anymore and dmrFABP5 was selected as inactive form of FABP5.

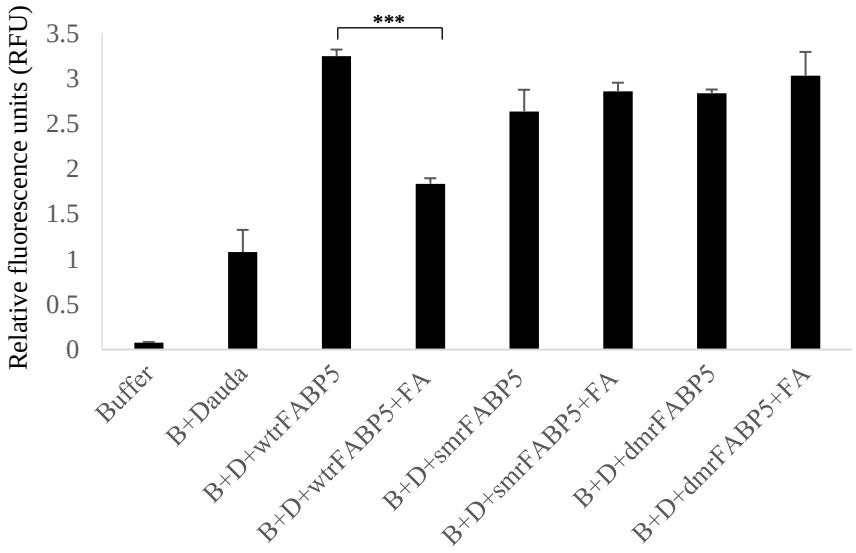

Figure 2.10 Fluorescence intensities of displaced DAUDA from recombinant FABP5s by linoleic acid. The value of fluorescence intensity produced by the buffer and DAUDA plus recombinant FABP5s was set as control. The results (mean ± SE) were obtained from 3 separate experiments (2-tailed unpaired Student's *t* test, ***, *P < 0.0001*).

2.4 Discussion

FABP5 binds to fatty acids with its carboxylate group through a binding motif that consist of 3 key amino acids (Arg^{109}, Arg^{129}, and Tyr^{131}) (226,229). During the past study on molecular mechanisms involved in the tumour-promoting activity of FABP5, it was found that the malignancy-promoting function of FABP5 in prostate cancer depends on its structural integrity of the 3 key amino acids-binding motifs. In addition, it was shown that the weakly malignant prostatic cancer cells LNCaP transfected with wild type *FABP5* DNA can greatly increase tumorigenicity and decrease apoptosis. The wtrFABP5, which is capable of binding and transporting fatty acids, can fully perform its tumour-promoting role. However, the mutated *FABP5* DNAs (either dmrFABP or smrFABP5), which had a greatly reduced capability or incapable of binding to fatty acids, lost or reduced their tumour-promoting function (192). Enlightened by the fact that mutant tumour suppressor p53 can promote tumorigenicity (227), we were curious to know whether the mutated FABP5s can play an opposite role to their wild type counterpart. The availability of a large quantity of recombinant materials is a prerequisite to perform further investigations.

To obtain 3 recombinant proteins (wtrFABP5, smrFABP5 and dmrFABP5), full length *FABP5 c*DNAs were cloned into the expression vector *pQE-32* to form 3 expression vectors that were transformed into the *E coli* cells, respectively **(Fig. 2.2) (Fig. 2.3)**. The maximum amount of protein synthesized in the *E coli* cells after IPTG induction was identified at the time point of hour 4. The fact that the no further increase in the amount of protein synthesised (or even decrease was observed) after 4-hour incubation in *E coli* cells suggested that the production of recombinant protein was ceased inside *E. coli* cells or even the synthesised protein started to degrade from their peak amount (**Fig. 2.5)**. After purification, the results from the Western blot analysis showed

that all 3 recombinant proteins isolated from *E. coli* cells are not only recognised by the specific anti-FABP5 antibody, but also exhibited a unique size, indicating a high purity **(Fig. 2.7)**.

The fatty acid-binding ability of all 3 recombinant FABP5s was tested by an assay using fluorescently labelled fatty acid DAUDA which binds with specific and nonspecific binding sites. If DAUDA binds to the protein, it will alter its fluorescence emission spectra and intensity (230). The degree of wavelength left shifting when DAUDA binds to protein indicate that DAUDA binds with specific and nonspecific site (polar and non-polar site) (231,232). Our results showed that Compared to maximum emission wavelength of DAUDA alone which is 560 nm. Reaction of wtrFABP5-DAUDA caused a significant left shift to 530nm **(Fig. 2.9, A)**. However, the reaction of DAUDA-smrFABP5 caused a left shift to 550nm **(Fig. 2.9, B)** and no shift in emission spectrum for dmrFABP5 **(Fig. 2.9, C)**. This results indicate that the degree of polarity of their binding sites is different and the dmrFABP5 loss the specific binding site.

In addition, a competitive study was performed by adding unlabelled linoleic acid to the reaction protein and DAUDA to displace DAUDA from the specific binding site (232). Our results showed that addition of fatty acid (linoleic acid) to wtrFABP5, DAUDA complex created a noticeable drop in the fluorescence intensity **(Fig. 2.9, A)**. Nevertheless, the addition of fatty acid to smrFABP5 or dmrFABP5, DAUDA complex was not able to decrease the fluorescence intensity **(Fig. 2.9, B** and **C)**. This results were confirmed by three separate experiment (mean ± SE). The results showed that when the fatty acid-binding ability of wtrFABP5 was set as 100%, it is significantly reduced to 43.7% after adding natural fatty acid to the reaction of wtrFABP5-DAUDA (Student's *t* test, $p < 0.0001$). However, for smrFABP5 and

dmrFABP5, no reduction in fluorescent intensity was showed after adding natural fatty acid to the reaction smrFABP5 and dmrFABP5-DAUDA **(Fig. 2.10)**. These results showed that mutating 2 of the 3 key amino acids in the fatty acid-binding motif (dmrFABP5) can almost completely deprive of the fatty acid-binding ability of this protein. These results showed that dmrFABP5 loss fatty acid-binding ability and can be used as a bio inhibitor to play a reverse function to the native FABP5.

Previous work in our research group proved that the tumour-promoting activity of FABP5 was reduced as the reducing fatty acid-binding capability and completely lost as the loss of fatty acid-binding capability (192). The availability of a large quantity of biologically inactive FABP5 obtained from this set of experiments will enable us to investigate whether the inactive FABP5 can play an opposite role to the native FABP5 inside the cancer cells.

Chapter Three

Identification of lead inhibitor of FABP5 from a group of chemical compounds

3.1 Introduction

The normal function of FABP5 is binding and transporting medium and long chain fatty acids into cells (212). Fatty acids are used as sources of energy in cancer cells and they are also used as signalling molecules (233) to play important roles in tumorigenicity and metastasis of cancer cells (234). After crucial role of FABP5 in promoting malignant progression of cancer cells was initially demonstrated (191,215), increased FABP5 expression in archival prostate cancer tissues is found to be significantly associated with a reduced patient survival time (189). Moreover, investigations in the past few years established that there is a novel fatty acid-initiated signalling pathway leading to malignant progression of prostatic cancer cells. Thus, when FABP5 expression is increased, excessive amounts of fatty acids are transported into the nucleus, where they act as signalling molecules to stimulate their nuclear receptor PPARγ. The activated PPARγ then modulates expression of its down-stream regulatory genes which finally lead to enhanced tumour expansion and aggressiveness caused by an overgrowth of cells with increased angiogenesis and reduced apoptosis (235).

To suppress the malignant progression of highly malignant CRPC cells by inhibiting FABP5 and its related signalling pathway, the availability of a highly effective FABP5 inhibitor is an important first step. Inhibition of FABPs activity was shown to be effective for treatment of inflammatory and metabolic diseases by chemically synthesized inhibitors, e.g. BMS309403 (206,220-222). Recently developed FABP5 inhibitors (SBFI26, SBFI19, SBFT27, SBFI31), which exhibited a higher inhibitory effect than BMS309403, were originally used effectively as analgesic and anti-inflammatory agents in mice (223-225). SBFI26 (α-truxillic acid 1-naphthyl mono-ester) was in fact, the active component of a Chinese herbal medicine (Incarvillea sinensis) which was used to treat pain and rheumatism in humans in Chinese traditional

medicine since hundreds of years ago (218,219). In a recently developed strategy to develop anti-inflammatory and anti-nociceptive reagents by targeting fatty acid protein anandamide transporters, SBFI26 was used to increase the brain anandamide levels and thus to produce analgesia effect (223,224).

To find out whether the above described, chemically synthesized FABP5 inhibitors can be used to suppress the malignant progression of the CRPC cells, identification of the most effective inhibitor which can produce a maximum suppressive effect is the first step. Thus, in this section, we tested this group of chemical inhibitors by comparing their binding affinities to FABP5 with wtrFABP5 through using the fluorescent displacement DAUDA assay. The most effective candidate was identified as the leading compound to be used for the treatment of CRPC in nude mouse.

3.2 Materials and Methods

3.2.1 Materials

Reagents are listed in Appendix A, Buffers in Appendix B and Equipment in Appendix C.

3.2.2 Methods

3.2.2.1 Fluorescence displacement DAUDA assay

3.2.2.1.1 wtrFABP5 delipidation

Removal of fatty acids from wtrFABP5 was performed as described in chapter 2 section 2.2.2.2.1.

3.2.2.1.2 Fluorescence emission spectroscope for wtrFABP5

Fluorescence emission spectroscope for wtrFABP5 was identified as described in chapter 2 section 2.2.2.2.2.

3.2.2.1.3 Calculation of dissociation DAUDA binding constants K_d (affinity)

The dissociation constant (K_d) is the concentration of ligand (DAUDA) which occupies half of the receptors (protein) at equilibrium. A small K_d means that the receptor has a high affinity for the ligand. However, a large K_d means that the receptor has a low affinity for the ligand (236). The K_d of wtrFABP5 was measured by titrating different concentration of DAUDA from (0.4-3µM) to a solution of 3µM wtrFABP5 in PBS for a total volume of 200µl per well. For calculation of K_d value, 345 and 530 nm were used as the excitation and emission wavelength. The fluorescence data was normalized to the peak fluorescence intensity for each experiment and subtracted from the data of samples without protein. To estimate the K_d and maximal fluorescence intensity (B_{max}) for wtrFABP5, the data was fitted by nonlinear regression techniques using GraphPad Prism software to a saturation binding curve model.

3.2.2.1.4 Inhibition constant K_i for different fatty acids and FABP5 chemical compounds

The inhibition constant (K_i) is the equilibrium dissociation constant for binding of the unlabelled ligand (fatty acids or chemical compounds) that will bind to half the binding sites of the protein at equilibrium in the presence of labelled ligand (DAUDA). The K_i is proportional to the IC50. If the K_i is low (i.e. the affinity is high), the IC50 will also be low (237). The affinities of several unlabelled ligand for wtrFABP5 were determined using DAUDA as a fluorescent probe. Ligand binding affinities (K_i) for an unlabelled ligand were measured to determine the binding affinity of different fatty acids (Linoleic, Oleic, Palmitic acid) (Sigma) for wtrFABP5 by evaluating their ability to displace DAUDA occupying wtrFABP5. In addition, the K_i values of different chemical compounds (SBFI26, SBFI19, SBFI27, and SBFI31) (ChemDiv) were evaluated by displace DAUDA occupying wtrFABP5 to determine the lead compound. 3µM wtrFABP5 was incubated with 2µM DAUDA in PBS in the presence or absence of each fatty acid and chemical inhibitor in different concentrations (0.5-20µM). The loss of fluorescence intensity was measured with Varioskan Flash with the excitation and emission of 345 and 530 nm and the data was fitted by nonlinear regression techniques using GraphPad Prism software to a one site binding affinity model to estimate the binding affinity. The K_i of each ligand was determined using the equation $K_i = IC_{50}/1+$ (DAUDA concentration $/K_d$) (238).

In addition, the chemical compounds and the fatty acids were then added to the assay at 10µM and tested in triplicate to confirm their activity by determine the degree of DAUDA displacement from wtrFABP5 by loss of fluorescence intensity.

3.2.2.2 Statistical analysis

Student's *t*-test was carried out using GraphPad Prism software to compare the differences of the means between control and experimental groups and the data is presented with SE. The difference is regarded as significant when $p<0.05$; in the results, *p* value is represented by asterisks as follow: ***, $P < 0.0001$.

3.3 Results

3.3.1 Determination of DAUDA binding constant (K_d) to wtrFABP5

The dissociation constant (K_d) of the wtrFABP5 was estimated by adding increasing concentrations of DAUDA analog from (0.4-3µM) to a solution of 3µM wtrFABP5. Then for calculation of K_d values, fluorescence data was normalized to the peak fluorescent intensity for each experiment and corrected for the background fluorescence of the ligand (DAUDA) alone at each concentration. The data was fitted by nonlinear regression techniques using GraphPad Prism software to a saturation binding curve model to estimate the apparent dissociation constant (K_d) and maximal fluorescence intensity (B_{max}) for the wtrFABP5. The K_d of DAUDA-wtrFABP5 was 1.86 ± 0.16 µM with B_{max} 3.58 µM **(Fig. 3.1)**.

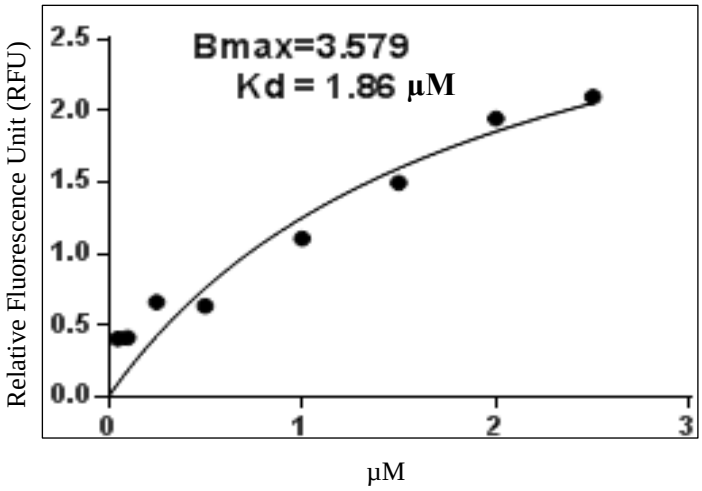

Figure 3.1 Titration curve of DAUDA binding to wtrFABP5. For calculation of the dissociation constant K_d values, the excitation and emission used was 345 and 530 nm, respectively. The apparent dissociation constant (K_d) for DAUDA to wtrFABP5 was calculated to be 1.86 ± 0.16 µM.

3.3.2 Detection of binding affinities (K_i) of 3 fatty acids and 4 candidate compounds to wtrFABP5

The K_i of 3 natural fatty acids (linoleic, oleic, palmitic acid) which inhibited 50% of DAUDA binding to wtrFABP5 were measured to find out the best fatty acid by measuring their ability to displace DAUDA from the wtrFABP5 binding cavity. In addition, the K_i of 4 chemical compounds (SBFI26, SBFI19, SBFT27 and SBFI31) which inhibited DAUDA binding to wtrFABP5 were measured to identify the most potent inhibitor by measuring their ability to displace DAUDA from the wtrFABP5. 3µM wtrFABP5 were incubated with 2µM DAUDA in the presence or absence of each fatty acid in different concentrations (0.5-20µM) to determine the best binding fatty acid. The loss of fluorescence intensity was measured with Varioskan Flash with the excitation and emission of 345 and 530 nm. The data was fitted by non-linear regression techniques using GraphPad Prism to a one site binding affinity model to determine the K_i of these select competitors by using the equation $Ki=IC_{50}/1+$ (DAUDA concentration $/K_d$). The K_d of DAUDA-stearate for wtrFABP5 from the previous results. The calculated K_i (µM) values of Linoleic, Oleic and Palmitic acid were 1.58 ± 0.14, 1.89 ± 0.18 and 4.30 ± 0.4, respectively **(Fig. 3.2, A, B, C) (Table3.1)**. Thus, linoleic acid had the strongest binding affinity for wtrFABP5.

Furthermore, the same protocol was performed to the other four candidate chemical compounds (SBFI26, SBFI-19, SBFI-27 and SBFI-31) to find out the lead inhibitor of FABP5 from these ligands. The most potent compound to bind wtrFABP5 was SBFI26 (K_i =1.69 ± 0.15 µM), whose affinity was about 7.4-times higher than those of SBFI19 and SBFI27 (K_i =12.54 ± 2.25 and 12.50 ± 2.07 µM, respectively). The K_i of SBFI31 did not converge **(Fig. 3.3, A, B, C, D) (Table3.1)**. Taken together, the binding

affinity (*Ki*) of the lead compound (SBFI26) for wtrFABP5 was similar to that of the best-binding fatty acid (linoleic acid).

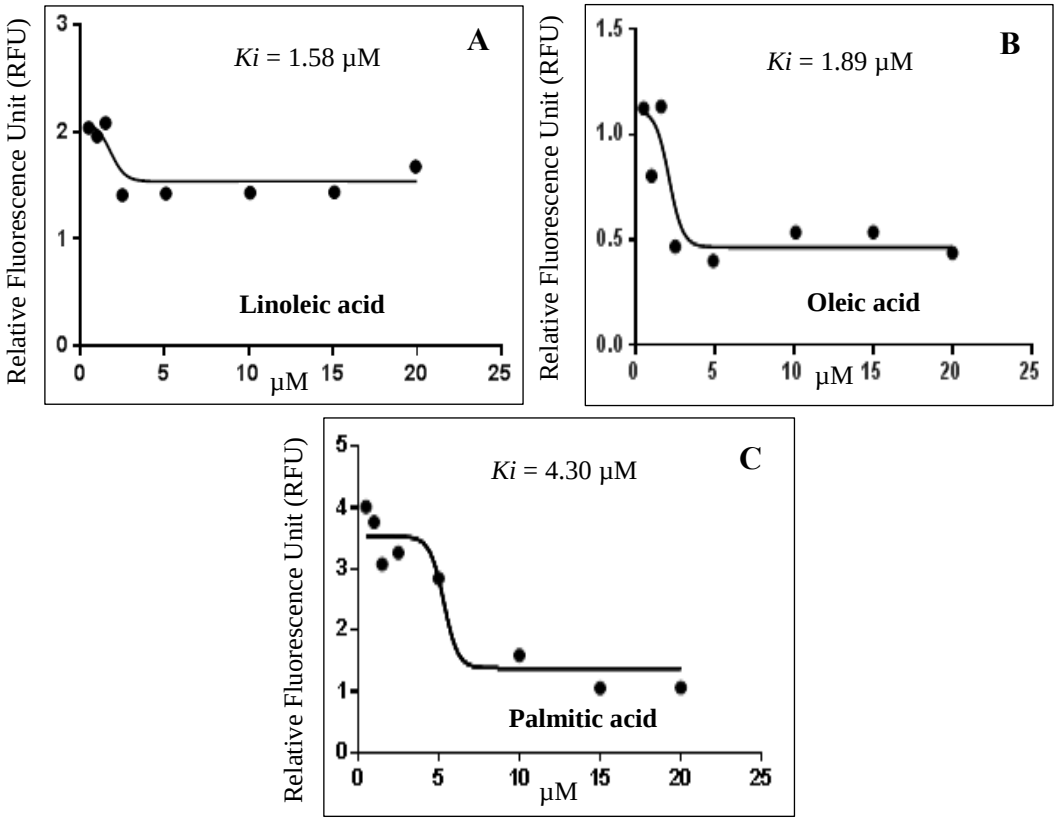

Figure 3.2 Chart records of binding affinity analysis of 3 different fatty acids of FABP5. Inhibition constant *Ki* (binding affinity) of **A,** Linoleic **B,** Oleic and **C,** Palmitic acids binding to wtrFABP5.

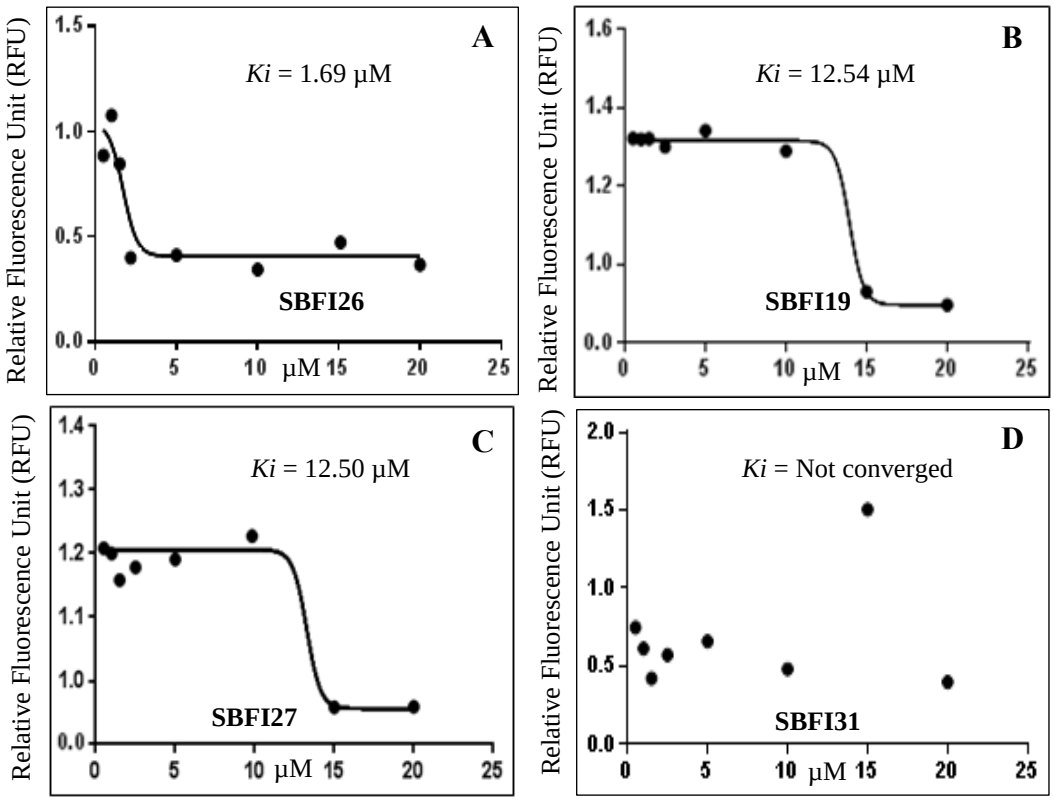

Figure 3.3 Chart records of binding affinity analysis of 4 different candidate chemical inhibitors of FABP5. Inhibition constant K_i of **A,** SBFI26 **B,** SBFI19 **C,** SBFI27, and **D,** SBFI31 to wtrFABP5.

Fatty acids/ Chemical inhibitors	Binding affinity (*Ki*) (µM)
Linoleic acid	1.58
Oleic acid	1.89
Palmitic acid	4.30
SBFI26	1.69
SBFI19	12.54
SBFI27	12.50
SBFI31	-----

Table 3.1 K_i values of 3 different fatty acids and 4 different candidate chemical compounds.

In addition, the activity of the lead compound was confirmed by adding 10µM of each fatty acid and candidate chemical compound to 3µM wtrFABP5 plus 2µM DAUDA to ascertain the degree of DAUDA displacement from wtrFABP5 by loss of fluorescence intensity and the results are shown in **(Fig. 3.4)**. The relative level of fluorescence intensity of wtrFABP5 with DAUDA was 2.65 ± 0.14. This was reduced to 1.37 ± 0.07, 1.68 ± 0.09 and 1.80 ± 0.08 after adding linoleic, oleic and palmitic acids, respectively, to the complex. After SBFI26, SBFI19, SBFT27, and SBFI31 were added to the complex, the intensity was reduced to 1.48 ± 0.06, 2.33 ± 0.08, 1.95 ± 0.17 and 2.58 ± 0.79, respectively. Linoleic acid and SBFI26 produced highly significant reductions in fluorescence intensities (Student's *t* test, $P < 0.0001$) and there was approximately similar binding affinity between the Linoleic acid and SBFI26 to the wtrFABP5.

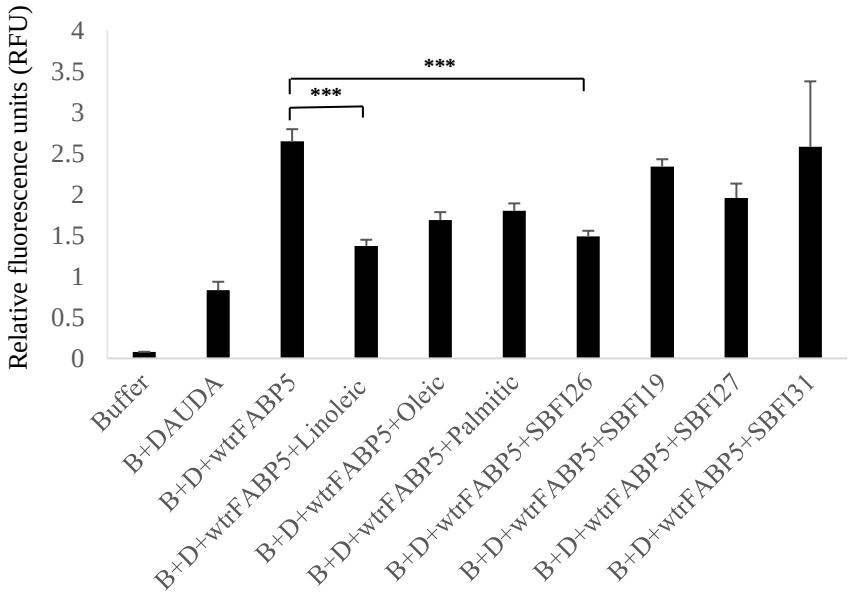

Figure 3.4 Fluorescence intensity of displacement of DAUDA from wtrFABP5 in the presence of 3 different fatty acids and 4 different candidate chemical inhibitors. The value of fluorescence intensity produced by the buffer and DAUDA plus wtrFABP5 was set as control. The results (mean ± SE) were obtained from 3 separate experiments (2-tailed unpaired Student's *t* test, ***, $P < 0.0001$).

3.4 Discussion

Recently several studies showed that inhibition of FABPs activity is an effective method for treatment of inflammatory and metabolic diseases by using chemically synthesized inhibitors (206,220-222). A group of 4 chemical compounds capable of suppressing the biological activity of FABP5, was originally used as anti-nociceptive agents by increasing levels of brain anandamide transported by FABP5 and produced analgesia (223,224).

Using DAUDA displacement assay, we aimed to identify the lead compound from 4 different potential chemical inhibitors. It has been confirmed that DAUDA binds to FABPs in a similar location to fatty acids (239). Ligand binding to wtrFABP5 using DAUDA as a fluorescent probe has been previously investigated (192). We found that a dissociation constant (K_d) of titration DAUDA with delipidated wtrFABP5 was 1.86μM, which was within the range of the other FABPs (240) **(Fig. 3.1)**.

The affinities of several ligands for wtrFABP5 were determined using DAUDA as a fluorescent probe. The *Ki* for a range of ligands were determined by measuring their ability to displace DAUDA from the wtrFABP5 binding cavity. Binding of non-fatty acid ligands to FABPs has been exemplified by their ability to displace bound fluorescent probes such as DAUDA from FABP (241,242). Although there is limited structural information on the binding sites of DAUDA within the different FABPs, they have been shown to bind competitively with fatty acids (239). To determine the best-fit value of *Ki* (the concentration of unlabelled ligand that blocks 50% of the specific binding of DAUDA), the nonlinear regression was used to determine the specificity at 100% (specific and nonspecific) (top plateaus) and 0% (nonspecific) (bottom plateaus) (243). If the labelled and unlabelled ligand compete for a single

binding site, the steepness of the competitive binding curve is determined by the law of mass action. The steepness of a binding curve can be quantified with a slope factor, or a Hill slope. A one-site competitive binding curve that follows the law of mass action has a slope of -1.0. If the curve is more shallow, the slope factor will be a negative fraction (-0.85 or -0.60) (236). Our result showed that the slope factor follows the law of mass action, indicating the labelled and unlabelled ligand compete for a single binding site of wtrFABP5.

Different natural fatty acids (Linoleic, Oleic, Palmitic acid) and chemical inhibitors (SBFI26, SBFI19, SBFI27, and SBFI31) were used to perform competitive experiments with DAUDA to bind to wtrFABP5. The calculated *Ki* values of different ligands in the presence of wtrFABP5 (via DAUDA displacement) are summarized in **Table 3.1**. DAUDA displacement assays showed that all 3 fatty acids had the ability to bind to wtrFABP5 **(Fig. 3.2)**. Linoleic and oleic acids are the better fatty acids with low *Ki* value 1.58 and 1.89µM respectively as compared with Palmitic acid 4.30µM. These results are in line with previous findings (192). In addition, this assays showed that 3 of these 4 compounds had the ability to bind to wtrFABP5, just as well as the 3 fatty acids tested **(Fig. 3.3)**. SBFI26 is the lead compound with low *Ki* value 1.58µM as compared with others.

We found that the fluorescence intensity reduced with increasing concentrations of Linoleic acid and SBFI26, suggesting that these two significantly displaced DAUDA from wtrFABP5 (mean ± SE) (Student's *t* test, $P < 0.0001$). While Linoleic acid had the highest binding ability amongst the 3 fatty acids, SBFI26 exhibited the highest FABP5 binding ability amongst the 4 compounds. Thus, SBFI26 was identified as the lead inhibitor of FABP5 **(Fig. 3.4)**.

Chapter Four

Suppressing the malignant progression of the PC3-M cells by SBFI26 and dmrFABP5 *in vitro* and *in vivo*.

4.1 Introduction

Increase expression of FABP5 may result in accumulation of excessive amounts of fatty acids in CRPC cells where fatty acids can act as signalling molecules to stimulate their nuclear receptor PPARγ. The activated PPARγ then modulates expression of its down-stream regulatory genes which finally lead to enhanced tumour expansion and aggressiveness caused by an overgrowth of CRPC cells with increased angiogenesis and reduced apoptosis (235). Recently, it was suggested that the FABP5-PPARγ-VEGF signalling transduction axis, rather than AR-modulated signal transduction pathway, that is the dominant signalling route in promoting malignant progression of CRPC cells (217). Based on previous long time investigations, it is reasonable to hypothesize that FABP5 is an important pharmacological target, and modulating FABP5 biological activity may provide an effective therapy for treatment of CRPC *in vitro* and *in vivo*.

When highly malignant CRPC PC3-M cells were orthotopically implanted into the mouse prostate gland, knockdown of *FABP5* gene by RNA interference produced reduction in average tumour size and metastasis (189). These results justified our hypothesis that FABP5 is indeed a treatment target for CRPC. Although knockdown *FABP5* RNA is highly effective in inhibition of malignancy of CRPC cells (189), siRNA molecules are not ideal agents for treatment due to their instability even when dissolved in a stabilizing agent (atolecollagen) (216). Thus, for an effective suppression of FABP5 function *in vivo*, inhibitors capable of suppressing the biological activity of FABP5, rather than completely knockdown the gene, may be more realistic tools for CRPC suppression. In this section, we targeted the FABP5-related signalling pathway to treat CRPC cells *in vitro* and in mouse model by using the bio-inhibitor (dmrFABP5) and chemical synthetic inhibitor (SBFI26) to suppress the biological activity of FABP5 and to cut

off the FABP5-related signalling transduction chain in CRPC cells. This is an entirely novel experimental approach to treat CRPC and is completely different from current treatments that are based on androgen-blockade therapy.

4.2 Materials and Methods

4.2.1 Materials

Reagents are listed in Appendix A, Buffers in Appendix B and Equipment in Appendix C.

4.2.2 Methods

4.2.2.1 *In vitro* assays

4.2.2.1.1 Cell growth assay

4.2.2.1.1.1 Preparation of standard curve

PC3-M cells were grown to 60-80% in median flask and harvested as previously mentioned and suspended in RPMI complete culture medium. Cells were counted using a haemocytometer as previously outlined and were diluted to 5×10^5 cells /ml of culture medium. Twenty-four well plate was used to set up serial dilution of cells as follow: $5x10^5$/ml, 2.5×10^5/ml, 1×10^5/ml, 5×10^4/ml, 2.5×10^4/ml, 1.25×10^4/ml and 6.25×10^3/ml. After that, 200µl from each dilution was seeded into a 96-well plate in triplicate. Plate was incubated overnight at 37°C, 5% CO_2 and the cell growth of the standard curve was checked by MTT assay.

4.2.2.1.1.2 Measuring number of cells by MTT assay

The MTT [3-(4, 5-dimethylthiazol-2-yl)-2, 5-diphenyltetrazolium bromide] tetrazolium assay is built on the capacity of a mitochondrial dehydrogenase enzyme from viable cells to convert MTT into a purple coloured known as formazan crystals product which are accumulate in live cells. The purple crystals were liquefied by adding DMSO. When cells die, they lose the ability to convert MTT into formazan, therefore colour formation serves as a valuable marker of viable cells. The MTT stock solution is prepared in PBS at a final concentration of 5mg/ml and stored at 4°C. After

overnight incubation of cells, 50µl of MTT solution was added to each 96-well plate and incubated at 37°C, 5% CO2 for 4 hours. 200µl of MTT and culture medium was removed slowly and carefully to avoid cells being disturbed. 200µl of DMSO was added to each well and blank and incubated at 37°C for 10 minutes. The optical density (OD) of the cells was measured with a Multiscan plate reader at 570nm. The standard curve for PC3-M was made by plotting OD against the number of cells. The growth rate was measured against its own standard curve to get the number of the cells per well.

4.2.2.1.1.3 Effect of SBFI26 and dmrFABP5 on cell growth

The growth rate of PC3-M treated by SBFI26 and dmrFABP5 were checked using MTT assay. Firstly, the optimal dose for both compounds was measured by seeding PC3-M cells in a 96 well plates ($5x10^4$/well) in a complete medium in triplicate with positive control and blank and incubated overnight at 37°C, 5% CO_2. The cells were washed with PBS and treated with different doses of SBFI26 (25-150µM) and dmrFABP5 (5-70µM) and incubated for 24 hours at 37°C, 5% CO_2. The MTT solution was added and incubated at 37°C, 5% CO2 for 4 hours. The cells were subsequently solubilized using DMSO and OD was measured at 570nm. The growth rate was measured against its own standard curve to get the best dose which caused high cytotoxicity. Furthermore, the anti-proliferative effect of the best concentration for each inhibitor was determined after 6 days of treatment with respect to the vehicle control using same assay.

4.2.2.1.2 Cell migration assay (scratch assay)

Scratch assay is an efficient and cheap method to estimate cancer cell migration *in vitro*. This method is constructed on the observation time that a new artificial wound gap (scratch) on a confluent cell monolayer will move toward the gap to close the

scratch until new cell–cell contacts are established again. PC3-M cells were grown to 60-80% in median flask and harvested as previously mentioned and suspended in RPMI complete culture medium. The assay was carried out in 24 well plates. When the cells become confluent, 1ml pipette tip was used to scratch and cells were removed from discrete area to form a cell free zone and wells were washed two times with PBS. Complete medium was added to control PC3-M cells and PC3-M treated with 100µM SBFI26 inhibitor or 50µM dmrFABP5 and the wells were photographed using microscopy at 0, 12, and 24 hours after treatment. A marker was used to create a reference point near the scratch in each well and analysed the minimum distance in micro meters between the wound edges of the scratch area using Image J software. All experiments were performed in triplicate.

4.2.2.1.3 Soft agar colony formation assay

The soft agar assay is a technique usually used to assess cellular tumorigenicity *in vitro*. The assay was carried out in 6-well plates which were pre-coated with 2ml of 1% (w/v) low melting agarose in routine culture medium and the mixture was solidified in refrigerator for 10 minutes. PC3-M cells were grown to 60-80% in median flask and harvested as previously mentioned and suspended in RPMI complete culture medium. The control PC3-M cells and cultures treated with 50µM dmrFABP5 or 100µM SBFI26 were seeded in triplicates into 0.5% agar in routine culture medium on top of a bed of first layer at 5×10^4 cells per dish and placed in refrigerator for 10 minutes until solidified. The 6-well plates were placed in the incubator at 37°C, 5% CO2 for two weeks. After one week of incubation, approximately 200µl of medium alone or medium with dmrFABP5 or SBFI26 according to the treatment plan were added to the dishes to avoid drying out and to ensure the cells had sufficient nutrients and treatment. After 2 weeks of growing, plates were treated with MTT at a

concentration of 0.5mg/ml and incubated for 4 hours in the incubator at 37°C, 5% CO2. Colonies larger than 250µm in diameters were counted by the GelCount (Oxford Optronix, UK).

4.2.2.1.4 Cell invasion assay using Boyden chamber system

The Boyden Matrigel chamber assay provides the condition to measure the invasive property of cancer cells *in vitro*. This assay is based on a chamber of two different medium compartments separated by 8 micron-pore size membrane. In general, cancer cells are seeded in the upper compartment and allowed to transport to the lower compartment through a membrane pores response to the presence of a chemo-attractant agents. After an incubation time, the membrane is stained and the cells that have migrated to the lower part of the membrane are counted by using microscope. For invasion assay, after PC3-M cells were grown up to 60-80% in median flask, cells were put in starvation by adding serum-free medium for 24 hours in the incubator at 37°C, 5% CO2. The invasion chambers were left in room temperature and the membrane was rehydrated by adding 0.5ml of warm serum-free medium for 2h in the incubator at 37°C, 5% CO2. The control PC3-M cells and cultures treated with 50µM dmrFABP5 or 100µM SBFI26 were seeded in triplicates at a density of 2.5×10^4 cells per well in 0.5ml serum-free medium in the upper chamber and allowed to invade through the Matrigel using medium containing 10% FCS in the lower chamber as a chemo-attractant for 24h in the incubator at 37ºC with 5% CO2. After 24h, cells in the upper chamber were removed with a cotton swab and cells on the bottom surface of the filter stained with 2% Crystal Violate for 10 minutes and washed with plane water. Chambers were left in the incubator for 2 hours for drying and the number of the invaded cells was counted under microscope. Every sample was analysed in triplicate and migrated cells were counted in mean ±SE.

4.2.2.2 Nude mouse tumorigenicity and metastasis assay

4.2.2.2.1 Nude mouse orthotopic tumour models

4.2.2.2.1.1 Establishment of a PC3-M cell lines stably expressing the luciferase gene

4.2.2.2.1.1.1 Stable transfection of PC3-M cell lines

PC3-M cells (2×10^5) were seeded in a 6 well plate and grown overnight in complete culture medium to reach 60-80% confluency. In the meantime, 3.3µg of the *pGL4.50* [*luc2*/CMV/Hygro] vector (Promega) was added to total volume of 155µl Opti-MEM I medium (Gibco, Invitrogen, Paisley, UK). Then, 9.9µl of FuGENE HD reagent (Promega) was added and mixed carefully by pipetting (15 times). The mixture was incubated at RT for 10 minutes and added drop wise to the wells. The transfection mixture was distributed evenly by rocking the plate back and forth. After 48-hour incubation, cells were split into 9cm cell culture plate and cultured in selective medium containing 200µg/mL Hygromycin (InvivoGen) which has been changed every three days for two weeks. Unsuccessfully transfected cells were killed by Hygromycin while successfully transfected cells were survived.

4.2.2.2.1.1.2 Ring cloning of transfected cells

After two weeks of incubation with antibiotic, colony formation was observed. Medium was removed from the dish and the colonies were washed with PBS. Glass cloning cylinders (Sigma) were fixed around the colonies. To isolate colonies, 100µl trypsin/EDTA solution was added and incubated for 3-4 minutes or until the cells were rounded-up at 37°C. The detached cells were re-seeded in 24 well plates and the medium was changed next day. Cells were allowed to grow within a controlled atmosphere of 5%CO_2 at 37°C before they analysed for expression of luciferase.

4.2.2.2.1.1.3 *In vitro* identification of stably luciferase expressing PC3-M colonies

To select the best colony with the highest luciferase gene expression, PC3-M parental cells and 33 different colonies of PC3-M cell transfected with luciferase vector were seeded at 1×10^5 in 96-well plate in triplicate. After 24 hours, the medium was removed and replaced with fresh medium containing 150µg/mL D-luciferin (Promega). Cells were immediately imaged in the Varioskan Flash Reader (Thermo Scientific) for a minute exposure. The wells that showed the highest relative luminescent units (RLU) were deemed to be the most highly expressing cells and were chosen as the colonies to take through into further *in vitro* check. To confirm that the luminescence intensity was associated with the number of cells, serial dilutions were performed on the PC3-M parental cells and three PC3-M luciferase expression cells at concentrations ranging from 20-100000 cells in black 96-well plate in duplicate. After overnight incubation, a fresh medium containing 150µg/mL D-luciferin was added and the plate was image for a minute by using IVIS imaging system (Perkin Elmer). The bioluminescent intensity was quantified as Total Flux (photons/second).

4.2.2.2.1.2 Surgical orthotopic implantation of PC3-M-*luc* cells

Before operation, (8-10 weeks old) Balb/c male nude mice (Charles River, UK) were analgised with Novalgin and then constantly anaesthetised with isofluorane during the operation. The mouse was placed in a supine position and immobilized using surgical adhesive tape. The lower abdomen was disinfected by 10% povidone-iodine and (1-1.5cm) midline skin and peritoneal incision approximately 1.5cm superior to the external genitalia was made using scissors. The urinary bladder was lifted as a yellow-light spherical organ and externalized using tissue forceps. Two distinct lobes of prostate gland (left and right) were located directly beneath the bladder. Suspension of

PC3-M-*luc* Cells (5×10^5) in 30µL PBS were injected orthotopically into the prostate gland and small bubble was observed in the prostate, as described previously (244). The peritoneum and skin were sutured with two layers using 6.0 absorbable vicryl monofilament. Post operationally, the mouse was subcutaneously analgised with Novalgin **(Fig. 4.1)**. In all mice, the same surgical conditions were preferred.

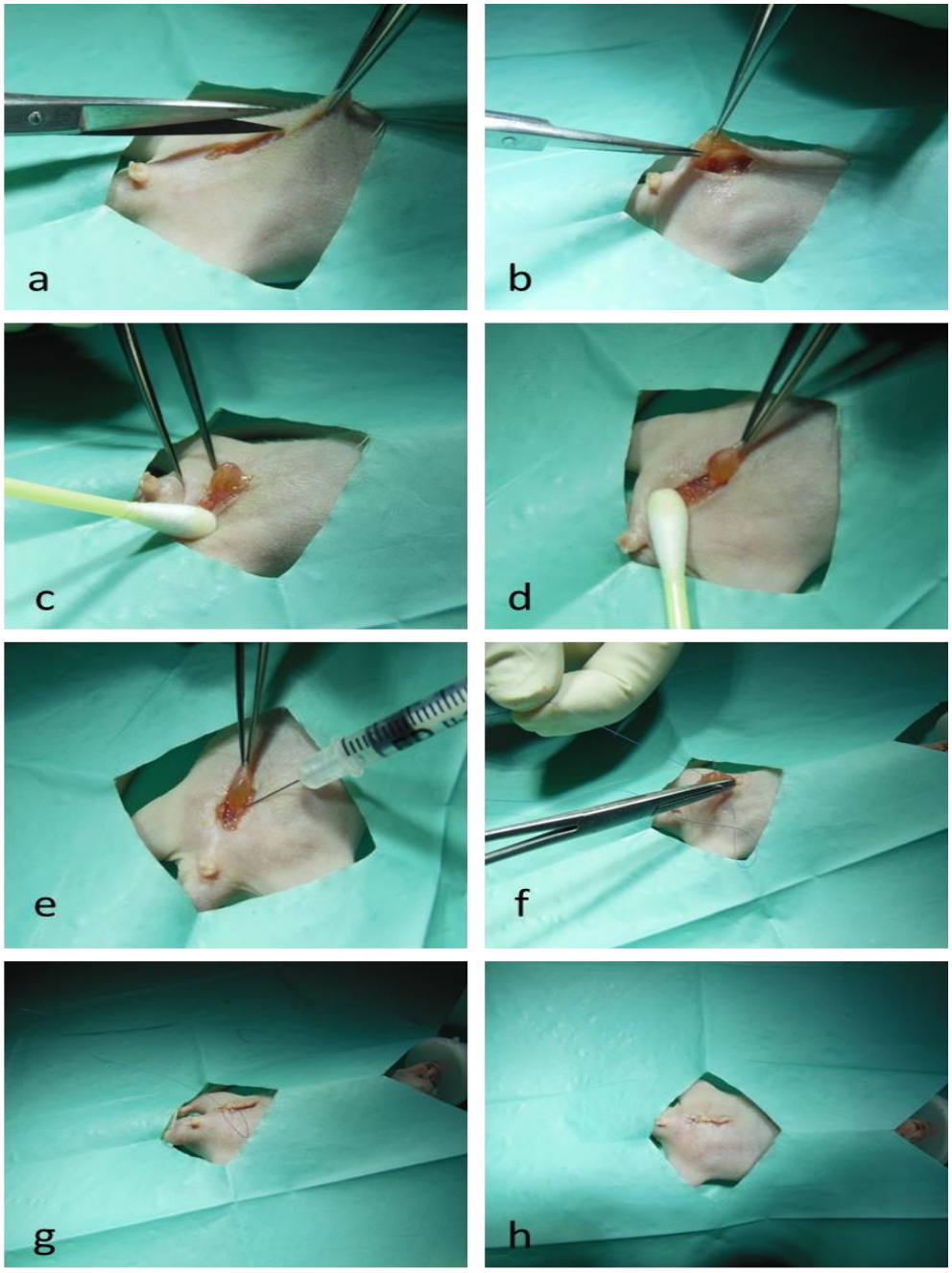

Figure 4.1 Orthotopic implantation of prostate cancer cells. a. Midline incision above the external genitalia. **b.** Midline incision in the peritoneal cavity. **c.** Light press on both sides of incision to protrude urinary bladder. **d.** Exteriorization of urinary bladder. **e.** Injection of cancer cells into one lobe of prostate gland. **f.** Suturing the peritoneal cavity using simple continuous suture method. **g.** Skin suturing using subcuticular suture method. **h.** End of the surgical operation

4.2.2.2.2 Experimental treatment of mice

One week after orthotopic implantation of PC3-M-*luc* cells, tumour bearing mice were divided into 4 groups (8 each) and subjected to following intraperitoneal injections: 1) control with PBS; 2) SBFI26, 1mg/kg; 3) dmrFABP5, 20μg/kg; 4) 1mg/kg SBFI26 plus 20μg/kg dmrFABP5. Injections were repeated every two days for 25 days.

4.2.2.2.3 Bioluminescence imaging of mice

Mice were imaged using IVIS imaging system (Perkin Elmer). 15mg/ml potassium D-luciferin (Promega) was dissolved in PBS and filtered through a 0.2μm filter. All mice were anesthetized with isoflurane and injected subcutaneously with 150mg/kg D-luciferin and imaged 15 minutes from injection. Tumour loci were monitored weekly using the IVIS after injection with D-luciferin. In the IVIS imaging chamber, mice were remained sedated with isoflurane administrated through nasal cones. After acquiring photographic images of mice, bioluminescent images were acquired with auto exposure time. The bioluminescent images were normally superimposed by the IVIS Living Image Software (Xenogen) and the measurements were based on total photons/second (p/s) within separate defined region of interest (ROI). ROI was manually drawn over the hull animal to assess the signal intensity emitted. Animal study was performed in accordance with UKCCCR guidelines under the Home Office Project License PPL40/2963.

4.2.2.3 Histological experiments and staining

4.2.2.3.1 Dissection of mice tissues

To check the metastasis of tumour in mice, samples of the livers and lungs were removed from the mice and fixed in 10% neutral buffered formalin (NBF) at least for 24 hours before processed routinely for histological examination.

4.2.2.3.2 Embedding in paraffin wax and sectioning

The fixed tissue samples were trimmed and placed within an embedding cassette and processed on a Tissue processor. Processed tissues were then embedded in paraffin wax at 60°C and cooled on iced plat. After solidification, the blocks were sectioned on a Microm HM355 microtome using a microtome knife containing a stainless steel disposal blade. Sections were cut to 4µm thickness and placed on 3-aminopropyl triethoxy-saline (APES) coated Superfrost microscope slides and incubated at 37°C overnight prior to processing with Haematoxylin and Eosin.

4.2.2.3.3 Haematoxylin and Eosin (H/E) staining of tissue sections

Paraffin-embedded tissue sections were deparaffinised and rehydrated in two-times xylene and a decreasing alcohol series (2×100%, 2×95% and 2×80% ethanol). The sections were stained in haematoxylin for 3-5 minutes and in eosin for 20 seconds, dehydrated in an alcohol series (2×80%, 2×95% and 2×100% ethanol) and rehydrated in two-times xylene before Coverslip slide were fixed by using Permount (xylene based).

4.2.2.4 Statistical analysis

For all the results in this work, Student's *t*-test and Fisher's Exact test were carried out using GraphPad Prism software to compare the differences of the means between control and experimental groups. All *in vitro* experiments were conducted in triplicate and repeated at least three times. The difference is regarded as significant when $p<0.05$; in the results, p value is represented by asterisks as follows: *, $P < 0.05$; **, $P < 0.001$; ***, $P < 0.0001$.

4.3 Results

4.3.1 Inhibitory effect of SBFI26 and dmrFABP5 on malignant characteristics of PC3-M cells *in vitro*

4.3.1.1 Effect of SBFI26 and dmrFABP5 on PC3-M cell growth

MTT assay was conducted to test the inhibitory effect of SBFI26 and dmrFABP5 on PC3-M cell growth *in vitro*. PC3-M cells standard growing curve, established as described in methods, was shown in **Fig. 4.2.**

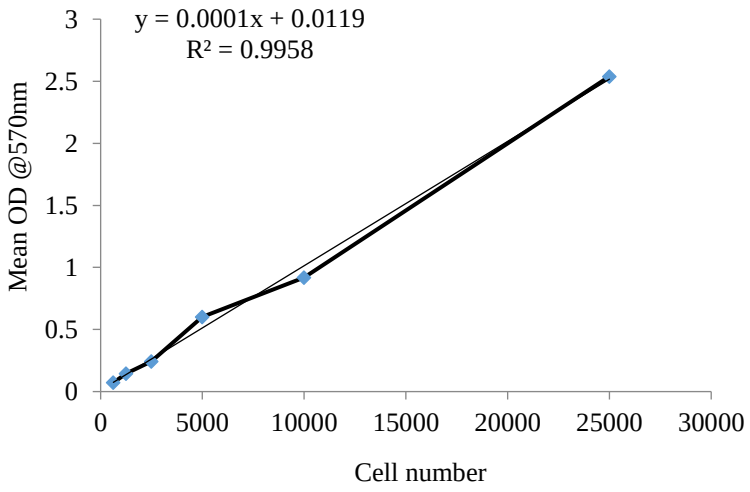

Figure 4.2 Standard curve of PC3-M cell lines. Using linear regression analysis, standard curve was established for the PC3-M cells by plotting absorbance (OD at 570 nm) (Y axis) against the cell numbers (X axis). The linear regression of the standard curve is presented in the figure and R=0.99. The numbers of cells were obtained by relating the OD values to the standard curve.

Cytotoxicity tests showed that treatment with either SBFI26 or dmrFABP5 significantly suppressed growth of PC3-M cells in a concentration-dependent pattern as compared to untreated cells. Maximum suppression was produced at 100μM for SBFI26 by 26% (Student's *t* test, $P < 0.001$); further increase in doses did not produce

any further significant suppression **(Fig. 4.3)**. Similarly, PC3-M cells were sensitive to treatment with dmrFABP5 and the Maximum suppression was found at 50µM for dmrFABP5 by 35% (Student's *t* test, $P < 0.001$); more increase in doses did not produce any further significant suppression **(Fig. 4.4)**.

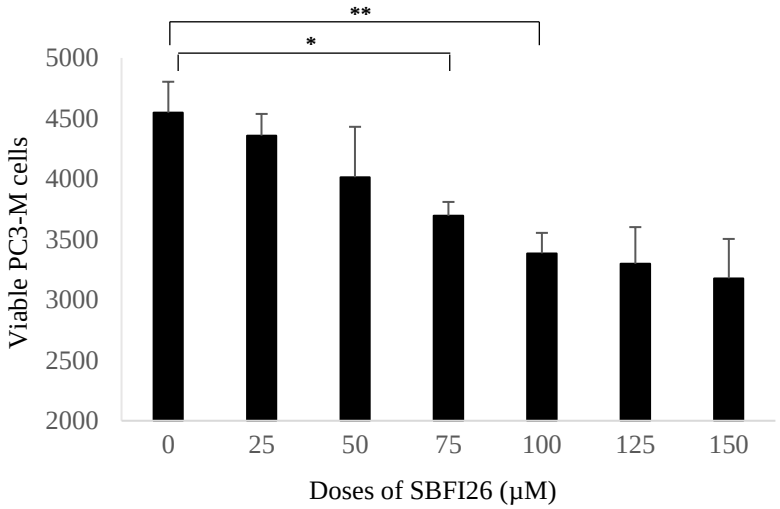

Figure 4.3 Determination of the optimal inhibitory concentration of SBFI26 on PC3-M cells. MTT assay was performed to measure the viable PC3-M cell numbers of the control (untreated) and those treated with different concentrations of SBFI26 (25-150µm) for 24h. Results were obtained from three separate measurements (mean ± SE).

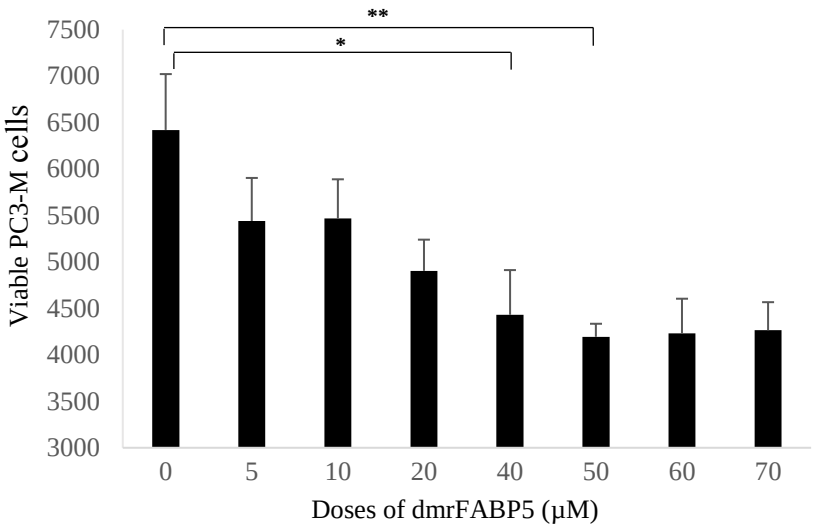

Figure 4.4 Determination of the optimal inhibitory concentration of dmrFABP5 on PC3-M cells. MTT assay was performed to measure the viable PC3-M cell numbers of the control (untreated) and those treated with different concentrations of dmrFABP5 for 24h. Results were obtained from three separate measurements (mean ± SE).

In addition, the inhibitory effect of 100µM SBFI26 or 50µM dmrFABP5 on proliferation of PC3-M cells was assessed over one-week experimental period by using MTT assay. The results showed that 100µM SBFI26 significantly reduced the proliferation rate of PC3-M cells at the end of the 7th day by 17-times (1667.6 ± 50.7) as compared to PC3-M cells without treatment (28290.6 ± 2068.6) (Student's *t* test, *P < 0.0001*) **(Fig. 4.5)**. 50µM dmrFABP5 reduced the proliferation rate of PC3-M cells at the end of the 6th day to 6414.3± 583.4; whereas in PC3-M cells without treatment was increased to 30046.6 ± 452.9. This dose significantly reduced the proliferation rate of PC3-M cells 4.7-times (Student's *t* test, *P < 0.0001*) **(Fig. 4.6)**.

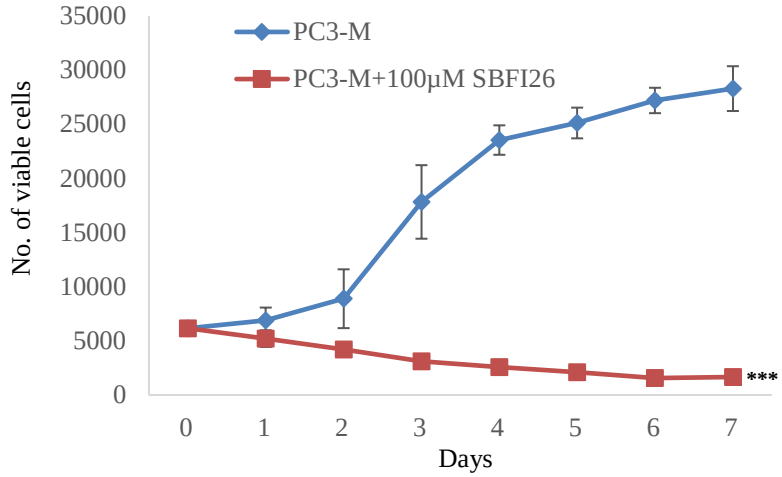

Figure 4.5 Inhibitory effect of 100µM SBFI26 on growth of PC3-M cells over the 7day experimental period. Results were obtained from three separate measurements (mean ± SE) and the differences between the control and the treatment was assessed at the last day by 2-tailed unpaired Student's *t* test. ***, *P < 0.0001*.

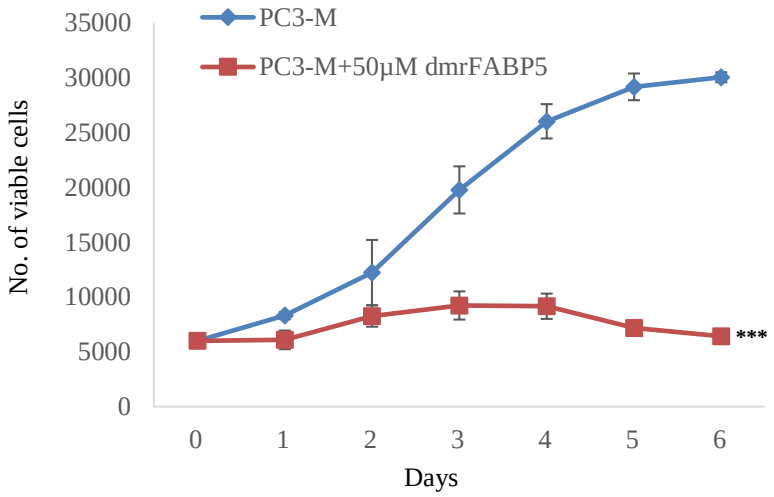

Figure 4.6 Inhibitory effect of 50µM dmrFABP5 on growth of PC3-M cells over the 6day experimental period. Results were obtained from three separate measurements (mean ± SE) and the differences between the control and treatment was assessed at the last day by 2-tailed unpaired Student's *t* test. ***, *P < 0.0001*.

4.3.1.2 Effect of SBFI26 and dmrFABP5 on migration of PC3-M cancer cells

To assess the effects of 100µM SBFI26 and 50µM dmrFABP5 on metastatic potential of PC3-M cells, cell migration was evaluated using wound healing assay. PC3-M cells were grown in 24-well plates to form a monolayer. Scratches were made using 1 mL sterile pipette tip. Cell migration capacity was measured by the reduction in wound size in control (untreated) and in cultures treated with 100µM SBFI26 or 50µM dmrFABP5, respectively. The photos were taken at 0, 12 and 24 hours, respectively, after treatment **(Fig. 4.7)**. Treatments with 100µM SBFI26 and 50µM dmrFABP5 produced only 19% and 21% reduction in wound sizes, respectively in 24h. These treatments significantly suppressed the migration rates of PC3-M cells (Student's *t* test, $p < 0.0001$), leading only to small changes in wound gaps for treated groups compared to an almost complete gap closure (94%) for the control (**Fig. 4.8)**.

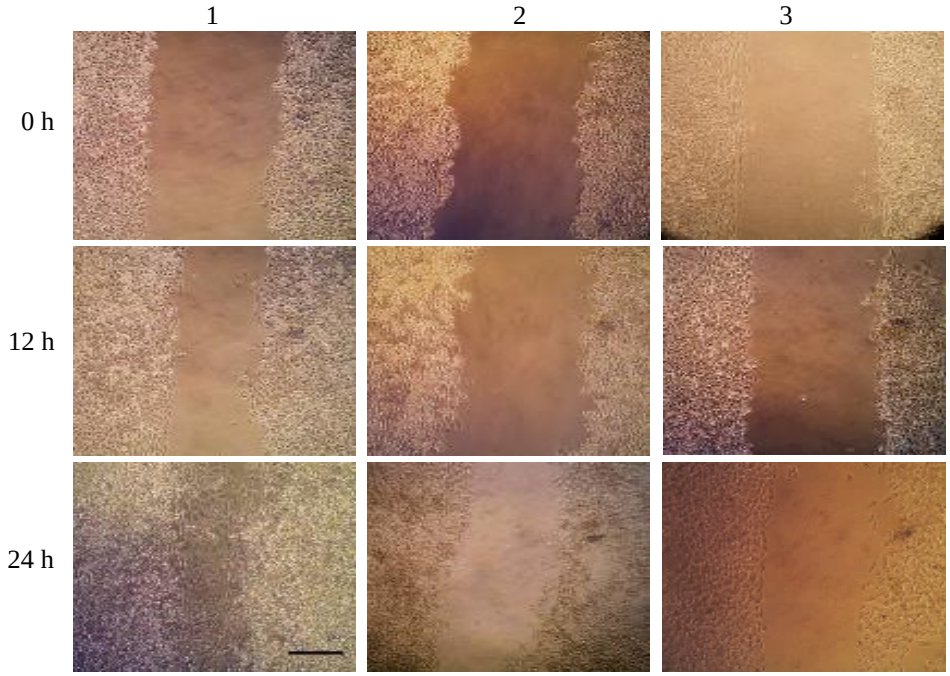

Figure 4.7 Representative photos of the wound healing assay. Cell migration capacity was measured by the reduction in wound size in control (1) and in cultures treated with 100µM SBFI26 (2) or 50µM dmrFABP5 (3) isolated at 0, 12 and 24 hours after treatment. Scale bar is 250µm.

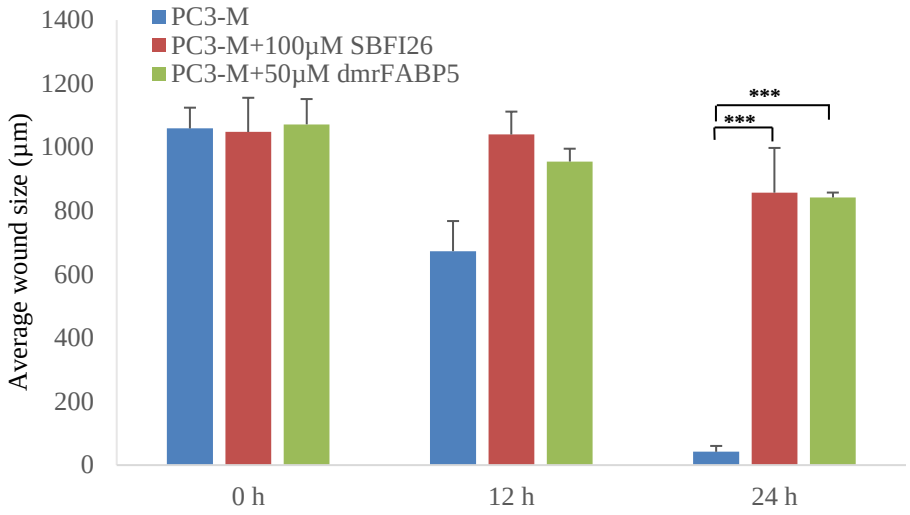

Figure 4.8 Average wound sizes (µm) of the control PC3-M and cultures treated groups. Average wound sizes (µm) of the control PC3-M and cultures treated with 100µM SBFI26 and 50µM dmrFABP5 isolated at 0, 12 and 24 hours after treatment. Data was collected by measuring image of the wound space and analysed by ImageJ software (National Institutes of Health). Results were obtained from three separate measurements (mean ± SE).

4.3.1.3 Effect of SBFI26 and dmrFABP5 on invasiveness of PC3-M cancer cells

The effect of SBFI26 and dmrFABP5 on invasiveness of PC3-M cancer cells was assessed using BD Matrigel coated invasion chambers. PC3-M cells in an active growth phase with confluency less than 80% were maintained in serum-free RPMI 1640 medium for 24 hours prior to setting up the invasion assay. After 24h starvation, cells were harvested and counted to prepare a mixture containing 5×10^4 cells in serum-free medium. Chambers were rehydrated for 2 hours before 2.5×10^4 cells in 0.5ml medium with inhibitors were loaded into every upper compartment of chambers. Routine medium (with 10% (v/v) FCS) was placed in lower compartments. Cell lines were set as triplicate and assay was run in a humidified tissue culture incubator for 24 hours. Finally, remaining cells in upper part were removed by gently using cotton

swabs and washed with PBS. Migrated cells were fixed and stained using 2% crystal violet for 10 minutes and counted in different random fields-of-view (5mm) using light microscope. Mean number of invaded cells from the control and the PC3-M cells treated with SBFI26 and dmrFABP5 were 22 ± 3, 1 ± 1 and 2 ± 1, respectively, representing significant suppressions of invasion by 95.5% and 91%, respectively (Student's *t* test, $P < 0.0001$) (**Fig. 4.9, A** and **B)**.

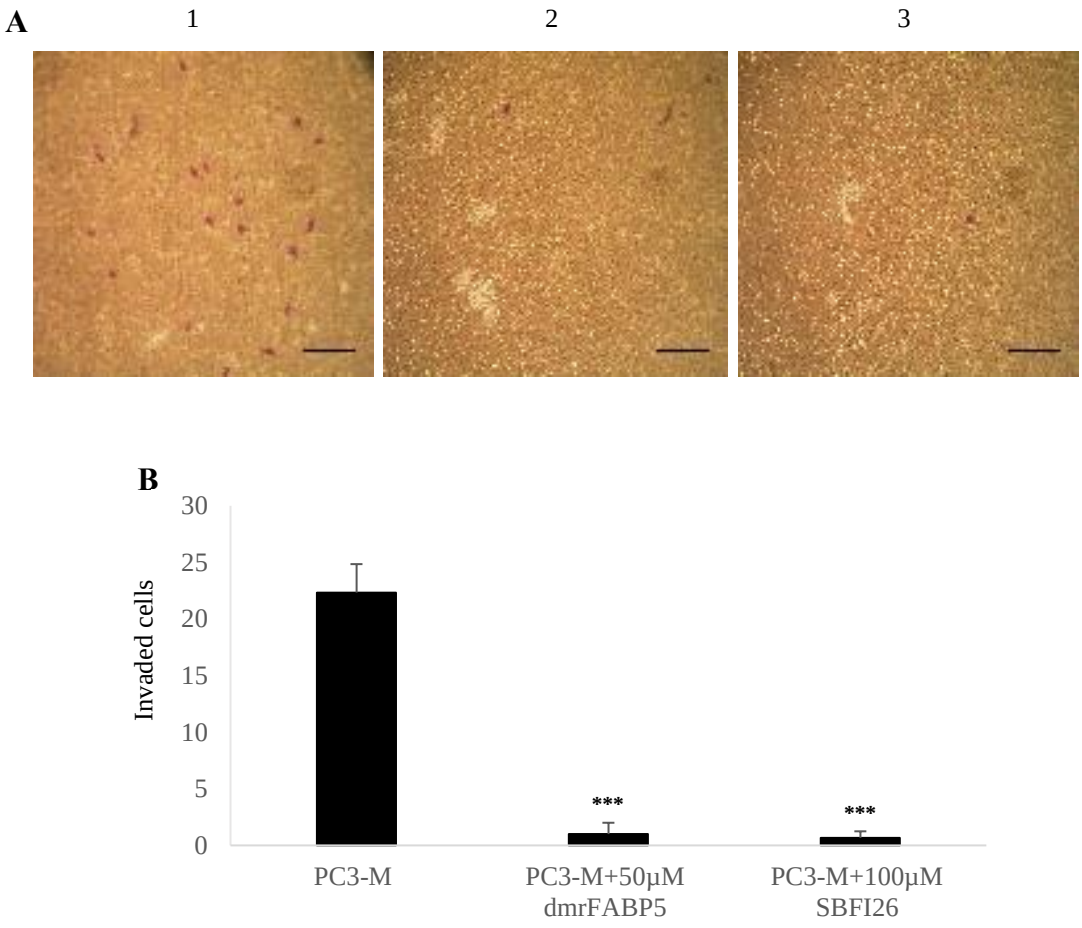

Figure 4.9 The impact of dmrFABP5 or SBFI26 on invasiveness of PC3-M cells. A, Representative fields-of-view (5mm) of invasion assay; Number of invading cells from the control PC3-M cells (1) and cultures treated with 50µM dmrFABP5 (2) or 100µM SBFI26 (3) for 24h after different treatments. Scale bar is 250µm. **B,** Number of invaded cells per field (5mm) in invasion assay. Results were obtained from three separate measurements (mean ± SE).

4.3.1.4 Effect of SBFI26 and dmrFABP5 on anchorage-independent growth of PC3-M cancer cells

To investigate the effect of SBFI26 and dmrFABP5 on tumorigenicity of PC3-M cells, their anchorage-independent growth in the soft agar were assessed. PC3-M cells, PC3-M cells treated with 50µM dmrFABP5 or 100µM SBFI26 were seeded in triplicates into 0.5% agar in routine culture medium on top of a bed of first layer at 5×10^4 cells per dish. After 1 week of incubation, approximately 200µl of medium alone or medium with dmrFABP5 or SBFI26 according to treatment were added to the dishes to avoid drying out and to ensure the cells had sufficient nutrients and treatment. Assay was set as triplicate and cells were grown for 2 weeks. Colonies were stained by adding 0.5ml of 2% MTT for 4 hours. Colonies larger than 250µm were counted using Gel Count. The soft agar showed that the number of colonies formed after 2 weeks by control PC3-M cells, PC3-M cells treated with dmrFABP5 or with SBFI26 were 124 ± 18, 27 ± 2, or 0, respectively, representing significant inhibitions by 78% and 100%, respectively, in comparison to control cells (Student's *t* test, $p < 0.0001$) **(Fig. 4.10, A** and **B)**.

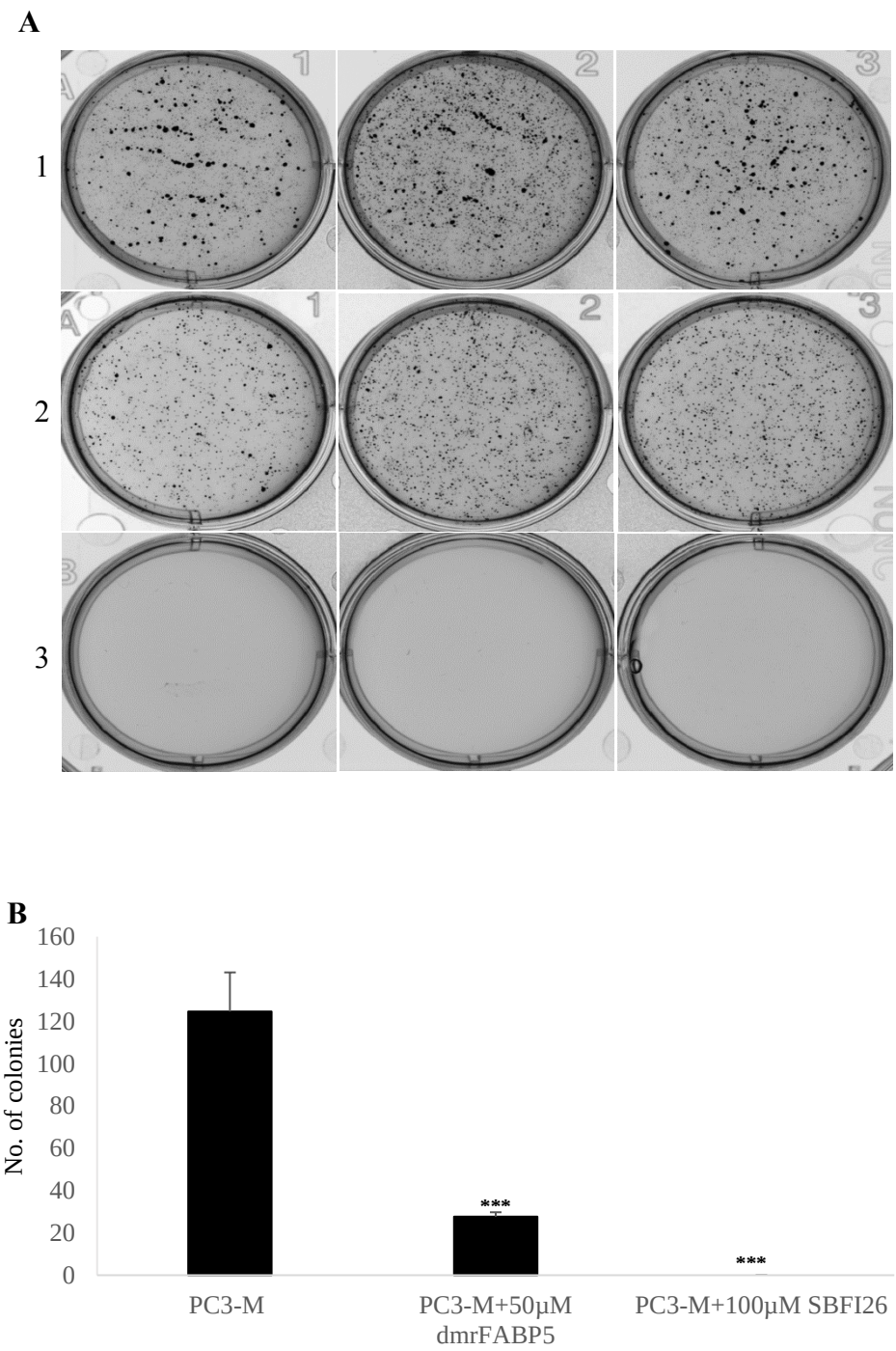

Figure 4.10 The impact of dmrFABP5 or SBFI26 on the anchorage-independent growth of PC3-M cells. A, Representative plates of soft agar colony formation with the control PC3-M cells (1) and cultures treated with 50µM dmrFABP5 (2) or 100µM SBFI26 (3). **B,** Colony counts of different treatments; Results (mean ±SE) are obtained from three separate plates in each treatment.

4.3.2 Effect of SBFI26 and dmrFABP5 on tumourigenicity and metastatic ability of PC3-M cells in mouse prostate gland

4.3.2.1 Establishment of stable PC3-M cells expressing strong bioluminescence signals

PC3-M cells were transfected with the *pGL4.50* [*luc2*/CMV/Hygro] vector using FuGene HD transfection reagent. After 48-hour incubation, cells were split into 9cm cell culture plate (petri dish) and continued to grow with selective medium containing 200μg/mL Hygromycin which has been changed every three days for two weeks. Single clones were appeared and visualized with naked eye. Then, using ring cloning method, thirty-three single colonies of PC3-M cells transfectants with *pGL4.50* were picked up and transferred onto a 24 well plates. The medium was changed next day and colonies were grown in normal cell culture conditions. To select the best colony with the highest luciferase gene expression, PC3-M parental cells and 33 different colonies of transfected PC3-M cell were imaged using Varioskan Flash Reader after adding fresh medium containing D-luciferin. The results showed that 2 transfectant colonies generated high luminescence signals and named PC3-M-Luc8 and 21 **(Fig. 4.11)**. The wells that showed the highest relative luminescent units were deemed to be the most highly expressing cells and were chosen as the colonies to take through into further *in vitro* check. To confirm that the luminescence intensity was associated with the number of cells, serial dilutions were performed on the PC3-M parental cells and three PC3-M luciferase expression cells. After overnight incubation, a fresh medium containing D-luciferin was added and the plate was image for minute by using an IVIS imaging system. The results showed that PC3-M-Luc8 produced the highest level of bioluminescence signal (**Fig. 4.12, A)** and there was a correlation between total flux and the number of labelled cells (R2 =0.98) **(Fig. 4.12, B)**.

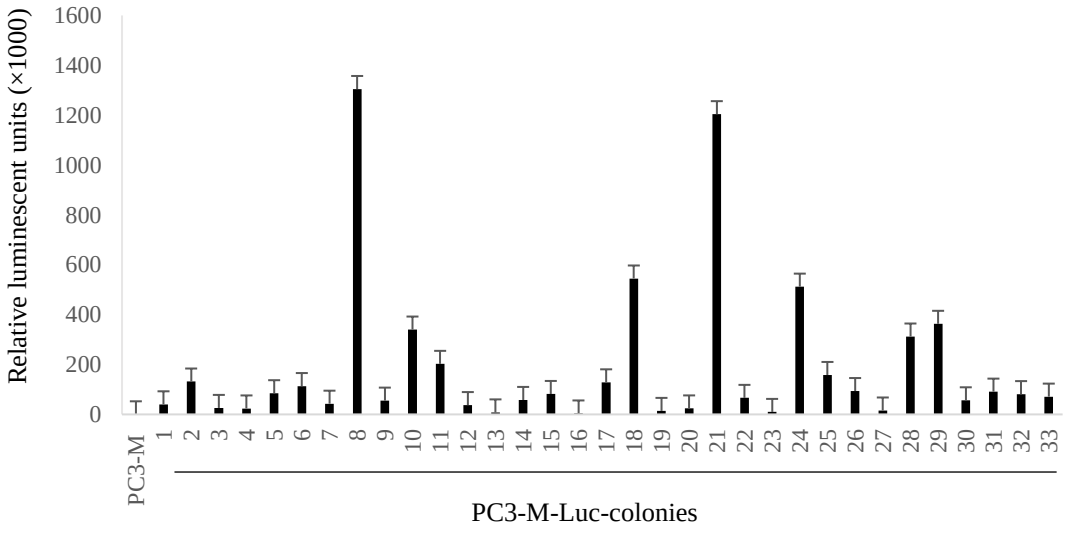

Figure 4.11 Establishment of stable PC3-M colonies expressing strong bioluminescence signals. Relative luminescent units (mean ±SE) of the PC3-M parental cells and 33 colonies derived from PC3-M cells were obtained from 3 separate measurements.

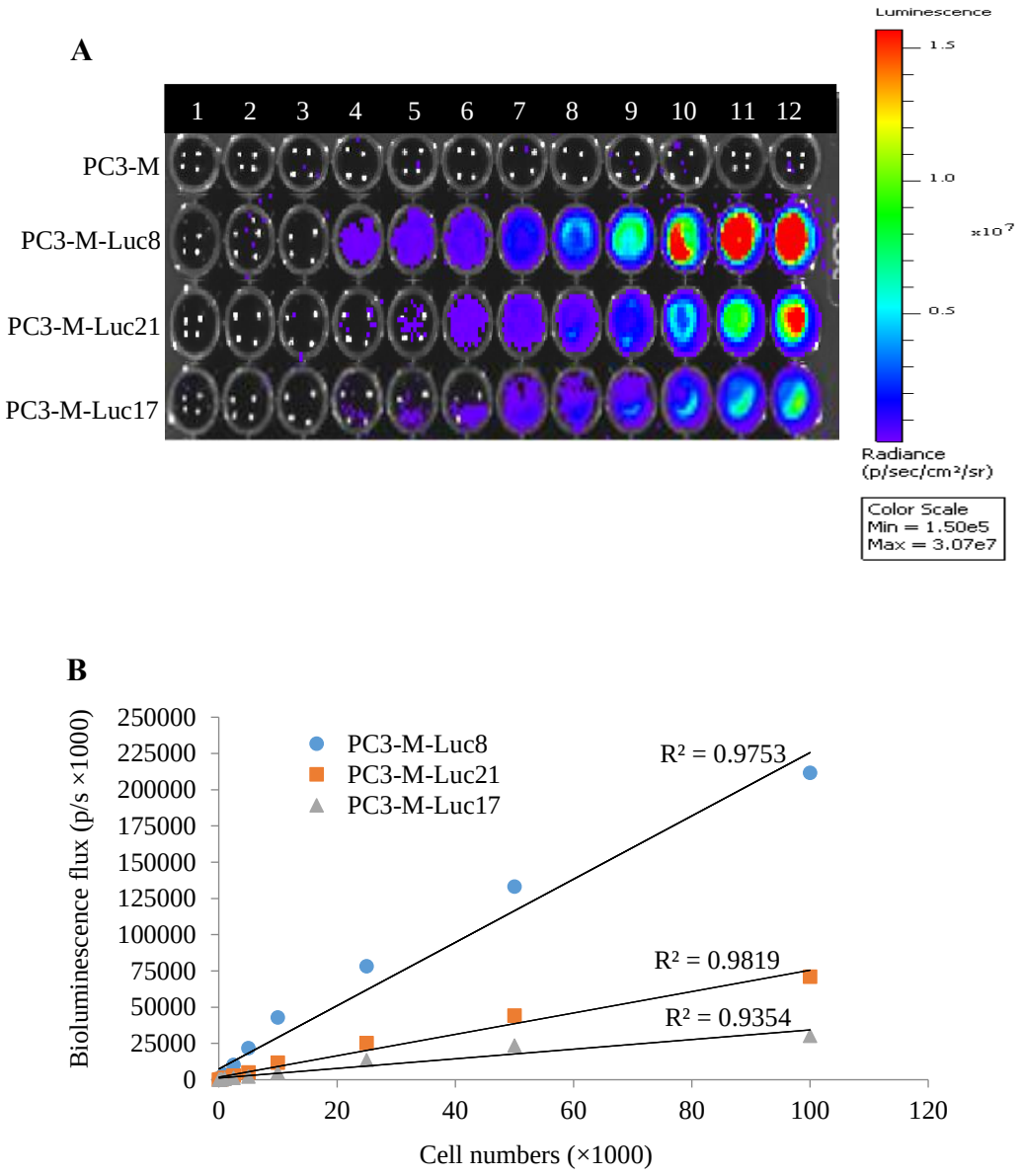

Figure 4.12 The intensities of the bioluminescence images of the serially-diluted PC3-M cells and 3 representative PC3M-Luc transfectants by IVIS. A, Detailed observation of the intensities of the bioluminescence images of the serially-diluted (20-100000) parental PC3-M cells and 3 representative PC3M-Luc transfectants. The colour bar on the right indicates the signal intensity range (photons/second/cm2). **B,** Correlation between the bioluminescence flux intensity (photons/second) and the number of cells derived from 3 different PC3-M-Luc colonies.

4.3.2.2 Inhibitory effect of SBFI26 and dmrFABP5 on tumorigenicity and metastatic ability of PC3-M cells implanted orthotopically into the nude mouse prostate gland.

Luciferase-labelled PC3-M-Luc8 Cells (5×10^5) were suspended in 30µL PBS and orthotopically implanted into the dorsal prostate of male Balb/c nude mice. One week later, tumour-bearing mice were divided into 4 groups (8 each) and subjected to the following intraperitoneally injections: 1) control with PBS, 2) SBFI26 (1mg/kg), 3) dmrFABP5 (20µg/kg), 4) SBFI26 plus dmrFABP5. Injections were repeated every two days for 25 days and the metastatic loci were monitored weekly using the IVIS after mice were subcutaneously injected with D-luciferin. At day 25, there was a massive decrease in bioluminescence signal (p/sec/cm2) in SBFI26 (6.66×10^8), dmrFABP5 (2.53×10^8) and combination of SBFI26, dmrFABP5 (3.67×10^8) groups, compared with control (31.5×10^8). On the basis of bioluminescence, our results showed about 4.9, 13 and 9-fold suppression in tumour mass by SBFI26, dmrFABP5 and a combination of both over those of control group (Student's *t* test, $P < 0.0001$) **(Fig. 4.13)**.

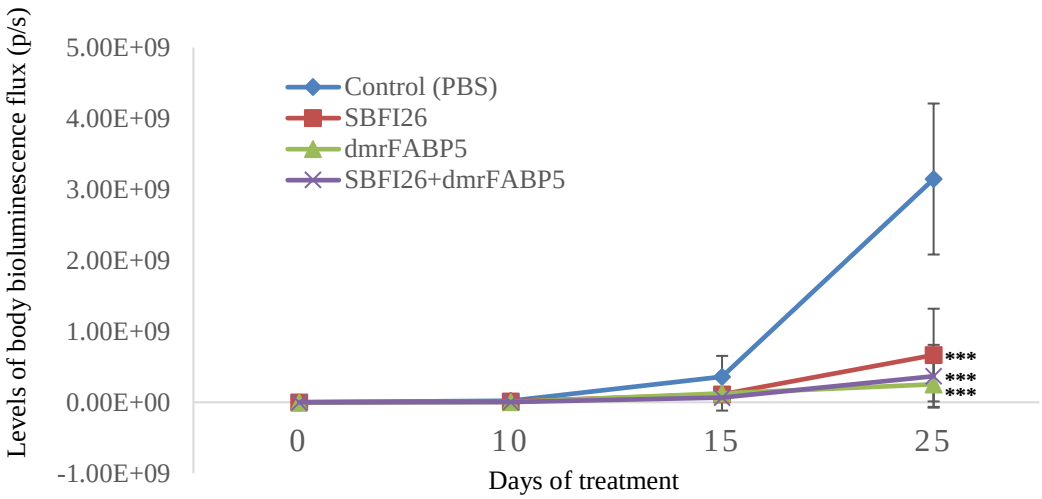

Figure 4.13 Whole body tumour bioluminescence flux produced by each group of nude mice after orthotopic implantation of luciferase-labelled PC3-M cells and different treatments for 25 days. Values were normalised to day 0. Values were plotted as mean ± SE (error bars) (n = 8); the difference between the control and each of the testing groups was assessed by two-tailed unpaired Student's *t* test ***, $P < 0.0001$.

In the control group, 7/7 (100%) mice produced metastases. In the group treated with SBFI26, 4/8 (50%) of mice produced visceral metastasis. In groups treated with dmrFABP5 and a combination of SBFI26 and dmrFABP5, no mice with metastases were detected, significant suppressions in metastasis was seen when compared to the control group (Fisher's Exact test, $P < 0.05$) **(Fig. 4.14, A** and **B)**. Histological staining showed that all mice developed metastases in the control group, mainly in the liver and lung. In the SBFI26 treated group, half of the mice developed liver metastases; none were found in groups treated with either dmrFABP5 or a combination of SBFI26 and dmrFABP5. One representative stained slide from each group/organ is shown in **(Fig. 4.15)**.

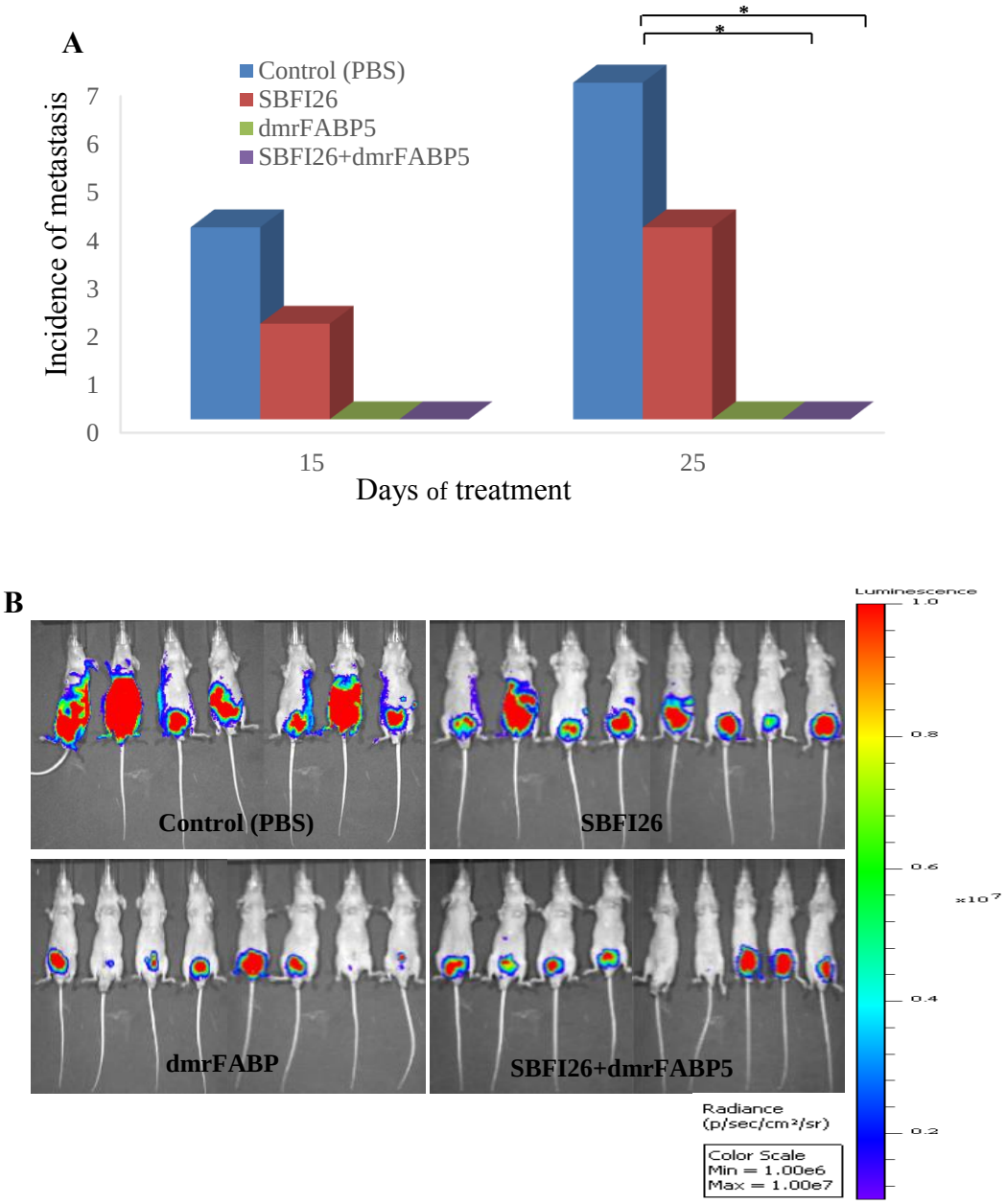

Figure 4.14 Inhibitory effect of SBFI26 and dmrFABP5 on tumorigenicity and metastatic ability of PC3-M cells implanted orthotopically in mice. A, Numbers of mice developed 1 or more metastases (or metastasis incidence, detected by bioluminescence signal) in the control and experimental groups, 15 and 25 days after treatment. The difference between the control and each of the experimental groups was assessed by 2-tailed Fisher's Exact test *, $P < 0.05$. **B,** Ventral bioluminescence images of primary tumours and metastases in all 4 groups of experimental mice 25 days after treatment. The colour bar on the right indicates the signal intensity range (photons/second/cm2).

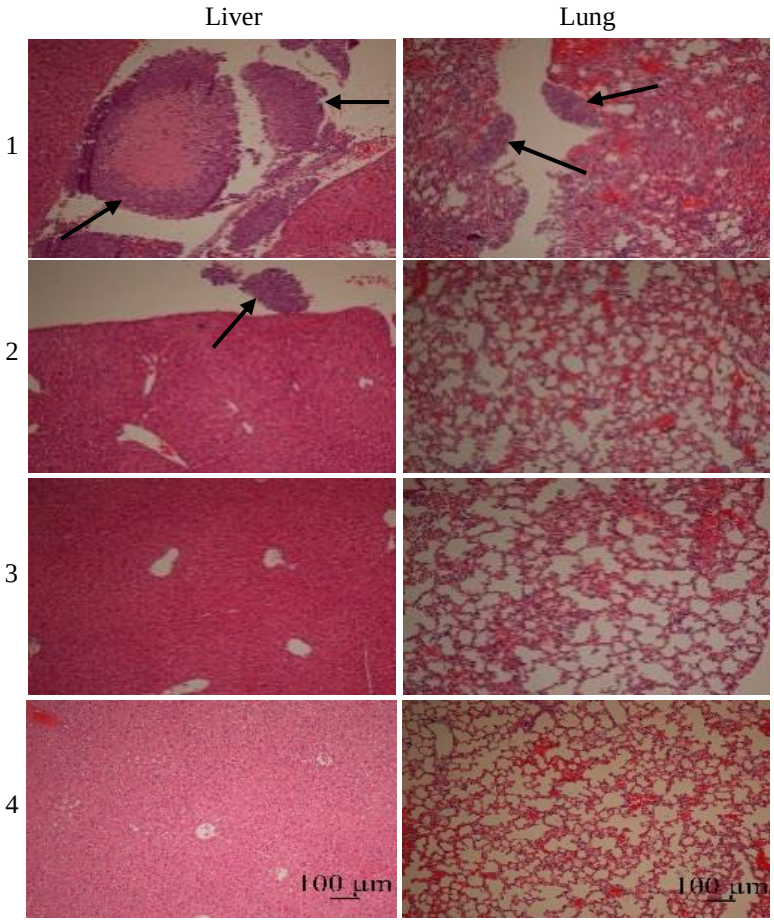

Figure 4.15 Representative photomicrographs of detection of liver and lung metastases. Representative photomicrographs of detection of liver and lung metastases (arrows) from mice which received injection of PBS (1), SBFI26 (2), dmrFABP5 (3) and combination of SBFI26 and dmrFABP5 (4). Sections of tissues were stained with H&E. Scale bar is 100µm.

4.4 Discussion

Androgen-independent prostate cancer cell line PC3-M (CRPC cells), expressing high levels of FABP5 and PPARγ, was an extremely malignant and metastatic cell line (217,245,246). When the biological function of FABP5 in the PC3-M CRPC cells was inhibited using SBFI26, significant anti-proliferation (by 17-time) **(Fig. 4.5)**, anti-invasive (by 95%) **(Fig. 4.9)**, anti-migration (by 81%) **(Fig. 4.8)** and anti-anchorage-independent growth (by 100%) **(Fig. 4.10)** were observed as compared to the control group. In addition, the effect of dmrFABP5 in the PC3-M cells was also tested. DmrFABP5 produced highly significant suppression of PC3-M cellular proliferation (by 4.7-time) **(Fig. 4.6)**, invasiveness (by 91%) **(Fig. 4.9)**, migration (by 97%) **(Fig. 4.8)** and colony formation (by 78%) **(Fig. 4.10)** *in vitro* as compared to the control group. This results were confirmed by three separate experiment (mean ± SE).

We tested whether suppressing FABP5 biological function could inhibit the growth of PC3-M CRPC cells *in vitro*. In PC3-M cells, SBFI26 and dmrFABP5 inhibited growth in a dose-dependent manner with optimal doses of 100 and 50μM respectively. Our results indicate that both SBFI26 and dmrFABP5 at concentrations >100 and >50 μM, respectively, are able to significantly inhibit PC3-M cells growth (Student's *t* test, $P < 0.001$). In the current study, we demonstrate the inhibitory effects of 100μM SBFI26 and 50μM dmrFABP5 on the proliferation of PC3-M cells *in vitro*. The results show that SBFI26 and 50μM dmrFABP5 each significantly suppressed the proliferation of human PC3-M cells after 1 week treatment (Student's *t* test, $P < 0.0001$). Interestingly, the results show that SBFI26 reduced the proliferation of human PC3-M cells below the initial density which indicated the cytotoxic effect. However, dmrFABP5 approximately kept the proliferation of PC3-M cells at the same as the initial density which indicated the cytostatic effect.

The major fatal event in cancerous disease is the metastasis, whereby, the cancer cells disseminate themselves from the primary site to the secondary site of the body. The effects of both inhibitors on migration and invasiveness of PC3-M cells were conducted **(Fig. 4.8) (Fig. 4.9)**. When cells were treated with SBFI26 or dmrFABP5 at concentrations of 100 or 50µM, significant differences were observed on the migration and invasiveness of PC3-M cells between treated and untreated cells (Student's *t* test, $P < 0.0001$). It was observed that the lack of migration and invasion of PC3-M cells treated with SBFI26 was due to cell death after 24-hour incubation **(Fig. 4.5)**. However, the lack of migration and invasion of PC3-M cells treated with dmrFABP5 may be due to loss of the proliferative activities after 24-hour incubation **(Fig. 4.6)**.

In line with these, SBFI26 as a lead inhibitor of FABP5 showed efficient anti-tumour roles in the mouse model for primary tumours implanted in the prostate gland (by 4.9-fold) (Student's *t* test, $P < 0.0001$) **(Fig. 4.13)**. Compared to the control group, in which all mice (100%) developed metastases, SBFI26 treatment suppressed metastases in half of the mice of the treated group (50%) **(Fig. 4.14)**. These results suggest that SBFI26 can be used as an anti-tumour agent to treat CRPC, which reduced the primary tumours by 4.9-times and suppressed the metastases by 50% in the experimental period.

In this study, the effect of dmrFABP5 was also tested. Here for the first time, we showed that dmrFABP5 has a dominant negative effect on tumorigenicity and metastatic ability of human PC3-M cells by suppressing the biological activity of FABP5. When tested in nude mice, dmrFABP5 was highly effective in suppressing the primary tumour growing in the prostate gland. Thus dmrFABP5 produced a 13-fold reduction in tumour mass in the prostate gland (Student's *t* test, $P < 0.0001$) **(Fig.**

4.13). Most importantly, dmrFABP5 produced a 100% suppression of metastasis in mice with CRPC cells implanted into the prostate gland (Fisher's Exact test, $P < 0.05$) **(Fig. 4.14)**.

Compared to SBFI26, the suppressive effect of dmrFABP5 was 2.7-fold higher in tumours growing in the prostate gland **(Fig. 4.13)**. Whilst, the suppression effect of dmrFABP5 on metastasis was 2 times that of SBFI26 **(Fig. 4.14)**. These results suggest that although both SBFI26 and dmrFABP5 are potent inhibitors, the suppression effect of dmrFABP5 is much stronger than that of SBFI26.

.

Chapter Five

The molecular mechanisms involved in the inhibitory effect of SBFI26 and dmrFABP5 on malignant progression of the CRPC cells

5.1 Introduction

Recently, it was confirmed that the increased expression of oncogenic cytoplasmic FABP5 significantly correlated with the increased nuclear PPARγ in CRPC cells. The increased levels of both proteins were associated with increased GS and connected with reduced patient survival time (211). It has been confirmed that the fatty acids, transporting by FABP5, stimulate PPARγ to activate the FABP5-PPARγ-VEGF signalling transduction axis which is the dominant signalling route in promoting malignant progression of CRPC cells (217). Previous studies also showed that suppression of FABP5 or PPARγ expression by RNAi in CRPC cells significantly reduced invasiveness *in vitro* and inhibited the tumorigenicity in mouse model (190,216,217).

In the previous set of experiments of this study, we tried to cut off the FABP5-related signalling transduction chain in CRPC cells to suppress the malignant progression of CRPC. To achieve this aim, we targeted FABP5 to treat CRPC in mice by using the chemical inhibitor SBFI26 and the bio-inhibitor dmrFABP5 to supress the biological activity of FABP5. Results of this work showed that suppression of FABP5 in CRPC cells by using both inhibitors produced a significant reduction in growth rate, invasiveness, migration and anchorage-independent growth. In addition, by orthotopic implantation of CRPC cells into prostate gland in nude mice, it was shown that both inhibitors could significantly reduce the size of tumours formed into the gland and the metastasis of the tumours.

To investigate whether the FABP5 inhibitors suppressed the malignant progression of CRPC through inhibiting the FABP5-related signalling transduction pathway, in this set of experiments, we first investigated whether these inhibitors inhibited tumourigenicity of CRPC cells in a similar manner to that of the PPARγ antagonist.

Then we investigated how these inhibitors cut off the FABP5-related signal transduction route and what connection points of the signal transduction chain were broken by these inhibitors so that the tumourigenicity and the metastatic ability of the CRPC cells was suppressed.

5.2 Materials and Methods

5.2.1 Materials

Reagents are listed in Appendix A, Buffers in Appendix B and Equipment in Appendix C.

5.2.2 Methods

5.2.2.1 Cell culture

5.2.2.1.1 Routine cell culture

Cells were grown in cell culture flasks and incubated in a humidified incubator at 37°C which contains 5% (v/v) CO2. Tissue culture hood found in the tissue culture laboratory was used for all routine cell culture procedures. Six cell lines were grown which are benign prostate cells (PNT2), low malignant prostate cancer cells (LNCaP), moderately malignant prostate cancer cells (22RV1) and highly malignant prostate cancer cells (DU145, PC3 and PC3-M). LNCaP cells were cultured in RPMI 1640 nutrient medium with 10% (v/v) fetal calf serum (FCS), 100IU penicillin/streptomycin, 2mM L-glutamine, 1mM sodium pyruvate. PNT2, 22RV1, DU145, PC3 and PC3-M cells were culture in the same complete medium without sodium pyruvate. Routine culture medium was replaced every three days.

5.2.2.1.2 Cells thawing

Vials of cells from liquid nitrogen were thawed in water bath at 37°C and directly moved into 10 ml of completed cell medium in a universal tube. The cell pellet was centrifuged for 3 minutes at 600×g. The supernatant was discarded and the pellet was suspended in a suitable volume of complete medium. The cells were cultured in a cell culture flask and incubated in a humidified incubator

5.2.2.1.3 Sub-culture of cell lines

Cells were sub-cultured when their confluency reached 60-80%. Medium was removed from the flask. Cells were washed by phosphate buffered saline (PBS) and adequate amount of 2.5% trypsin/versene solution was added to the flask and incubated at 37°C for 3-5 minutes until the cells were starting to detach from the flask. Double amount of medium was added to deactivate the effect of trypsin/versene solution and the cells were transferred to a universal tube and centrifuged at 600×g for 3 minutes. The supernatant was removed and pellet was washed with PBS and centrifuged. Finally, the cells were seeded at the required concentration and incubated in a humidified incubator.

5.2.2.1.4 Cell count

Improved double counting chambers hemocytometer was used to calculate the number of the cells. Cells were detached as described previously, suspended in complete medium and 20µl of cell suspension was loaded to a counting chamber of hemocytometer with 9 (3×3) squares. The cells were counted in four corner squares under the microscope. The total number of cells was calculated using the equation below.

Total number of cells= Average cell count per square × Dilution× 10^4 × Total volume (ml)

5.2.2.1.5 Freezing down Cells

Cells were frozen down when their confluency reached to approximately 60-80%. The cells were detached and washed as described previously. After washing the supernatant was removed and the cell pellet broke up by repeated pipetting with freezing medium (complete medium and 7.5% (v/v) DMSO). Cell suspension (1ml) were put into

cryogenic vials and placed into a Nalgene cryo-preserver box containing 250ml of isopropyl alcohol. The box was stored in a freezer at -80°C overnight before vials were transferred to liquid nitrogen for long term storage.

5.2.2.2 Nude mouse xenograft tumour models

Two rounds of animal studies were performed using 6-8 weeks old male Balb/c nude mice (Charles River, UK). They were weighted in their arrival and ranged between 18-20g. After one week of settling down, PC3-M cell lines were cultured up to 80% confluency. On the day of inoculation, cells were harvested and re-suspended in PBS at the concentration of 1×10^7/ml. 2×10^6 PC3-M cells in 200µL PBS were subcutaneously injected into the right flank region of the mouse to test the suppression effect of the inhibitors on tumorigenicity. In the first round, 5 groups of mice (8 each) were used: 1) control with PBS; 2) 1mg/kg SBFI26, injected from the 1st day after cell inoculation; 3) 1mg/kg SBFI26, injected from the 7th day after cell inoculation; 4) 20µg/kg dmrFABP5, injected from the 1st day after cell inoculation; 5) 20µg/kg dmrFABP5, injected from the 7th day after cell inoculation. In the second round, 4 groups of mice (5 each) were used and at 7 days after the cell inoculation, each group was subjected to different intra-tumoural injections: 1) control with PBS; 2) 1mg/kg SBFI26 plus 20µg/kg dmrFABP5; 3) PPARγ antagonist (GW9662, 1mg/kg) (Sigma); 4) 1mg/kg SBFI26, 20µg/kg dmrFABP5 plus 1mg/kg GW9662. The injections were repeated every 2 days for 30 days and tumour size measured every 3-4 days and calculated by the formula of L×W×H×0.5236 (247). All animal studies were performed in accordance with UKCCCR guidelines under the Home Office Project License PPL40/2963.

5.2.2.3 Fatty acid uptake assay

Fatty acid uptake assay offers a sensitive and simple method for the measurement of long-chain fatty acids (LCFAs) uptake in cells containing fatty acid transporters. The red fluorescence-labelled LCFA, BODIPY 558/568C_{12} [4, 4-difluoro-5-(2-thienyl)-4-bora-3a, 4a-diaza-s-indacene-3-dodecanoic acid] (Invitrogen) was used as a fluorescently labelled fatty acid that permits fatty acid transport to be measured using flow cytometry (248). BODIPY analogue acts as natural fatty acid for the detection of fatty acid uptake in cells and to screen for inhibitors of fatty acid binding proteins. Fluorescent fatty acid stock solution of 2mM were prepared in ethanol as suggested by the company and stored at −20°C.

5.2.2.3.1 Fatty acid uptake for different prostate cells

PNT2, LNCaP, 22RV1and PC3-M cells were plated (1×10^5 cells) in 2ml routine culture medium into 6-well plates in triplicate and incubated at 37°C, 5% CO_2 overnight. The medium was replaced with 2ml of solution (PBS containing 5% FBS) containing 2µM of BODIPY 558/568C_{12} with a blank solution, and cells were incubated for 30mins at 37°C, 5% CO_2. The fatty acid uptake was finished by removal of labelled fatty acid solution and adding 3ml of an ice-cold stop solution (PBS containing 5% FBS). The cells were washed another two times using 3ml of fresh ice-cold solution and were kept on ice for 2 minutes. Cells were detached using 2.5% (v/v) trypsin/versene on ice and then re-suspended using fresh ice-cold solution. The fluorescence intensity of the cell was measured with an EPICS XL Cytometer (Beckman) at the wavelength of 570nm to assess the different expression of FABP5 between different cell lines by measuring fatty acid uptake 30 min before and after adding fluorescence-labelled fatty acid.

5.2.2.3.2 Effect of SBFI26 and dmrFABP5 on the fatty acid uptake of PC3-M cells

Fatty acid uptake assay was performed to determine the inhibitory and competitive effect of SBFI26 and dmrFABP5 which inhibit fatty acid uptake of PC3-M cells. Highly malignant prostate cancer cells (PC3-M) were seeded in 6 well plates as mentioned in 5.2.2.2.1. The medium was replaced with 2ml of solution (PBS containing 5% FBS) containing 2µM of BODIPY 558/568C_{12} and different concentration of unlabelled SBFI26 (50-200µM) or dmrFABP5 (25-75µM) with a blank solution to make competition between inhibitors and BODIPY 558/568C_{12} for binding with FABP5, the cells were incubated for 30mins at 37°C, 5% CO_2. The next steps were as mentioned in section 5.2.2.2.1. The fluorescence intensity of PC3-M cells was measured with an EPICS XL Cytometer at 570nm wavelength.

5.2.2.4 Analysis of protein expression using Western blot

5.2.2.4.1 Treatment of cultured cells

1×10^6 of different prostate cells were grown in 6-well plate and incubated overnight at 37°C, 5% CO2. The medium was removed and new medium containing different compounds (inhibitors or activators) was added and incubated for 24 hours.

5.2.2.4.2 Isolation of protein extracts from cultured cells

After 24 hours' treatment, the cells were detached and suspended in 2ml of medium to inactivate the trypsin. Cell suspensions were centrifuged at 600×g for 3 minutes, the supernatant was decanted and washed with PBS which was removed by centrifugation. The cell pallet was lysed by adding CelLytic-M reagent supplemented with protease inhibitor and incubated on roller mixer for 15 minutes at room temperature. The mixture was centrifuged for 20 minutes at 10,000×g to remove the cellular debris. The supernatant containing proteins was collected into a fresh micro-centrifuge tube.

5.2.2.4.3 Determination of protein concentration

Protein concentration was calculated as described in chapter 2 section 2.2.2.1.2.6.

5.2.2.4.4 Sodium dodecyl sulphate polyacrylamide protein gel electrophoresis (SDS-PAGE)

SDS-PAGE was performed as described in chapter 2 section 2.2.2.1.2.7.

5.2.2.4.5 Transfer of proteins from SDS gel to nitrocellulose membrane

Transfer of proteins from SDS gel to nitrocellulose membrane SDS-PAGE was performed as described in chapter 2 section 2.2.2.1.2.9.

5.2.2.4.6 Immunoblotting for detection of protein expression

In general, Immunoblotting for detection of protein expression was performed as described in section 2.2.2.1.2.10 using different primary and secondary antibodies. Here, the membrane was incubated on a shaker with a primary antibody in an appropriate concentration **(Table 5.1)** at 4°C overnight. The following day, the membrane was washed with TBS-T, 3 times to remove the primary antibody and then incubated with secondary antibody with an appropriate concentration **(Table 5.1)** for 1 hour at RT. To standardise the loading difference, the expression level of β-actin expression was examined. The expression level (EL) of each target protein was calibrated using the formula listed below.

Normalised EL of target protein= EL of target protein/ El of β-actin

Target protein	Primary antibody	Secondary antibody
PPARγ	Monoclonal Mouse Anti-Human PPARγ (1:200)	Polyclonal Rabbit Anti-Mouse IgG-HRP (1:2000)
p-PPARγ	Polyclonal Rabbit Anti-Human p-PPARγ (1:200)	Polyclonal Goat Anti-Rabbit IgG-HRP (1:2000)
β-actin	Monoclonal Mouse Anti-β-actin (1:5000)	Polyclonal Rabbit Anti-Mouse IgG-HRP (1:2000)

Table 5. 1 Primary and secondary antibodies used in Western blot.

5.2.2.5 Statistical analysis

Student's *t*-test were carried out using GraphPad Prism software to compare the differences of the means between control and experimental groups. All experiments were conducted in triplicate and repeated at least three times. The difference is regarded as significant when $p<0.05$; in the results, p value is represented by asterisks as follows: *, $P < 0.05$; **, $P < 0.001$; ***, $P < 0.0001$.

5.3 Results

5.3.1 SBFI26 and dmrFABP5 inhibited tumourigenicity of PC3-M cells in nude mice in a similar way to PPARγ antagonist

PC3-M cancer cells (2×10^6) in 200µL PBS were subcutaneously implanted into right flank of Balb/c male nude mice and the FABP5 inhibitors were injected subcutaneously to compare their anticancer effect with that of PPARγ antagonists. In the first round, 5 groups of mice (8 each) were subcutaneously injected with PBS (control), SBFI26 (1mg/kg) and dmrFABP5 (20µg/kg) every other day for 4 weeks; started from day 1 or from day 7 after the inoculation. Tumour sizes were measured every 3-4 days and the volume calculated by the formula of L×W×H×0.5236. Although remarkable suppression of tumour growth was found in mice treated with both inhibitors (**Fig. 5.2)**, no significant difference in treatment effect was found when inhibitors were applied from day 1 or from day 7 after the inoculation. On termination, average volumes of tumours in groups treated with SBFI26 and dmrFABP5 were 302 ± 86 mm^3 and 161± 61 mm^3, respectively, compared to 627± 120 mm^3 in the control group; significant suppressions of 52% and 75% (Student's *t* test, $p < 0.001$ and $P < 0.0001$), respectively (**Fig. 5.1, A** and **B)**. When tumours were weighed on termination, the difference amongst control and treated groups were similar to those measured by tumour volume (**Fig. 5.3)**.

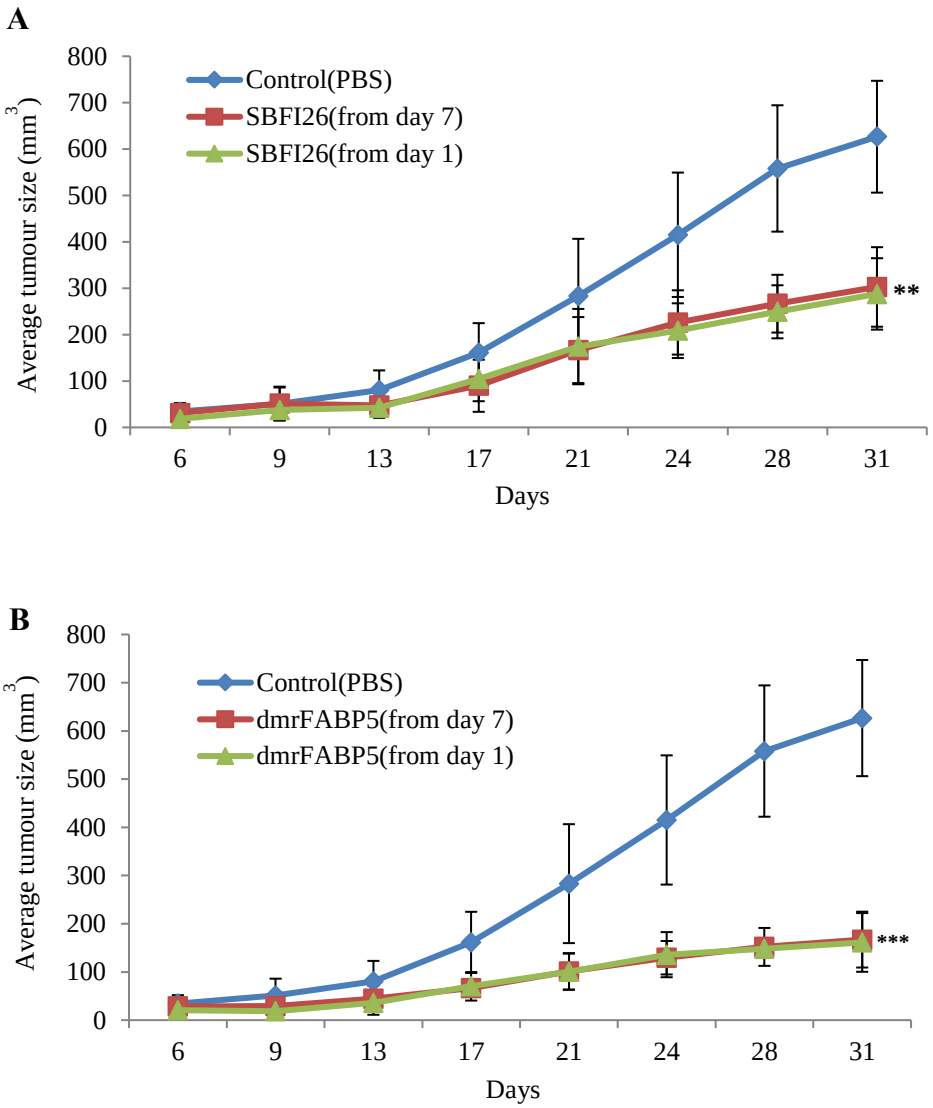

Figure 5.1 Effect of SBFI26 and dmrFABP5 on tumorigenicity in prostate cancer xenograft mice. A, Average volume of tumours produced by each group of male nude mice after subcutaneous inoculation of PC3-M cells and treated with PBS (control) or SBFI26 (1mg/kg) for 4 weeks; started on day 1 and day 7 after inoculation. Values are plotted as mean ± SE (error bars) (n = 8); difference between the control group and the experimental groups were assessed by 2-tailed unpaired Student's *t* test, **, $P < 0.001$. **B,** Average volume of tumours produced by each group of male nude mice after subcutaneous inoculation of PC3-M cells and treated with PBS (control) or dmrFABP5 (20µg/kg) for 4 weeks, starting on day 1 or day 7 after inoculation. Values were plotted as mean ± SE (error bars) (n = 8); differences between the control and the experimental groups were assessed by 2-tailed unpaired Student's *t* test ***, $P < 0.0001$.

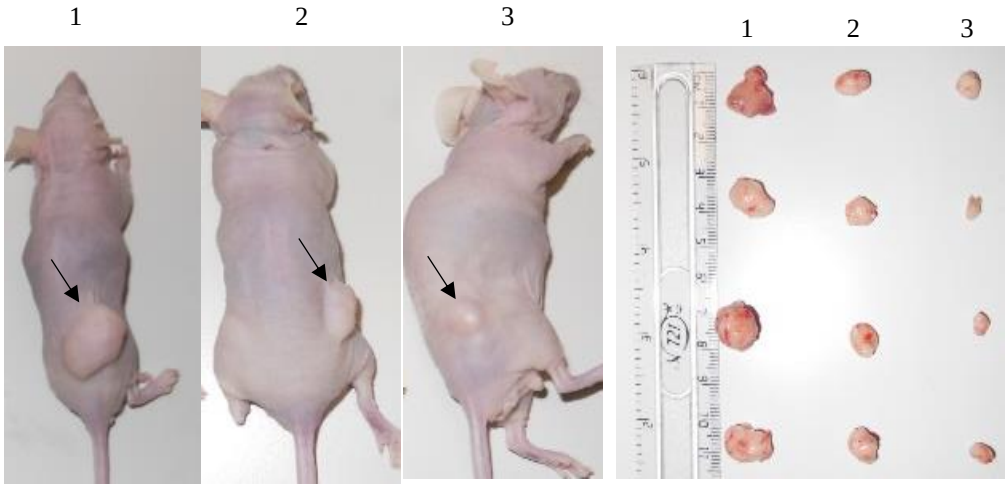

Figure 5.2 Representative mouse and its corresponding tumours from control (1), SBFI26 (2) and dmrFABP5 (3) groups.

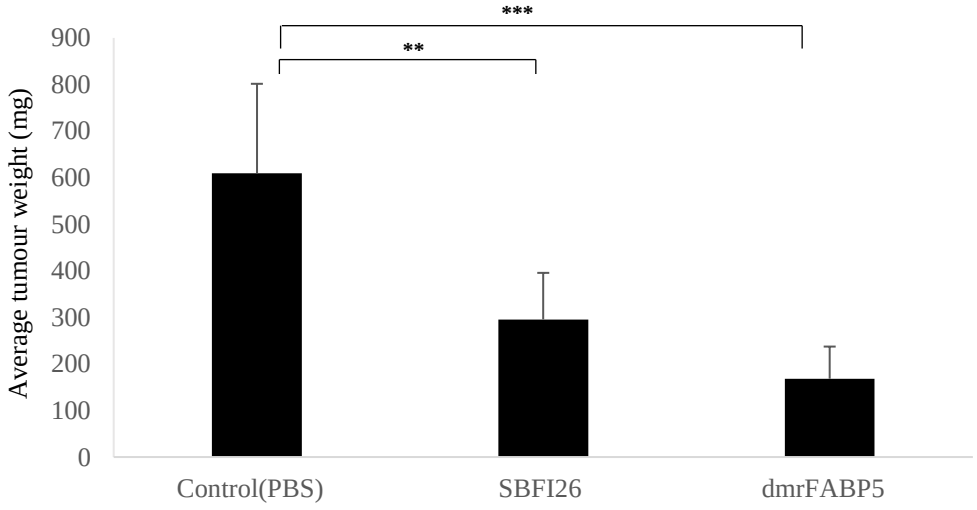

Figure 5.3 Average weight (mg) of tumours from control and treated groups of mice. Values were plotted as mean ± SE (error bars). The differences between the control and the experimental groups were assessed by 2-tailed unpaired Student's *t* test **, $P < 0.001$; ***, $P < 0.0001$.

In the second round, PC3-M cells were inoculated into the right flank of nude mice and the FABP5 inhibitors were injected subcutaneously to compare their anticancer effect with that of PPARγ antagonists. Mice were treated in the following 3 ways from

day 7 after inoculations: SBFI26 plus dmrFABP5; GW9662; and SBFI26 plus dmrFABP5 plus GW9662 (**Fig. 5.5)**. Compared to the average size of tumours (774 ± 202 mm^3) in control group, the average sizes of tumours in these 3 groups of mice were 186 ± 25 mm^3, 252 ± 84 mm^3, and 244 ± 22 mm^3, respectively, highly significant reductions by 76%, 67%, and 68%, respectively (Student's *t* test, p < *0.0001*) (**Fig. 5.4)**. No significant differences were found in inhibitory effects between these 3 treatments. When tumour weight was measured at autopsy, any differences between control and treated groups were similar to those measured by tumour volume (**Fig. 5.6)**.

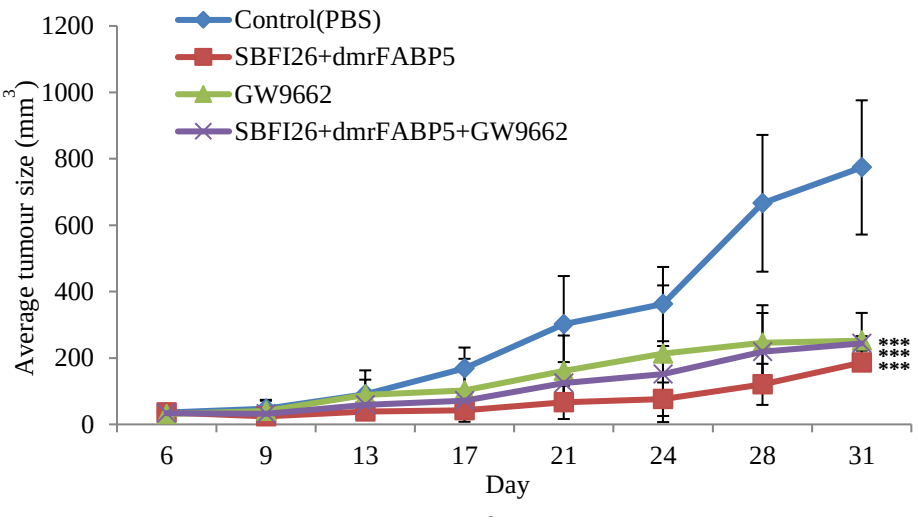

Figure 5.4 Effect of SBFI26, dmrFABP5 and GW9662 on tumorigenicity in prostate cancer xenograft mice. Average volume of tumours produced by each group of male nude mice after subcutaneous inoculation with PC3-M cancer cells and treated with PBS (control), SBFI26 (1mg/kg) plus dmrFABP5 (20µg/kg), PPARγ antagonist (GW9662;1mg/kg) and the combination of SBFI26, dmrFABP5, GW9662 for 4 weeks. Values were plotted as mean ± SE (error bars) (n = 5); differences between the control and the experimental groups were assessed by 2-tailed unpaired Student's *t* test ***, *P < 0.0001*.

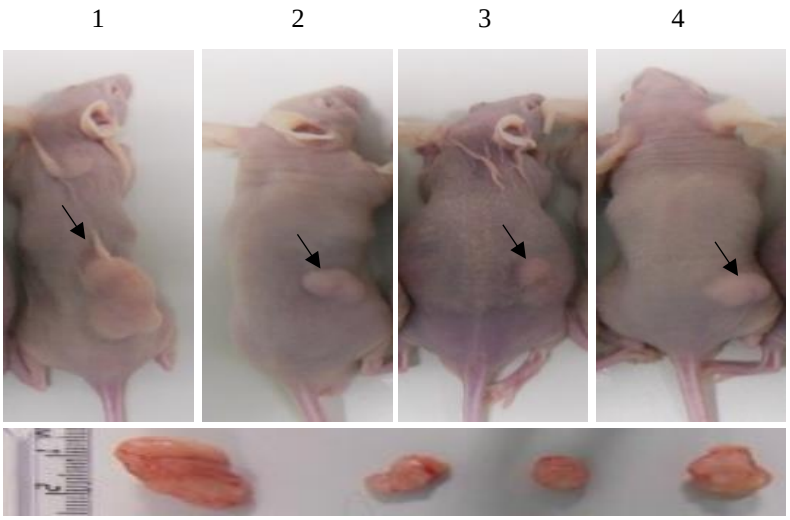

Figure 5.5 Representative mouse and its corresponding tumour. Control (1), GW9662 (2), SBFI26 and dmrFABP5 (3) and the combination of SBFI26, dmrFABP5, GW9662 (4) groups.

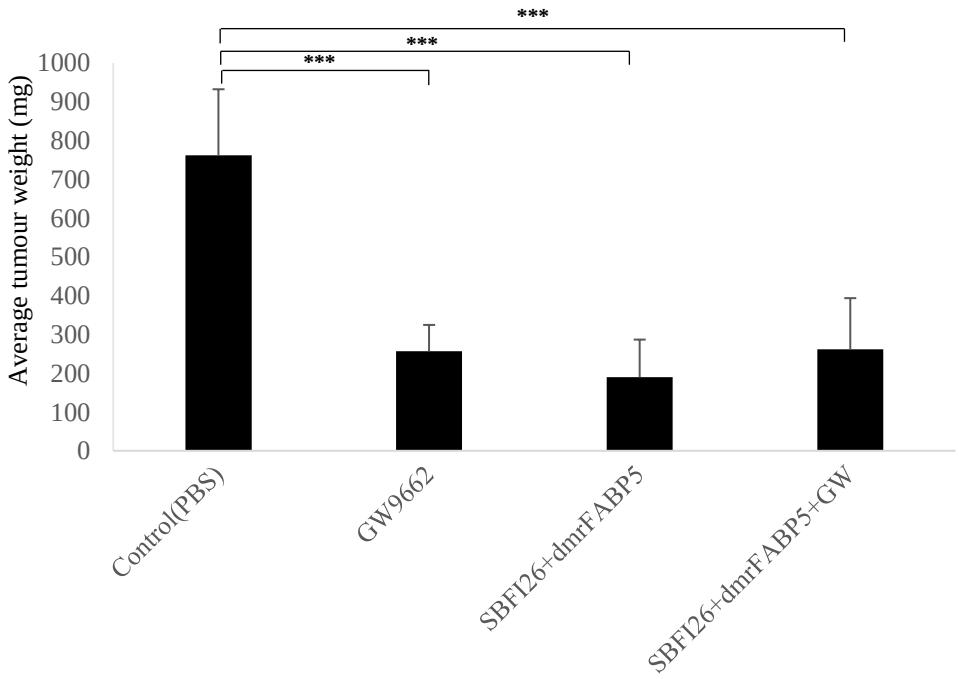

Figure 5.6 Average weight (mg) of tumours in the control and experimental groups of mice. Values were plotted as mean ± SEM (error bars). Differences between the control and the experimental groups were assessed by 2-tailed unpaired Student's *t* test **, $P < 0.001$; ***, $P < 0.0001$.

5.3.2 SBFI26 inhibited fatty acid uptake of FABP5 in PC3-M cells

5.3.2.1 Determination the fatty acid uptake of different prostate cells

Fatty acid uptake assay offers a sensitive and simple method for the measurement of long-chain fatty acids (LCFAs) uptake in cells containing fatty acid transporters. The red fluorescence-labelled LCFA, BODIPY 558/568C12 was used as a fluorescently labelled fatty acid that permits fatty acid transport to be measured using flow cytometry. To identify the uptake of fatty acids in benign prostate epithelial cells (PNT2), and low (LNCaP), moderately (22RV1) and highly (PC3-M) malignant prostate cancer cells. Cells were incubated with BODIPY for 30 mins at 37°C and the fluorescence intensity of cells was measured with an EPICS XL Cytometer at the wavelength of 570nm. Unstained cells (without BODIPY) were present in M1 zone (**Fig.5.7, A)** but fluorescence-labelled BODIPY stained cells were present in the M2 zone after 30mins incubation with BODIPY (**Fig. 5.7, B)**. The fatty acid uptake of PNT2, LNCaP, 22RV1and PC3-M cells were 68, 66, 88 and 93%, respectively. In contrast to benign PNT2, significantly more than 20% and 25% of cells took up fatty acid in moderately malignant 22RV1 and highly malignant PC3-M (Student's *t* test $p < 0.01$ and $p < 0.001$) cells, respectively. Levels of fatty acid uptake between benign PNT2 and weakly malignant LNCaP cells were similar (**Fig. 5.8)**.

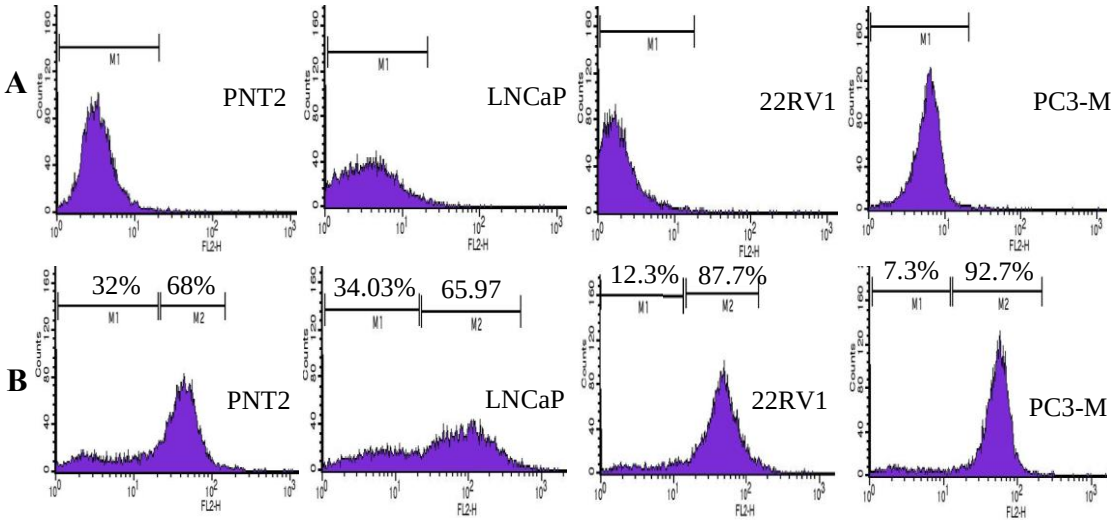

Figure 5.7 Fatty acid uptake of different prostate epithelial cell lines. A, Representative histograms for unstained PNT2, LNCaP, 22RVI and PC3-M cells without adding BODIPY-labelled fatty acid. The marker M1 highlights negative peaks of the subclass control. **B,** Representative histograms for fluorescence of stained PNT2, LNCaP, 22RVI and PC3-M cells 30min after adding BODIPY-labelled fatty acid and the marker M2 is placed to the right of M1 to highlight positive events (total percentage of cells with BODIPY-labelled fatty acid).

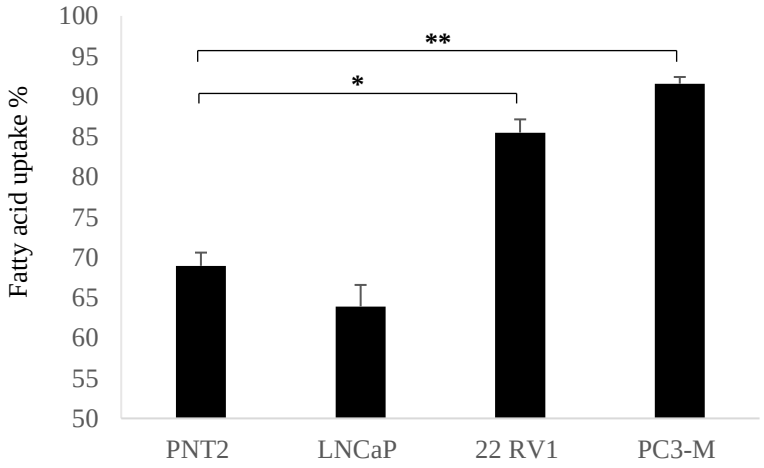

Figure 5.8 Percentages of cells taking up BODIPY-labelled fatty acid from different prostate epithelial cell lines. Values were plotted as mean ± SE (error bars). The differences between groups were assessed by 2-tailed unpaired Student's *t* test. *, *P < 0.01*; **, *P < 0.001*.

5.3.2.2 Effect of SBFI26 or dmrFABP5 on the fatty acid uptake of FABP5 in PC3-M cells

To investigate possible effect of FABP5 inhibitors on fatty acid uptake of PC3-M cells, Fatty acid uptake assay was performed to determine the effect of increasing concentration of SBFI26 or dmrFABP5 on fatty acid uptake in PC3-M cells. PC3-M cells were seeded in 6 well plates for 24h. The medium was replaced with 2ml of solution (PBS containing 5% FBS) containing 2µM of BODIPY and different concentration of SBFI26 (50-200µM) (**Fig. 5.9, A)** or dmrFABP5 (25-75µM) (**Fig. 5.9, B)** with a blank solution to make competition between inhibitors and BODIPY for binding with FABP5. When inoculated with SBFI26, cellular fatty acid uptake into PC3-M cells was reduced from 92.9% in the control in a dose-dependent manner, the significant maximum reduction with 100µM was 67.7% (Student's *t* test $p < 0.001$). No reduction was produced by dmrFABP5 on fatty acid uptake in PC3-M cancer cells (**Fig. 5.10)**.

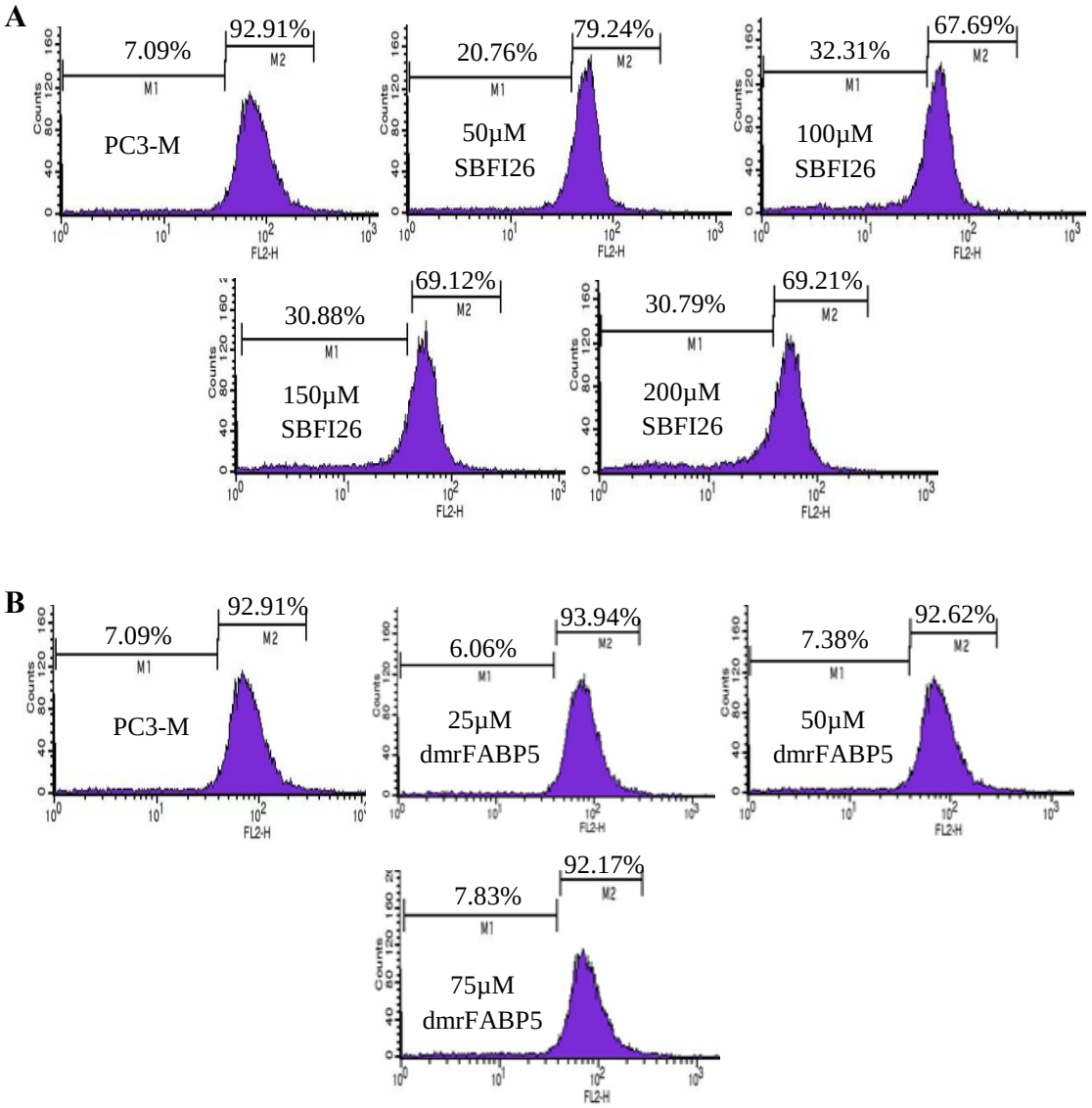

Figure 5.9 Inhibitory effect of increasing concentration of SBFI26 or dmrFABP5 on fatty acid uptake in PC3-M cells. A, Representative histograms for fatty acid uptake of PC3-M cells at a fixed concentration of BODIPY-labelled fatty acid with different concentrations of SBFI26. M1, unstained cells; M2, stained cells. **B,** Representative histograms for fatty acid uptake of PC3-M cells at a fixed concentration of BODIPY-labelled fatty acid with different concentrations of dmrFABP5. M1, unstained cells; M2, stained cells.

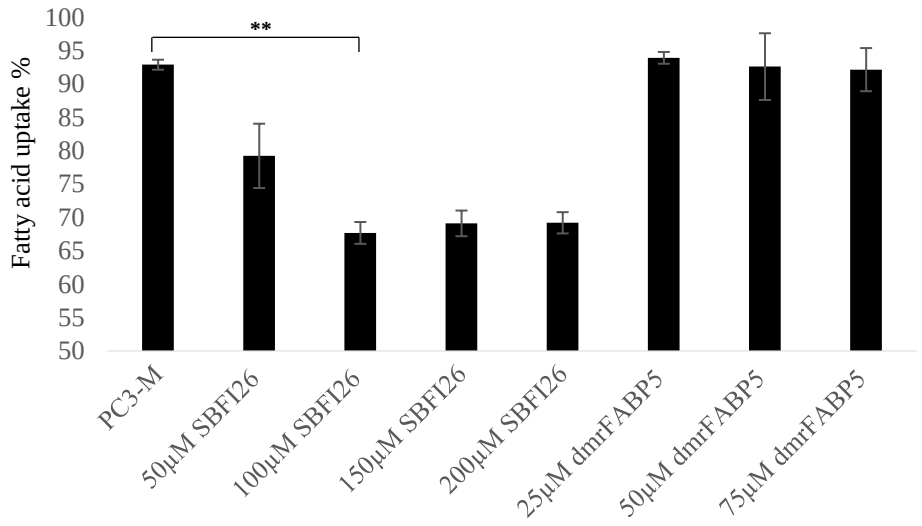

Figure 5.10 Percentages of cells with fatty acid uptake from PC3-M control (untreated) and those treated with different concentrations of SBFI26 or dmrFABP5 for 30min with a fixed concentration of BODIPY. Fluorescence intensity of each cell line was measured with an EPICS XL Cytometer (Beckman) at 570nm and data analysis was performed with SYSTEM II™ Software. Values were plotted as mean ± SE (error bars). The differences between the control and the experimental groups were assessed by 2-tailed unpaired Student's *t* test. **, $P < 0.001$.

5.3.3 SBFI26 and dmrFABP5 inhibited PPARγ activation

The effect of FABP5 inhibitors on levels of PPARγ or biologically active phosphorylated PPARγ (p-PPARγ1 and p-PPARγ2) in benign and malignant prostate epithelial cells was checked by using Western blot. Western blot detected a PPARγ band at 55kDa in most of the cell lines used (**Fig. 5.11, A**). When the level of PPARγ in PNT2 was set at 1.0, relative levels of PPARγ in LNCaP, 22RV1, DU145, PC3 and PC3-M were 0.70 ± 0.03, 0.02 ± 0.01, 0.22 ± 0.001, 0.4 ± 0.0 and 0.64 ± 0.04, respectively (**Fig. 5.11, B**). When Western blot was used to detect p-PPARγ, 2 bands representing isoforms of p-PPARγ1 and p-PPARγ2 were found at 54 and 57kDa, respectively (**Fig. 5.12, A**). If levels of p-PPARγ1 and p-PPARγ2 in PNT2 were set at 1 and 1, relative levels in LNCaP, 22RV1, DU145, PC3 and PC3-M were 9.54 ± 1.81

and 9.5 ± 0.5; 25.4 ± 1.8 and 47.0 ± 1.7; 26.99 ± 1.72 and 85.5 ± 14.5; 12.08 ± 1.8 and 30 ± 5; and 21.99 ± 2.63 and 80 ± 5, respectively (**Fig. 5.12, B**). Levels of p-PPARγ, particularly p-PPARγ2, were significantly increased in all malignant cell lines (Student's *t* test, $p < 0.001$).

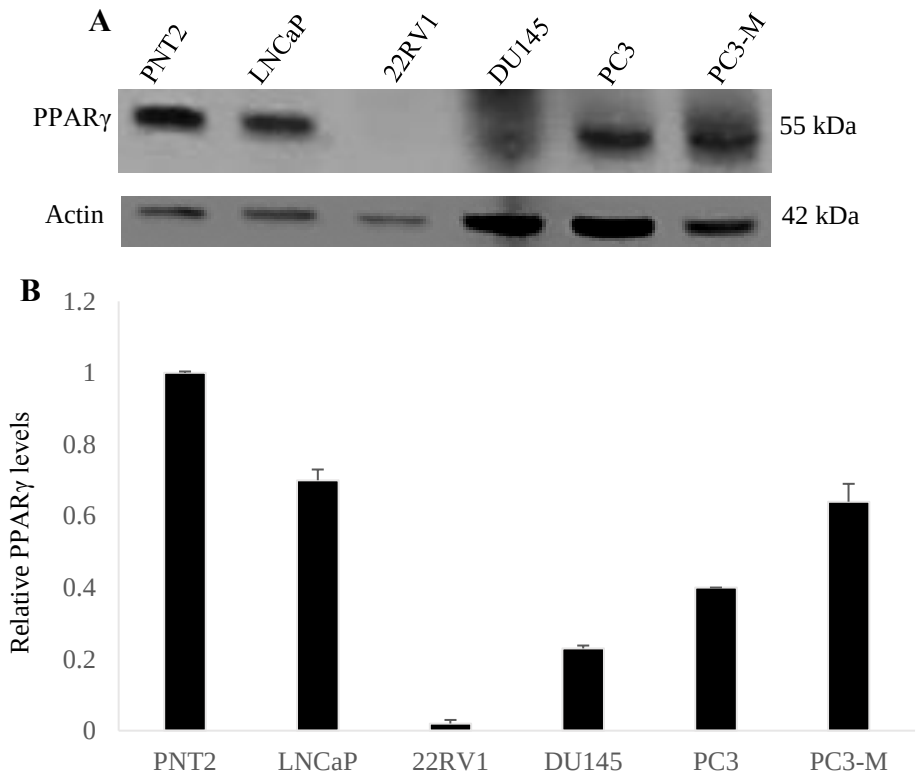

Figure 5.11 The expression of PPARγ in benign and malignant prostate epithelial cells. **A,** Western blot of PPARγ expression in benign and malignant prostate epithelial cells. **B,** Quantitative assessment of levels of PPARγ in benign and malignant prostate epithelial cells. The level of PPARγ in the benign prostate PNT2 cells was set at 1; levels in the other prostate cell lines were obtained by comparison with that in PNT2. For each Western blot, anti-β-actin was incubated with the same blot to normalize for possible loading errors. Results (mean ± SE) were obtained from 3 separate experiments.

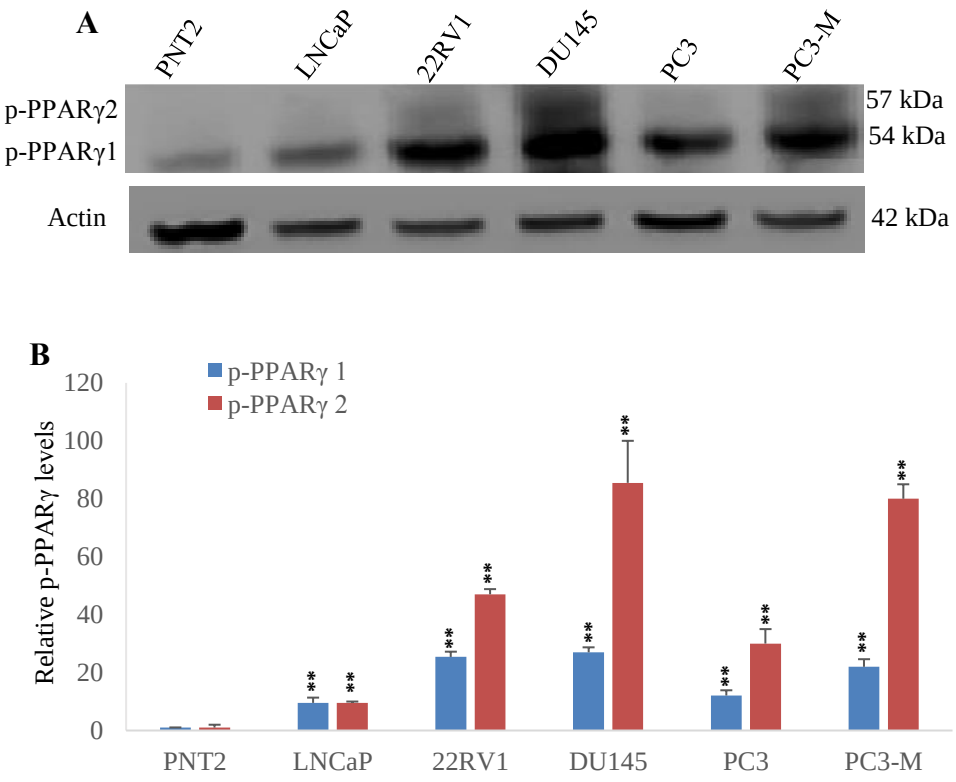

Figure 5.12 The expression of p-PPARγ in benign and malignant prostate epithelial cells. A, Western blot analysis of p-PPARγ1 and p-PPARγ2 in benign and malignant prostate epithelial cells. **B,** Quantitative assessment of the levels of p-PPARγ1 and p-PPARγ2 in prostate cells. Levels of p-PPARγ1 and 2 in benign PNT2 cells were set at 1; levels in the other prostate cells were obtained by comparison with those in PNT2. For each Western blot, anti-β-actin was incubated with the same blot to normalize for possible loading errors. Results (mean ± SE) were obtained from 3 separate experiments and the differences between the benign PNT2 cells and other cells in each experiment were assessed by 2-tailed unpaired Student's *t* test. **, $P < 0.001$.

In order to investigate the effect of FABP5 inhibitors or activators on p-PPARγ, PC3-M, LNCaP or 22RV1 (1×10^6) cells were plated in 6 well plates and treated with different inhibitors or activators. After 24hour treatment, cells were washed with PBS and lysed on ice in lysis buffer supplemented with protease inhibitor. Lysates were

centrifuged and the protein concentration was measured using Bradford assay. Proteins from cell lysates were subjected to SDS-PAGE and the proteins were transferred to nitrocellulose membrane. PC3-M cells were treated with SBFI26, PPARγ antagonist GW9662, PPARγ agonist Rosiglitazone, dmrFABP5 and a combination of SBFI26 and dmrFABP5 for 24 hours (**Fig. 5.13, A**). If levels of p-PPARγ1 and p-PPARγ2 in untreated cells were set at 1 and 1, the levels after treatment with SBFI26, GW9662 and dmrFABP5 were reduced significantly by 44% and 46%; 52% and 51%; and 50% and 65%, respectively (Student's *t* test, $p< 0.001$). Interestingly, treatment with a combination of SBFI26 and dmrFABP5 dramatically reduced the level of p-PPARγ2 by 90%, whereas it also reduced the levels of p-PPARγ1 by 52%. However, those treated with rosiglitazone, significantly increased levels of both p-PPARγ isoforms were observed (Student's *t* test, $p < 0.01$) (**Fig. 5.13, B**). For LNCaP cells which expressed low levels of p-PPARγ1 and 2, treatments with wtrFABP5 increased levels of both isoforms by 1- and 0.9- fold, respectively. However, these increases were reversed completely by adding dmrFABP5. Furthermore, addition of dmrFABP5 even reduced the level of p-PPARγ2 by 5-times (Student's *t* test, $p < 0.001$) to a level lower than that obtained in pretreatment (**Fig. 5.14, A** and **B**). When treatments with wtrFABP5, SBFI26 and dmrFABP5 were tested in androgen-sensitive 22RV1 cells (**Fig. 5.15, A**), wtrFABP5 significantly increased levels of both p-PPARγ1 and 2 (Student's *t* test, $P < 0.01$) **(Fig. 5.15, B)**. However, treatments with the inhibitors suppressed the levels of both p-PPARγ isoforms.

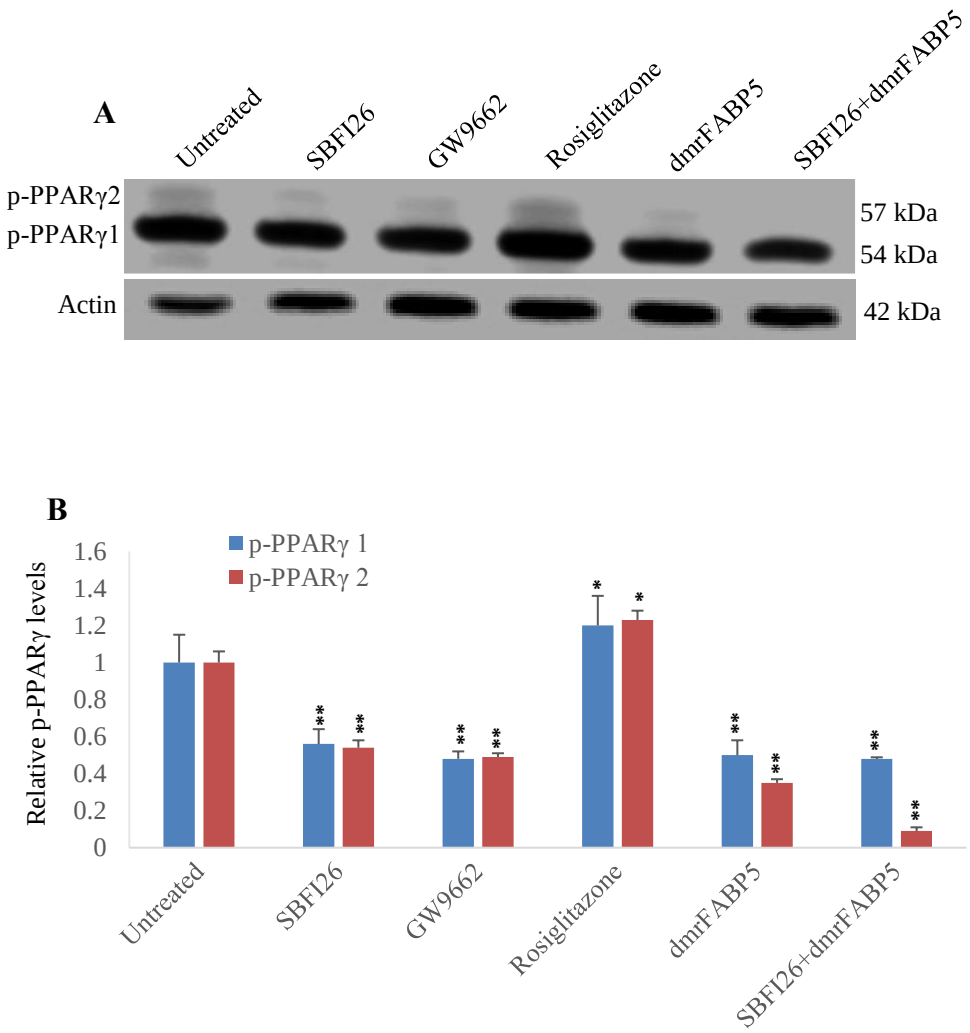

Figure 5.13 Effects of inhibitors and activators on levels of p-PPARγ in PC3-M cells. A, Effect of 24 h treatments with SBFI26, PPARγ antagonist (GW9662), PPARγ agonist (Rosiglitazone), dmrFABP5 and a combination of SBFI26 and dmrFABP5 on levels of p-PPARγ1 and 2 in PC3-M cells. **B,** Quantitative assessment of p-PPARγ1 and 2 levels in PC3-M cells after treatments with SBFI26, GW9662, Rosiglitazone, dmrFABP5, and a combination of SBFI26 and dmrFABP5. Levels of both p-PPARγ1 and 2 in untreated PC3-M cells were set at 1; levels in the other treated cells were obtained by comparison with those in untreated PC3-M. For each Western blot, anti-β-actin was incubated with the same blot to normalize for possible loading errors. Results (mean ± SE) were obtained from 3 separate experiments and the differences between the control and the treatments in each experiment were assessed by 2-tailed unpaired Student's *t* test. *, $P < 0.05$; **, $P < 0.001$.

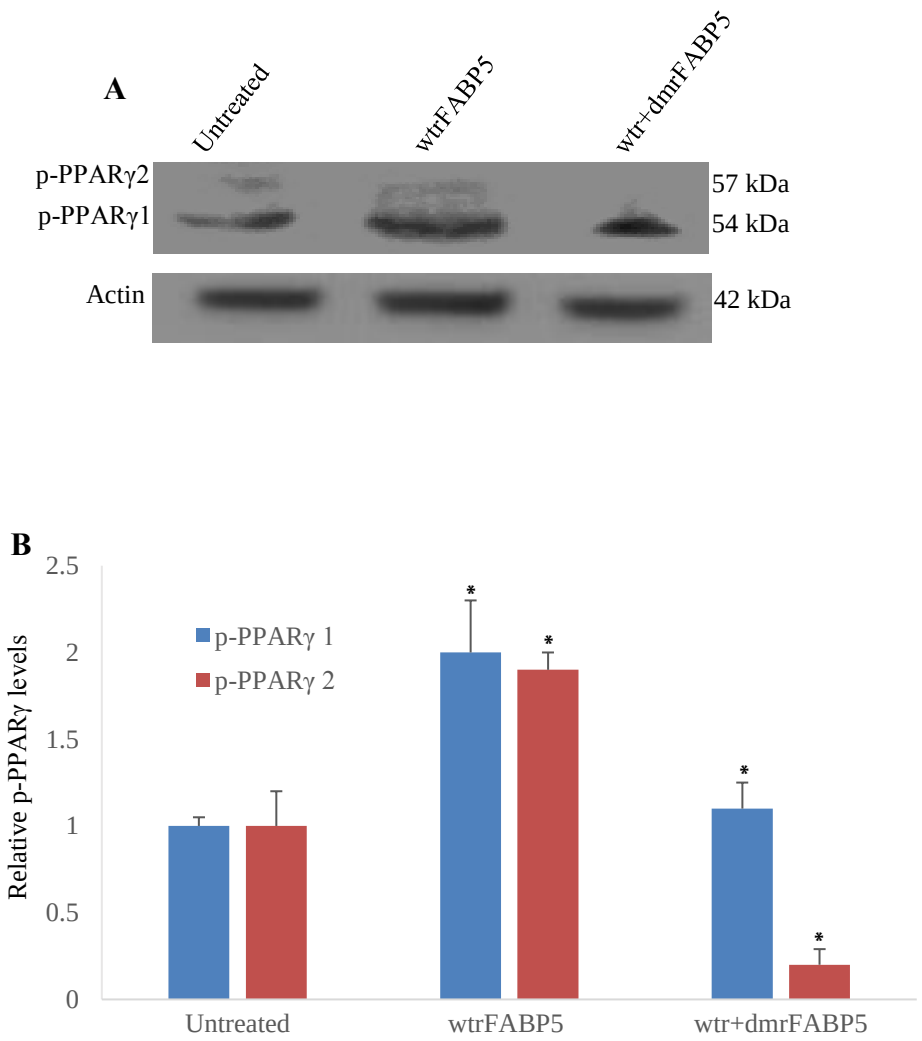

Figure 5.14 Effects of wtrFABP5 and dmrFABP5 on levels of p-PPARγ in LNCaP cells. A, Effect of 24h treatments with wtrFABP5 and a combination of wtrFABP5 and dmrFABP5 on levels of p-PPARγ1 and 2 in LNCaP cells. **B,** Quantitative assessment of levels of p-PPARγ1 and 2 in control (untreated) and in treated LNCaP cells. Levels of p-PPARγ1 and 2 in control LNCaP cells were set at 1; levels in the other treated cells were obtained by comparison with those in control. For each Western blot, anti-β-actin was incubated with the same blot to normalize for possible loading errors. Results (mean ± SE) were obtained from 3 separate experiments and the differences between the control and the treatments in each experiment were assessed by 2-tailed unpaired Student's *t* test. *, $P < 0.05$; **, $P < 0.001$.

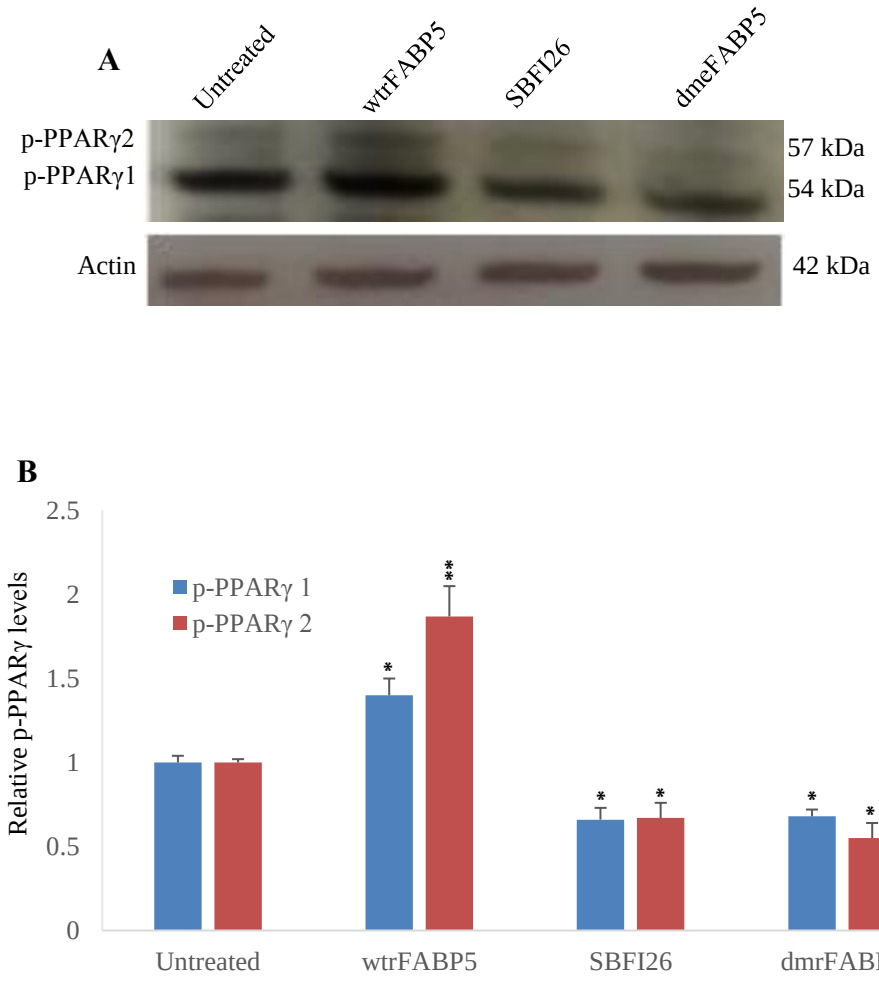

Figure 5.15 Effects of wtrFABP5 and FABP5 inhibitors on levels of p-PPARγ in 22RV1 cells. A, Effect of 24 h treatments with wtrFABP5, SBFI26 and dmrFABP5 on levels of p-PPARγ1 and 2 in 22RV1 cells. **B,** Quantitative assessment of levels of p-PPARγ1 and 2 in 22RV1 cells. Levels of both p-PPARγ1 and 2 in the control were set at 1; levels in the other treated cells were obtained by comparison with those in controls. For each Western blot, anti-β-actin was incubated with the same blot to normalize for possible loading errors. Results (mean ± SE) were obtained from 3 separate experiments and the differences between the control and the treatments in each experiment were assessed by 2-tailed unpaired Student's *t* test. *, $P < 0.05$; **, $P < 0.001$.

5.4 Discussion

Previous work on investigating the molecular mechanisms involved in the tumour-promoting role of FABP5, our research team identified a FABP5-PPARγ-VEGF signalling transduction axis, and it is this axis, rather than AR modulated route, is the dominant signalling route in CRPC cells (217). It has been identified that prostate cancer cell lines and clinical samples exhibit elevated levels of PPARγ (249,250). To find out the possible molecular mechanisms on how SBFI26 and dmrFABP5 inhibited the malignant progression of the prostate cancer cells, we investigated the role of the PPARγ antagonist, GW9662, on tumour suppression in mouse. Our results showed that the treatment of PC3-M cells with GW9662 produced a similar suppression of tumour growth to those produced by SBFI26 and dmrFABP5 (Student's *t* test, $p < 0.0001$) **(Fig. 5.4)** (**Fig. 5.6)**. These results indicate that SBFI26 and dmrFABP5 may played their suppressive role through affecting PPARγ and thus the suppressive mechanisms of both inhibitors may be related to the FABP5-PPARγ-signal transduction pathway.

In this work, no difference on the tumour-suppression effect was observed when the administration of the inhibitors started either at day 1 or at day 7 after the inoculation of the cancer cells (**Fig. 5.1)**. No significant difference was observed in tumour-suppression effect obtained by each inhibitor alone or by the combination of both **(Fig. 5.3)** (**Fig. 5.6)**. These results suggested that there was no synergistic treatment effect when both inhibitors were used in a combined manner.

In the work described in chapter 3, the highly binding affinity of SBFI26 with FABP5 was found when DAUDA displacement assay was performed. In this set of experiments, we used the BODIPY-labelled fatty acid analogues to test the effect of SBFI26 and dmrFABP5 on fatty acid uptake of the CRPC cells. The results showed

that fatty acid uptake by the highly malignant PC3-M cells was 25% higher than that by the benign prostate PNT2 cells (mean ± SE) (Student's *t* test $p < 0.001$) **(Fig. 5.7)** (**Fig. 5.8)**, indicating that the increased fatty acid uptake is positively related to the high degree of malignancy. When the possible effect of SBFI26 on fatty acid uptake was studied, 100μM of SBFI26 produced a reduction of fatty acid uptake by 25% in 30 min incubation (mean ± SE) (Student's *t* test $p < 0.001$) **(Fig. 5.9, A)** (**Fig. 5.10)**. These results suggest that SBFI26 may be a competitive inhibitor of fatty acids which competitively binds to FABP5 and hence prevent extra amount of intra- and extra-cellular fatty acids from being transported into the cytoplasm. The reduced fatty acid uptake produced by SBFI26 may result in a remarkable reduction or cessation of the stimulation of PPARγ by fatty acids. Thus PPARγ may no longer be able to upregulate the down-stream cancer-promoting genes, such as VEGF, and to suppress apoptosis (251,252). Surprisingly, dmrFABP5 did not produce any noticeable changes in fatty acid uptake of PC3-M cells **(Fig. 5.9, B)** (**Fig. 5.10)**, which suggests that dmrFABP5 acts through a mechanism different from that of SBFI26.

Over expression of FABP5 and PPARγ has been observed in malignant prostate cancer cells. Therefore, suppression the biological activity of FABP5 may limit the expression of PPARγ and hence inhibit the expression of its down-stream controlling genes such as VEGF. In this axis, the role of PPARγ is essential. Although the total PPARγ expressed in the malignant cell lines was not higher than that in the benign PNT2 cells **(Fig. 5.11, A** and **B)**, the biologically-active PPARγ isoforms (or phosphorylated PPARγ) p-PPARγ1 and p-PPARγ2 (250,253) both increased with increasing cellular malignancy **(Fig. 5.12, A** and **B)**. Both activated PPARγ isoforms were increased by wtrFABP5 stimulation and these increases were inhibited by dmrFABP5 **(Fig. 5.14, A** and **B)** in LNCaP cells which expressed low levels of activated PPARγ. In contrast,

PPARγ isoforms in PC3-M cells, which expressed high levels, were further increased by rosiglitazone (PPARγ agonist). But their levels greatly reduced by treatments with SBFI26, dmrFABP5, GW9662, and by SBFI26 plus dmrFABP5 **(Fig. 5.13, A** and **B)**. These results suggest that both SBFI26 and dmrFABP5 may act as inhibitors to block the stimulation of fatty acids transported by natural wild type FABP5 and hence prevent activation of PPARγ.

In androgen-responsive, moderately-malignant 22RV1 cells, both SBFI26 and dmrFABP5 produced a reduction in both PPARγ activated isoforms by an average of 33.5% **(Fig. 5.15, A** and **B)**. This level of reduction was much smaller than that caused by SBFI26 and dmrFABP5 in the androgen-independent, highly malignant PC3-M cells (average reduction was about 50%). These results suggest that the proportion of activated PPARγ regulated by the FABP5-related pathway was much higher in PC3-M cells than that in 22RV1 cells, a result which suggests that treatment by suppression of the FABP5-pathway is more effective in CRPC cells.

Chapter Six

General discussion, Conclusions and Future work

6.1 General discussion

Since it was discovered that prostate cancer cell growth is dependent on the promoting effect of male hormone supplied through peripheral blood circulation (108), ADT targeting AR and circulating male hormone has been the main therapeutic method to treat prostate cancer patients during the past 4 decades. ADT is an effective treatment as an initial therapy. However, the disease relapses within a period of time with a more aggressive form, called androgen-independent prostate cancer or CRPC, this does not respond to ADT effectively since the growth and progression of CRPC cells do not rely on circulation hormone anymore. The conversion of androgen-dependent cancer cells to androgen independent CRPC cells is a fundamental change and the molecular mechanisms involved in this change is not fully understood. Currently, there are several different hypotheses on how the androgen-dependent cells were transformed to androgen-independent cells. The main theory is that the biological sensitivity of AR is amplified after the first round of ADT to such an extent that even micro-quantities of remaining hormone in peripheral blood can still promote the malignant progression of CRPC cells (254,255). Thus, further ADT on CRPC was a general clinical practice. However, an opposite opinion to this practice was proposed recently to suggest that ADT may lead to a treatment dead end (256). Our previous work suggested that AR may not be relevant to malignant progression of CRPC and that targeting FABP5-PPARγ-VEGF axis, rather than the AR-mediated signalling pathway, which was gradually replaced by the FABP5-related pathway, could be a more effective way for CRPC treatment (217). It has been found that ADT had little effect to suppress fatty acid synthase expression which is important enzyme for the control of fatty acid synthesis (188). It has been confirmed that cancer cells rely on fatty acids as cellular

building and production of signalling molecules (233) and play an important role in carcinogenesis and metastasis of cancer cells (234).

High expression of FABP5 has long been considered as a promoter for cell growth and metastatic in prostate cancer (190). FABP5 delivers fatty acids and enhance the transcriptional activity of their nuclear receptor PPARγ in prostate cancer cells (211,217,257). Targeting FABP5 biological function may constitute a new way for therapy of CRPC. Although, siRNA knockdown of FABP5 was previously shown an effectively inhibit CRPC cells growth *in vivo* (216), the efficient delivery of siRNA remains problem and very unstable and thus loss their function quickly. Here for the first time, we targeted the FABP5 and its related signal transduction pathway and successfully used both a chemically-synthesized inhibitor (SBFI26) and a bio-inhibitor (dmrFABP5) for FABP5 to treat CRPC in nude mice by suppressing the biological activity of FABP5.

6.1.1 DmrFABP5 and SBFI26 can be used as a bio-inhibitor and a lead chemical inhibitor of FABP5

The malignancy-promoting function of FABP5 in CRPC cells depends on its structural integrity of the 3 key amino acids which consist of the fatty-acid-binding motif (192,226,229). In this work, we produced a biologically inactive FABP5 (dmrFABP5) by making double mutation to change 2 of the 3 key amino acids in the fatty acid-binding motif and used it as a bio-inhibitor of the wild type FABP5 to treat CRPC. The mutant protein dmrFABP5 has the same structure as wtrFABP5, but it is incapable of binding to fatty acids **(Fig. 2.9) (Fig. 2.10)**. Our results confirmed that dmrFABP5 incapable of binding to fatty acids can be used as a bio-inhibitor to inhibit the biological activity of the native FABP5 inside the CRPC cells. The chemically-synthesized inhibitor SBFI26 can competitively bind to the wtrFABP5 in a similar

affinity to that of the best fatty acid (Linoleic acid) **(Fig. 3.4)**. Linoleic acid and SBFI26 are the best fatty acid and lead compound with high binding affinity *Ki* value 1.58 and 1.69 μM respectively **(Table 3.1)**. Therefore, SBFI26 can be used as a FABP5 inhibitor to prevent the excessive amounts of fatty acids being transported to activate PPARγ in CRPC cells.

6.1.2 SBFI26 and dmrFABP5 are potent inhibitors on malignant characteristics of PC3-M cells *in vitro* and *in vivo*

PC3-M (CRPC cells) is an extremely malignant cell line and expressing high levels of FABP5 and PPARγ (217,245,246). Suppression of FABP5 biological functions may be a therapeutic approach for treatment of CRPC. SBFI26 and dmrFABP5, the potent inhibitors of FABP5 function allowed us to test the effects on the growth and metastasis of PC3-M cell lines *in vitro* and *in vivo*.

In vitro results showed that both SBFI26 and dmrFABP5 can suppress the malignant characteristics of PC3-M CRPC cells via inhibiting the biological activity of FABP5. When tested *in vivo*, SBFI26 and dmrFABP5 were highly effective in suppressing both the primary tumours growing in the prostate gland (by 4.9-fold and 13-fold, respectively) **(Fig. 4.13)** and subcutaneous tumours growing in the flank (by 52% and 75%, respectively) **(Fig. 5.1)**. In addition, SBFI26 and dmrFABP5 treatment suppressed metastases of the tumours growing in the prostate gland by 50% and 100%, respectively compared to 0% in the control group **(Fig. 4.14)**. Comparing with SBFI26, the anti-tumour effect of dmrFABP5 was 2.7-fold higher in tumours growing in the prostate gland **(Fig. 4.13)**, and 30% higher in tumours growing in the flank **(Fig. 5.1)**. In addition, the anti-metastatic effect of dmrFABP5 was 2-folds of that of SBFI26 **(Fig. 4.14)**.

The migrating ability and invasiveness are essential characteristics for cancer cells to be able to metastasise to the secondary sites of the body (258). Cancer cells own a unique ability to adapt themselves to different secondary environments (259). After cancer cells acquire the ability to penetrate the tissues, the process of invasion is initiated as these motile cancer cells pass through the basement membrane and penetrate the vascular circulation (260). The pathological processes of cancer cell invasion and metastasis is regulated by a number of molecules that have been identified as having important roles to play in modulating signalling pathways leading to malignant progression (260). It has been confirmed that high level of fatty acids uptake provided an important source of signalling molecules that led to the promotion of cell migration and invasion (261). Our results in this study showed that suppression the biological function of FABP5 by both inhibitors inhibited the migration and invasion of PC3-M cells *in vitro* and *in vivo*. These results suggest that both SBFI26 and dmrFABP5 are potent inhibitors on malignant progression of CRPC cells *in vitro* and *in vivo* and the suppression effect of the bio-inhibitor dmrFABP5 is much stronger than that of the chemically synthesised SBFI26.

6.1.3 Possible problems to use PPARγ agonist and antagonist as direct therapeutic agents for CRPC

Investigations in the past few years established that there is a novel FABP5-PPARγ-VEGF signalling pathway leading to malignant progression of CRPC cells (217). PPARγ is highly expressed in adipose tissue and plays an important role to regulate adiposity and insulin sensitivity (262). The potential of using PPARγ as a direct target for cancer treatment has been widely investigated during the past decade but still remains debatable. Both PPARγ agonist and antagonist have shown some anticancer effect through PPARγ-dependent and -independent pathways (263,264). However,

there are safety concerns: side effects, including dose limited side effects linked to PPARγ drug treatments, increased the risk of cardiac failure and potential carcinogenicity in rodents (265). It has been found that PPARγ stimulation using synthetic agonists (high doses) suppresses *in vitro* and *in vivo* growth of PC3 prostate cell lines (246,266,267). However, evidence suggested that these agonists may work through a PPARγ-independent pathway to induce cell cycle arrest and apoptosis in prostate cancer (264,266,268). In addition, PPARγ agonist inhibitors have been shown to suppress cell growth and induce apoptosis of prostate cancer cells by both PPARγ-dependent (genomic) and - independent (non-genomic) signalling pathways. Thus, it remains unclear whether the non-genomic effects are essentially on PPARγ pathways (269). On the other hand, although most of Thiazolidinediones (TZDs) are potent PPARγ agonists, they also have some affinity to PPARα or PPARβ/δ (270,271). In addition, it has been showed that TZDs had inhibitory effects on cholesterol biosynthesis, independently from PPARγ pathway (272).

It was proved that the irreversible, potent and specific PPARγ antagonist (GW9662) prevented activation of PPARγ, suppressed growth of cancer cells and efficiently blocked tumour growth in an animal model (263,273,274). However, the results from another study indicated that GW9662 has a protective role in cancer by blocking cannabinoids-induced apoptosis in xenograft-induced tumours in mice (275). It was found that down-regulation of PPARγ using the GW9662 compound reduced the malignant characteristic of PC3 and PC3M cells (276). GW9662 has a significant effect on adipose tissue weight and glucose metabolism *in vivo*. Gene expression analyses showed that GW9662 suppressed the expression of many lipogenic genes, for example FASN which is important for fatty acid synthesis (273). If GW9662 is administrated continuously for a long time, it can reduce weight and suppress any

increase in the amount of visceral adipose tissue (277). In addition, GW9662 upregulates the expression of several genes associated with the transcription, processing, splicing and translation of RNA (278). Thus, due to PPARγ versatile nature, directly targeting PPARγ by its agonists and antagonists as a treatment for CRPC is difficult to achieve.

6.1.4 Possible problems to use anti-VEGF therapy in the treatment of CRPC

VEGF protein has been detected in prostate cancer, but not in BPH or normal prostate samples (279). Over-expression of FABP5 induced metastasis through up-regulation of VEGF and thus VEGF played a crucial role in malignant progression of CRPC cells (190,191). It is known that increases in uptake of fatty acids will contribute to the switch in energy production from aerobic to anaerobic sources as well as the downstream effect of increased production of VEGF to stimulate angiogenesis. These changes are induced by increased expression levels of FABP5 and may contribute to the amelioration of the effects of chronic hypoxia which is known to occur as prostate cancer develops (280,281). Suppressing *FABP5* gene in CRPC cells has reduced the expression of VEGF and down-regulated angiogenesis (189,190). In androgen-dependent prostate cancer cells, androgen has mediated the up-regulation of VEGF expression through a Sp1/Sp3 binding site in the VEGF core promoter (282). However, in CRPC cells, it has been found that androgen-Sp1/Sp3-VEGF signalling pathway disappeared as the cells gradually lost their androgen dependency and was replaced by the FABP5-PPARγ-VEGF pathway (217). It was suggested that the suppression of tumorigenicity of CRPC cells by knocking down *PPARγ* gene was achieved through inhibiting the biological activity of VEGF (217). Anti-angiogenic treatment with VEGF inhibitors such as Bevacizumab, Sunitinib or Sorafenib reduced progression rate of CRPC and increased patient survival time (283). However, anti-VEGF therapy

in the treatment of cancer can be accompanied by a variety of side effects, which are increased by concurrent chemotherapeutic agents (284). The most common adverse effect for anti-angiogenic treatment are hypertension, proteinuria, upper respiratory infection, epistaxis, anorexia, headache, dyspnea, stomatitis, fatigue (285). Infrequent serious side events include haemorrhage, arterial thromboembolic events, gastrointestinal perforation, wound healing difficulties, nephrotic syndrome, and congestive heart failure (286). Thus, due to the side effect of anti-VEGF therapy, directly targeting VEGF by its inhibitors as a treatment for CRPC is difficult to achieve.

6.1.5 PPARγ antagonist, GW9662, produced a similar suppression of tumour growth to that obtained by SBFI26 and dmrFABP5

To compare the effect of SBFI26 and dmrFABP5 with GW9662 which is specific target to PPARγ on tumour suppression in mice. The results in current work showed that the treatment of CRPC cells with GW9662 produced a similar suppression of tumour growth to that obtained by SBFI26 and dmrFABP5 **(Fig. 5.4)** (**Fig. 5.6)**. This result suggests that the suppressive mechanisms of both inhibitors may be similar to that achieved by GW9662 which is related to the FABP5-PPARγ-signal transduction pathway. In addition, we did not observe similar changes when tumour was treated with first and seven-days after inoculation, indicate that there is no effect in the tumour incidence **(Fig. 5.1)**. Furthermore, the results showed that no significant changed in tumour growth between combination treatment and each inhibitor alone **(Fig. 5.3) (Fig. 5.6)**. Although our results in this study showed that GW9662 produced significant reduction in the sizes of primary tumours developed from cancer cells inoculated subcutaneously in flanks of the mice, using GW9662 as a therapeutic reagent is hardly possible because of its none-specificity.

After SBFI26 and dmrFABP5 treatment, primary tumours became much smaller in the treated mice. The reduction in the number of metastases in the treated mice may be related to the decrease in sizes of primary tumours. It has been reported that reduction in the size of primary tumour in a patient with prostate metastasis may be used as a further therapeutic indication for a relatively prolonged patient survival time (287). From biological point of view, growth and expansion of primary tumours request increased level of blood supply and hence the increased angiogenesis. The newly increased blood vessels can provide increased escaping routes by which cells can leave the primary tumour and arrest in a new organ in the secondary sites (288). It has been known that treatment of primary tumour may not only have a inhibitive effect on the localized tumour growth but also in the distant tumours that grow as metastasis (289). Thus, the results obtained in this work suggest that both inhibitors may delay the progression of metastatic disease and may translate to prolonged survival, especially when treated with dmrFABP5.

6.1.6 SBFI26 inhibited the biological function of FABP5 through block its transportation of fatty acids

Based on the highly binding affinity of SBFI26 with FABP5, we identify a mechanism of cellular inhibition whereby SBFI26 suppress FABP5 to transport fatty acids by using BODIPY-labelled fatty acid analogues. BODIPY binds to FABPs with high affinity at a site similar to that for the natural fatty acid, endoplasmic reticulum, mitochondria, and lipid droplets in cells (248).

Our results of FABP5 expression in benign and malignant prostate cells using BODIPY observed that the highly malignant prostate cancer PC3-M cells were 25% higher uptake of BODIPY compared to benign prostate PNT2 cells **(Fig. 5.7) (Fig. 5.8)**. This results suggest that the highly expression of FABP5 seems to be the cause

of that difference in PC3-M and the other 75% BODIPY uptake is related to bind with other cellular compartments and the similar results have been observed by others (290). It has been confirmed that BODIPY provide a useful drug discovery tool as a competitor to screen for inhibitors of FABPs into a variety of cell types (291). The results of fatty acid uptake assay using BODIPY-labelled fatty acid analogues showed that addition of SBFI26 to PC3-M cells inhibited BODIPY uptake **(Fig. 5.9, A)** (**Fig. 5.10)**. However, dmrFABP5 did not produce any noticeable changes in fatty acid uptake of PC3-M cells **(Fig. 5.9, B)** (**Fig. 5.10)**. These results suggested that the mechanism of action of SBFI26 is directly prevent FABP5 from transporting fatty acids. SBFI26 prevented the natural cellular fatty acids from being transported into the cells and being delivered to PPARγ and may result in a reduction of the stimulation of PPARγ by fatty acids. Therefore, PPARγ is no longer able to upregulate the down-stream cancer-promoting genes and to suppress apoptosis or promote angiogenesis (251,252). Since dmrFABP5 did not reduce the fatty acid uptake by PC3-M cells, it may act through a mechanism different from SBFI26 to interfere PPARγ.

6.1.7 SBFI26 and dmrFABP5 act as inhibitors to prevent PPARγ to be activated by fatty acids transported by FABP5

Recent study showed that the FABP5-PPARγ-VEGF signalling transduction axis, not the AR-initiated pathway, is a dominant route for transduction of malignant signals in CRPC cells (217). When FABP5 expression is increased, excessive amounts of fatty acids are transported into the nucleus, where they act as signalling molecules to stimulate their nuclear receptor PPARγ. It has been identified that prostate cancer cell lines and clinical samples exhibit elevated levels of PPARγ (249,250). Two biologically active isoforms of PPARγ, PPARγ1 and PPARγ2, are expressed in human tissues (250,253). In this work, for accurate quantitation of Western blots, results were

depended on a linear relationship between the signals (OD) and the amount of protein loaded. Our results showed that low malignant prostate LNCaP cells expressed low levels of PPARγ isoforms. Treatment of LNCaP cells with wtrFABP5 increased the expression of two isoforms. However, this expression was abolished by dmrFABP5 treatment **(Fig. 5.14, A** and **B)**. In addition, CRPC PC3-M cells expressed high levels of two PPARγ isoforms. Treatment of PC3-M cells with SBFI26 or dmrFABP5 reduced the expression of two isoforms **(Fig. 5.13, A** and **B)**. These results suggest that both SBFI26 and dmrFABP5 may act as inhibitors to block the stimulation of PPARγ by fatty acids transported by FABP5. Previous work suggested that the dependency of the prostate cancer cells on the FABP5-related pathway was gradually increased with a correspondingly reduced dependency on the AR-initiated pathway until the former became completely dominant (217). The results of this work showed that both SBFI26 and dmrFABP5 produced a reduction in both PPARγ isoforms in androgen-responsive, moderately-malignant 22RV1 cells by an average of 33.5% **(Fig. 5.15, A and B)**. The level of PPARγ isoforms reduction in 22RV1 cells after treatment with SBFI26 and dmrFABP5 was much smaller than that caused in CRPC PC3-M cells (average reduction was about 50%). These results suggest that treatment by suppression of the FABP5-pathway is more effective in CRPC cells. These results support the previous finding that ADT would lose its effect gradually as the cancer cell become more independent of androgen for growth (217,256).

6.1.8 Suppression of FABP5 and its downstream pathways reduced the tumorigenicity and metastases of CRPC cells

In normal condition FABPs including FABP5 are responsible for binding hydrophobic ligands (fatty acids) and for transporting these ligands to the appropriate compartments within the normal cells (292). As fatty acids are essential for the formation of

membrane components, energy sources, and the stimulation of cellular signalling molecules during normal cell proliferation (182,199), over expression of FABP5 might play an important role in cancer cell proliferation. Our previous work found that FABP5 acted with PPARγ in a coordinated manner to promote malignant progression in CRPC cells and hence, PPARγ is more likely to be the receptor for the fatty acids transported by FABP5 (192). PPARγ is a fatty acid receptor localised in the nuclear membrane (198,293,294). It has been suggested that transporting fatty acids to PPARγ through FABP5 may be a short delivery process, after which FABP5 may return to the cytoplasm, rather than staying on the nuclear membrane (217). However, it has been confirmed that the expression of FABP5 in prostate cancer tissues localised in the cytoplasm and nucleus (211). It has been demonstrated that a high affinity with structural molecular interaction between FABPs and PPARs families by protein-protein contacts (198,295). In addition, it was confirmed that the observed interaction of both proteins is independent of ligand binding (198).

In our results, the inhibition of phosphorylation of PPARγ by SBFI26 is likely to cause inhibition of fatty acid uptake. It has been suggested that SBFI26 is a weak agonist of PPARγ (223). Since SBFI26 suppressed fatty acid uptake by replacing fatty acids which bind to FABP5, it is possible that some SBFI26 may be delivered to activate PPARγ in a weaker way than with the fatty acids. This may be the reason why SBFI26 is a less effective inhibitor than dmrFABP5. Thus, SBFI26 interferes with the FABP5 signalling pathway at the initial stage of this signal by binding directly to FABP5 to inhibit cellular fatty acid uptake. Since the structure of dmrFABP5 is very similar to native wild type FABP5, it is possible that dmrFABP5 may occupy the same binding site as native wild type FABP5 so as to prevent it from delivering fatty acids to PPARγ. Therefore, dmrFABP5 indirectly suppresses FABP5, works by blocking PPARγ

receptor and prevents it from activating the down-stream regulated cancer-promoting genes. Since the inhibitory effects of SBFI26 and dmrFABP5 are exerted at 2 different points in the same signal transduction pathway, no further suppression is anticipated when used in combination.

6.1.9 Potential clinical implementation of FABP5 inhibitors in CRPC

Clinically, ADT is a main therapy against prostate cancer, because growth of prostate cancer is dependent on androgen at early stages of treatment. ADT alone does not fully cure prostate cancer and prolonged therapy often make conversion to CRPC. Therefore, based on results in this study and other studies, right treatment at early stages of prostate cancer is important. Previous pathological studies have shown that FABP5 overexpression is strongly associated with prostate cancer progression and metastasis. Interestingly, this study indicates that inhibition the biological functions of FABP5 can be an effective treatment to suppress multiple steps that are important in tumour progression and metastasis in nude mice. The results obtained from targeting FABP5 biological function provided important clues for the treatment of human patients with CRPC and a theoretical basis for resolving some possible problems raised from the treatment by targeting PPARγ or VEGF.

In summary, we have targeted the FABP5-PPARγ signalling pathway by suppressing the biological activity of FABP5 so that the signalling molecules fatty acids cannot be passed to PPARγ. Thus, this signalling axis is ceased to functioning due to the lack of fatty acids stimulation. Therefore, the FABP5 inhibitors suppressed the malignant progression of CRPC by cutting off the FABP5-related signalling transduction chain and they may be candidate reagents for a CRPC treatment.

6.2 Conclusion

Based on the data achieved in this study, several important findings have been established:

1- This study clearly establishes that a mutated FABP5 (dmrFABP5) incapable of binding to fatty acids can be used as a bio-inhibitor to suppress the biological activity of FABP5.

2- SBFI26, a lead inhibitor selected from a group of chemical compounds, has a highly binding affinity with FABP5.

3- Both novel inhibitors of FABP5 (SBFI26 and dmrFABP5) can suppress the proliferation, migration, invasion and colony formation of castration resistant prostate cancer PC3-M cells *in vitro*.

4- Both inhibitors produce a highly significant suppression of both primary tumours and metastases of cancer cells implanted orthotopically into the mouse prostate gland. DmrFABP5, incapable of binding to fatty acids, produced a greater suppression of both primary tumour and metastases than the chemical inhibitor SBFI26.

5- SBFI26 competitively binds to FABP5 and hence suppresses cellular fatty-acid uptake. SBFI26 directly suppresses the biological function of FABP5 and work as a weak agonist to PPARγ to suppress the CRPC by inhibiting fatty acid uptake.

6- DmrFABP5 indirectly suppresses the biological function of FABP5, works by blocking the fatty-acid stimulation of PPARγ and prevents it from activating the down-stream regulated cancer-promoting genes.

6.3 Future work

In this work, we suppressed the malignant progression of CRPC by using FABP5 inhibitors to cut off the FABP5-PPARγ related signalling transduction chain at two different points. SBFI26 interferes with this pathway at the original stage of the initial signal transduction by binding competitively to FABP5 to inhibit cellular fatty acid uptake. The mechanism involved in the biological action of SBFI26 is now fully understood. The bio-inhibitor dmrFABP5 indirectly suppresses the biological function of FABP5 and works by blocking the fatty-acid stimulation of PPARγ to prevent it from activating the down-stream regulatory cancer-promoting genes. Since the exact route of fatty-acid delivery to PPARγ is not known, how dmrFABP5 inhibits PPARγ is not fully understood. Further study is needed to understand fully the detailed molecular mechanisms involved in the suppressive effect of dmrFABP5 on PPARγ activation. In addition, further preclinical work on toxicity and pharmacokinetics studies are needed before the true clinical application of these inhibitors.

References

1. Ferlay J, Soerjomataram I, Dikshit R, Eser S, Mathers C, Rebelo M, et al. Cancer incidence and mortality worldwide: sources, methods and major patterns in GLOBOCAN 2012. International journal of cancer Journal international du cancer 2015;136(5):E359-86.

2. Torre LA, Bray F, Siegel RL, Ferlay J, Lortet-Tieulent J, Jemal A. Global cancer statistics, 2012. CA: a cancer journal for clinicians 2015;65(2):87-108.

3. Walters S, Quaresma M, Coleman MP, Gordon E, Forman D, Rachet B. Geographical variation in cancer survival in England, 1991-2006: an analysis by Cancer Network. Journal of epidemiology and community health 2011;65(11):1044-52.

4. Bray F, Jemal A, Grey N, Ferlay J, Forman D. Global cancer transitions according to the Human Development Index (2008-2030): a population-based study. The Lancet Oncology 2012;13(8):790-801.

5. CRUK. 2014 The 10 Most Commonly Diagnosed Cancers, World, 2012 Estimates. Cancer Research UK <http://www.cancerresearchuk.org/health-professional/cancer-statistics/worldwide-cancer/incidence>.Accessed October 2016.

6. CRUK. 2016 All Cancers Excluding Non-Melanoma Skin Cancer (C00-C97 Excl. C44), European Age-Standardised Incidence Rates, Great Britain, 1979-2013.Cancer Research UK<http://www.cancerresearchuk.org/health-professional/cancer-statistics/incidence/all-cancers-combined>.Accessed October 2016.

7. Ferlay J SI, Ervik M, et al. GLOBOCAN 2012 v1.0. 2013 Cancer Incidence and Mortality Worldwide: IARC CancerBase No. 11 [Internet]. Lyon, France: International Agency for Research on Cancer. <http://globocan.iarc.fr (link is external), accessed December 2013.>.

8. Hsing AW, Tsao L, Devesa SS. International trends and patterns of prostate cancer incidence and mortality. International journal of cancer Journal international du cancer 2000;85(1):60-7.

9. Bray F, Lortet-Tieulent J, Ferlay J, Forman D, Auvinen A. Prostate cancer incidence and mortality trends in 37 European countries: an overview. European journal of cancer (Oxford, England : 1990) 2010;46(17):3040-52.

10. Ferlay J, Steliarova-Foucher E, Lortet-Tieulent J, Rosso S, Coebergh JW, Comber H, et al. Cancer incidence and mortality patterns in Europe: estimates for 40 countries in 2012. European journal of cancer (Oxford, England : 1990) 2013;49(6):1374-403.

11. ONS. 2014 Cancer Registration Statistics, England Statistical bulletins. Office for National Statistics < http://www.ons.gov.uk/ons/rel/vsob1/cancer-statistics-registrations--england--series-mb1-/index.htm>.

12. WCISU. 2015 Prostate Cancer, The Latest Welsh Statistics. Welsh Cancer Intelligence and Surveillance Unit <http://www.wales.nhs.uk/sites3/page.cfm?orgid=242&pid=59080>.

13. CRUK. 2016 Prostate Cancer (C61), Average Number of New Cases per Year and Age-Specific Incidence Rates, Males, UK, 2012-2014. Cancer Research UK<http://www.cancerresearchuk.org/health-professional/cancer-statistics/statistics-by-cancer-type/prostate-cancer/incidence>.Accessed December 2016.

14. CRUK. 2016 Prostate Cancer (C61), European Age-Standardised Incidence Rates, by Age, Males, Great Britain, 1979-2013. Cancer Research UK <http://www.cancerresearchuk.org/health-professional/cancer-statistics/statistics-by-cancer-type/prostate-cancer/incidence>. Accessed October 2016.

15. ONS. 2015 Deaths registered in England and Wales Statistical bulletins. Office for National Statistics <https://www.ons.gov.uk/peoplepopulationandcommunity/birthsdeathsandmarriages/deaths/bulletins/deathsregistrationsummarytables/previousReleases>.

16. CRUK. 2016 Prostate Cancer (C61) Average Number of Deaths per Year and Age-Specific Mortality Rates, Males, UK, 2012-2014. Cancer Research UK <http://www.cancerresearchuk.org/health-professional/cancer-statistics/statistics-by-cancer-type/prostate-cancer/mortality>. Accessed October 2016.

17. NRS. 2015 Births, Deaths and Other Vital Events - Preliminary Annual Figures. Natinal Record of Scotland <http://gro-scotland.gov.uk/statistics/theme/vital-events/general/ref-tables/index.html>.

18. CRUK. 2016 Prostate Cancer (C61), European Age-Standardised Mortality Rates, By Age, Males, UK, 1971-2014. Cancer Research UK <http://www.cancerresearchuk.org/health-professional/cancer-statistics/statistics-by-cancer-type/prostate-cancer/mortality>.Accessed October 2016.

19. Brenner H, Arndt V. Long-term survival rates of patients with prostate cancer in the prostate-specific antigen screening era: population-based estimates for the year 2000 by period analysis. Journal of clinical oncology : official journal of the American Society of Clinical Oncology 2005;23(3):441-7.

20. Holmberg L, Robinson D, Sandin F, Bray F, Linklater KM, Klint A, et al. A comparison of prostate cancer survival in England, Norway and Sweden: a population-based study. Cancer epidemiology 2012;36(1):e7-12.

21. Lin DW, Porter M, Montgomery B. Treatment and survival outcomes in young men diagnosed with prostate cancer: a population based cohort study. Cancer 2009;115(13):2863-71.

22. NCRAS. 2010 Prostate Cancer Survival - NCIN Data Briefing. National Cancer Registration and Analysis Service <http://www.ncin.org.uk/publications/data_briefings/prostate_cancer_survival>.

23. Woods VD, Montgomery SB, Belliard JC, Ramírez-Johnson J, Wilson CM. Culture, Black Men, and Prostate Cancer: What Is Reality? Cancer control : journal of the Moffitt Cancer Center 2004;11(6):388-96.

24. Crawford ED. Epidemiology of prostate cancer. Urology 2003;62(6, Supplement 1):3-12.

25. Gann PH. Risk Factors for Prostate Cancer. Reviews in Urology 2002;4(Suppl 5):S3-S10.

26. Goldgar DE, Easton DF, Cannon-Albright LA, Skolnick MH. Systematic population-based assessment of cancer risk in first-degree relatives of cancer probands. Journal of the National Cancer Institute 1994;86(21):1600-8.

27. Cerhan JR, Parker AS, Putnam SD, Chiu BC, Lynch CF, Cohen MB, et al. Family history and prostate cancer risk in a population-based cohort of Iowa men. Cancer epidemiology, biomarkers & prevention : a publication of the American Association for Cancer Research, cosponsored by the American Society of Preventive Oncology 1999;8(1):53-60.

28. Powell IJ. The Precise Role of Ethnicity and Family History on Aggressive Prostate Cancer: A Review Analysis. Archivos espanoles de urologia 2011;64(8):711-19.

29. Kicinski M, Vangronsveld J, Nawrot TS. An epidemiological reappraisal of the familial aggregation of prostate cancer: a meta-analysis. PloS one 2011;6(10):e27130.

30. Anderson DE, Badzioch MD. Familial effects of prostate and other cancers on lifetime breast cancer risk. Breast cancer research and treatment 1993;28(2):107-13.

31. Beebe-Dimmer JL, Yee C, Cote ML, Petrucelli N, Palmer N, Bock C, et al. Familial clustering of breast and prostate cancer and risk of postmenopausal breast cancer in the Women's Health Initiative Study. Cancer 2015;121(8):1265-72.

32. Castro E, Eeles R. The role of BRCA1 and BRCA2 in prostate cancer. Asian Journal of Andrology 2012;14(3):409-14.

33. Levy-Lahad E, Friedman E. Cancer risks among BRCA1 and BRCA2 mutation carriers. British journal of cancer 2007;96(1):11-5.

34. Wolk A. Diet, lifestyle and risk of prostate cancer. Acta oncologica (Stockholm, Sweden) 2005;44(3):277-81.

35. Niclis C, Diaz Mdel P, Eynard AR, Roman MD, La Vecchia C. Dietary habits and prostate cancer prevention: a review of observational studies by focusing on South America. Nutrition and cancer 2012;64(1):23-33.

36. Sonn GA, Aronson W, Litwin MS. Impact of diet on prostate cancer: a review. Prostate cancer and prostatic diseases 2005;8(4):304-10.

37. Baade PD, Youlden DR, Krnjacki LJ. International epidemiology of prostate cancer: geographical distribution and secular trends. Molecular nutrition & food research 2009;53(2):171-84.

38. Barnard RJ, Ngo TH, Leung PS, Aronson WJ, Golding LA. A low-fat diet and/or strenuous exercise alters the IGF axis in vivo and reduces prostate tumor cell growth in vitro. The Prostate 2003;56(3):201-6.

39. Pelser C, Mondul AM, Hollenbeck AR, Park Y. Dietary fat, fatty acids, and risk of prostate cancer in the NIH-AARP diet and health study. Cancer epidemiology, biomarkers & prevention : a publication of the American Association for Cancer Research, cosponsored by the American Society of Preventive Oncology 2013;22(4):697-707.

40. Rose DP, Connolly JM. Effects of fatty acids and eicosanoid synthesis inhibitors on the growth of two human prostate cancer cell lines. The Prostate 1991;18(3):243-54.

41. Hori S, Butler E, McLoughlin J. Prostate cancer and diet: food for thought? BJU international 2011;107(9):1348-59.

42. Hiatt RA, Armstrong MA, Klatsky AL, Sidney S. Alcohol consumption, smoking, and other risk factors and prostate cancer in a large health plan cohort in California (United States). Cancer causes & control : CCC 1994;5(1):66-72.

43. Wilson AH. The prostate gland: a review of its anatomy, pathology, and treatment. Jama 2014;312(5):562.

44. Bhavsar A, Verma S. Anatomic Imaging of the Prostate. BioMed Research International 2014;2014:728539.

45. BFGallery. 2010 Anatomy and physiology/prostate gland. Biology Forums Gallery <http://biology-forums.com>.

46. Cohen RJ, Shannon BA, Phillips M, Moorin RE, Wheeler TM, Garrett KL. Central zone carcinoma of the prostate gland: a distinct tumor type with poor prognostic features. The Journal of urology 2008;179(5):1762-7.

47. Kayhan A, Fan X, Oommen J, Oto A. Multi-parametric MR imaging of transition zone prostate cancer: Imaging features, detection and staging. World Journal of Radiology 2010;2(5):180-87.

48. McNeal JE. The zonal anatomy of the prostate. The Prostate 1981;2(1):35-49.

49. Vargas HA, Akin O, Franiel T, Goldman DA, Udo K, Touijer KA, et al. Normal Central Zone of the Prostate and Central Zone Involvement by Prostate Cancer: Clinical and MR Imaging Implications. Radiology 2012;262(3):894-902.

50. Wadhera P. An introduction to acinar pressures in BPH and prostate cancer. Nat Rev Urol 2013;10(6):358-66.

51. Mawhinney M, Mariotti A. Physiology, pathology and pharmacology of the male reproductive system. Periodontology 2000 2013;61(1):232-51.

52. Cunha GR, Hayward SW, Dahiya R, Foster BA. Smooth muscle-epithelial interactions in normal and neoplastic prostatic development. Acta anatomica 1996;155(1):63-72.

53. Liu AY, True LD. Characterization of Prostate Cell Types by CD Cell Surface Molecules. The American Journal of Pathology 2002;160(1):37-43.

54. Czyz J, Szpak K, Madeja Z. The role of connexins in prostate cancer promotion and progression. Nat Rev Urol 2012;9(5):274-82.

55. Prajapati A, Gupta S, Mistry B, Gupta S. Prostate Stem Cells in the Development of Benign Prostate Hyperplasia and Prostate Cancer: Emerging Role and Concepts. BioMed Research International 2013;2013:107954.

56. De Marzo AM, Meeker AK, Epstein JI, Coffey DS. Prostate stem cell compartments: expression of the cell cycle inhibitor p27Kip1 in normal, hyperplastic, and neoplastic cells. The American journal of pathology 1998;153(3):911-9.

57. Long RM, Morrissey C, Fitzpatrick JM, Watson RW. Prostate epithelial cell differentiation and its relevance to the understanding of prostate cancer therapies. Clinical science (London, England : 1979) 2005;108(1):1-11.

58. Papini S, Rosellini A, Campani D, DeMatteis A, Selli C, Revoltella RP. Selective growth of epithelial basal cells from human prostate in a three-dimensional organ culture. The Prostate 2004;59(4):383-92.

59. Bonkhoff H, Stein U, Remberger K. The proliferative function of basal cells in the normal and hyperplastic human prostate. The Prostate 1994;24(3):114-8.

60. Wang Y, Hayward S, Cao M, Thayer K, Cunha G. Cell differentiation lineage in the prostate. Differentiation; research in biological diversity 2001;68(4-5):270-9.

61. Aumuller G, Leonhardt M, Janssen M, Konrad L, Bjartell A, Abrahamsson PA. Neurogenic origin of human prostate endocrine cells. Urology 1999;53(5):1041-8.

62. Bonkhoff H. Neuroendocrine cells in benign and malignant prostate tissue: morphogenesis, proliferation, and androgen receptor status. The Prostate Supplement 1998;8:18-22.

63. Cohen RJ, Glezerson G, Taylor LF, Grundle HA, Naude JH. The neuroendocrine cell population of the human prostate gland. The Journal of urology 1993;150(2 Pt 1):365-8.

64. Huang J, Wu C, di Sant'Agnese PA, Yao JL, Cheng L, Na Y. Function and molecular mechanisms of neuroendocrine cells in prostate cancer. Analytical and quantitative cytology and histology / the International Academy of Cytology [and] American Society of Cytology 2007;29(3):128-38.

65. Sun Y, Niu J, Huang J. Neuroendocrine differentiation in prostate cancer. American Journal of Translational Research 2009;1(2):148-62.

66. van Leenders GJLH, Gage WR, Hicks JL, van Balken B, Aalders TW, Schalken JA, et al. Intermediate Cells in Human Prostate Epithelium Are Enriched in Proliferative Inflammatory Atrophy. The American Journal of Pathology 2003;162(5):1529-37.

67. Elterman DS, Barkin J, Kaplan SA. Optimizing the management of benign prostatic hyperplasia. Therapeutic Advances in Urology 2012;4(2):77-83.

68. Berry SJ, Coffey DS, Walsh PC, Ewing LL. The development of human benign prostatic hyperplasia with age. The Journal of urology 1984;132(3):474-9.

69. Dhingra N, Bhagwat D. Benign prostatic hyperplasia: An overview of existing treatment. Indian Journal of Pharmacology 2011;43(1):6-12.

70. Miah S, Catto J. BPH and prostate cancer risk. Indian Journal of Urology : IJU : Journal of the Urological Society of India 2014;30(2):214-18.

71. Ellis WJ, Brawer MK. PSA in benign prostatic hyperplasia and prostatic intraepithelial neoplasia. The Urologic clinics of North America 1993;20(4):621-5.

72. Polascik TJ, Oesterling JE, Partin AW. Prostate specific antigen: a decade of discovery--what we have learned and where we are going. The Journal of urology 1999;162(2):293-306.

73. Jung K, Elgeti U, Lein M, Brux B, Sinha P, Rudolph B, et al. Ratio of free or complexed prostate-specific antigen (PSA) to total PSA: which ratio improves differentiation between benign prostatic hyperplasia and prostate cancer? Clinical chemistry 2000;46(1):55-62.

74. Sershon PD, Barry MJ, Oesterling JE. Serum prostate-specific antigen discriminates weakly between men with benign prostatic hyperplasia and patients with organ-confined prostate cancer. European urology 1994;25(4):281-7.

75. Zlotta AR, Djavan B, Petein M, Susani M, Marberger M, Schulman CC. Prostate specific antigen density of the transition zone for predicting pathological stage of localized prostate cancer in patients with serum prostate specific antigen less than 10 ng./ml. The Journal of urology 1998;160(6 Pt 1):2089-95.

76. Izumi K, Mizokami A, Lin W-J, Lai K-P, Chang C. Androgen Receptor Roles in the Development of Benign Prostate Hyperplasia. The American Journal of Pathology 2013;182(6):1942-49.

77. van der Sluis TM, Meuleman EJ, van Moorselaar RJ, Bui HN, Blankenstein MA, Heijboer AC, et al. Intraprostatic testosterone and dihydrotestosterone. Part II: concentrations after androgen hormonal manipulation in men with benign prostatic hyperplasia and prostate cancer. BJU international 2012;109(2):183-8.

78. Brawer MK. Prostatic Intraepithelial Neoplasia: An Overview. Reviews in Urology 2005;7(Suppl 3):S11-S18.

79. Foster CS, Bostwick DG, Bonkhoff H, Damber JE, van der Kwast T, Montironi R, et al. Cellular and molecular pathology of prostate cancer precursors. Scandinavian journal of urology and nephrology Supplementum 2000(205):19-43.

80. Zlotta AR, Schulman CC. Clinical Evolution of Prostatic Intraepithelial Neoplasia. European Urology 1999;35(5-6):498-503.

81. Cheville JC, Reznicek MJ, Bostwick DG. The focus of "atypical glands, suspicious for malignancy" in prostatic needle biopsy specimens: incidence, histologic features, and clinical follow-up of cases diagnosed in a community practice. American journal of clinical pathology 1997;108(6):633-40.

82. Bostwick DG, Liu L, Brawer MK, Qian J. High-Grade Prostatic Intraepithelial Neoplasia. Reviews in Urology 2004;6(4):171-79.

83. Harnden P, Shelley MD, Coles B, Staffurth J, Mason MD. Should the Gleason grading system for prostate cancer be modified to account for high-grade tertiary components? A systematic review and meta-analysis. The Lancet Oncology 2007;8(5):411-9.

84. Humphrey PA. Gleason grading and prognostic factors in carcinoma of the prostate. Modern pathology : an official journal of the United States and Canadian Academy of Pathology, Inc 2004;17(3):292-306.

85. NCI. 1977 MORPHOLOGY & GRADE. National Cancer Institute <http://training.seer.cancer.gov/prostate/abstract-code-stage/morphology.html>.

86. Epstein JI, Zelefsky MJ, Sjoberg DD, Nelson JB, Egevad L, Magi-Galluzzi C, et al. A Contemporary Prostate Cancer Grading System: A Validated Alternative to the Gleason Score. European urology 2015.

87. Shah RB. Current perspectives on the Gleason grading of prostate cancer. Archives of pathology & laboratory medicine 2009;133(11):1810-6.

88. Cussenot O, Berthon P, Berger R, Mowszowicz I, Faille A, Hojman F, et al. Immortalization of human adult normal prostatic epithelial cells by liposomes containing large T-SV40 gene. The Journal of urology 1991;146(3):881-6.

89. Berthon P, Cussenot O, Hopwood L, Leduc A, Maitland N. Functional expression of sv40 in normal human prostatic epithelial and fibroblastic cells - differentiation pattern of nontumorigenic cell-lines. International journal of oncology 1995;6(2):333-43.

90. Horoszewicz JS, Leong SS, Chu TM, Wajsman ZL, Friedman M, Papsidero L, et al. The LNCaP cell line--a new model for studies on human prostatic carcinoma. Progress in clinical and biological research 1980;37:115-32.

91. Horoszewicz JS, Leong SS, Kawinski E, Karr JP, Rosenthal H, Chu TM, et al. LNCaP model of human prostatic carcinoma. Cancer research 1983;43(4):1809-18.

92. Sramkoski RM, Pretlow TG, 2nd, Giaconia JM, Pretlow TP, Schwartz S, Sy MS, et al. A new human prostate carcinoma cell line, 22Rv1. In vitro cellular & developmental biology Animal 1999;35(7):403-9.

93. Hartel A, Didier A, Pfaffl MW, Meyer HH. Characterisation of gene expression patterns in 22RV1 cells for determination of environmental androgenic/antiandrogenic compounds. The Journal of steroid biochemistry and molecular biology 2003;84(2-3):231-8.

94. Stone KR, Mickey DD, Wunderli H, Mickey GH, Paulson DF. Isolation of a human prostate carcinoma cell line (DU 145). International journal of cancer Journal international du cancer 1978;21(3):274-81.

95. Pulukuri SM, Gondi CS, Lakka SS, Jutla A, Estes N, Gujrati M, et al. RNA interference-directed knockdown of urokinase plasminogen activator and urokinase plasminogen activator receptor inhibits prostate cancer cell invasion, survival, and tumorigenicity in vivo. The Journal of biological chemistry 2005;280(43):36529-40.

96. Kaighn ME, Narayan KS, Ohnuki Y, Lechner JF, Jones LW. Establishment and characterization of a human prostatic carcinoma cell line (PC-3). Investigative urology 1979;17(1):16-23.

97. Tai S, Sun Y, Squires JM, Zhang H, Oh WK, Liang C-Z, et al. PC3 Is a Cell Line Characteristic of Prostatic Small Cell Carcinoma. The Prostate 2011;71(15):1668-79.

98. Pettaway CA, Pathak S, Greene G, Ramirez E, Wilson MR, Killion JJ, et al. Selection of highly metastatic variants of different human prostatic carcinomas using orthotopic implantation in nude mice. Clinical cancer research : an official journal of the American Association for Cancer Research 1996;2(9):1627-36.

99. Taplin ME, Ho SM. Clinical review 134: The endocrinology of prostate cancer. The Journal of clinical endocrinology and metabolism 2001;86(8):3467-77.

100. Cunha GR, Donjacour AA, Cooke PS, Mee S, Bigsby RM, Higgins SJ, et al. The endocrinology and developmental biology of the prostate. Endocrine reviews 1987;8(3):338-62.

101. Srinivas-Shankar U, Wu FC. Drug insight: testosterone preparations. Nature clinical practice Urology 2006;3(12):653-65.

102. Dehm SM, Tindall DJ. Molecular regulation of androgen action in prostate cancer. Journal of cellular biochemistry 2006;99(2):333-44.

103. Heinlein CA, Chang C. Androgen receptor in prostate cancer. Endocrine reviews 2004;25(2):276-308.

104. Freedland SJ, Humphreys EB, Mangold LA, Eisenberger M, Dorey FJ, Walsh PC, et al. Death in patients with recurrent prostate cancer after radical prostatectomy: prostate-specific antigen doubling time subgroups and their associated contributions to all-cause mortality. Journal of clinical oncology : official journal of the American Society of Clinical Oncology 2007;25(13):1765-71.

105. Magnan S, Zarychanski R, Pilote L, Bernier L, Shemilt M, Vigneault E, et al. Intermittent vs Continuous Androgen Deprivation Therapy for Prostate Cancer: A Systematic Review and Meta-analysis. JAMA oncology 2015;1(9):1261-9.

106. Miyamoto H, Messing EM, Chang C. Androgen deprivation therapy for prostate cancer: current status and future prospects. The Prostate 2004;61(4):332-53.

107. Attar RM, Takimoto CH, Gottardis MM. Castration-Resistant Prostate Cancer: Locking Up the Molecular Escape Routes. Clinical Cancer Research 2009;15(10):3251-55.

108. Huggins C, Stevens RE, Jr, Hodges CV. Studies on prostatic cancer: Ii. the effects of castration on advanced carcinoma of the prostate gland. Archives of Surgery 1941;43(2):209-23.

109. Dar JA, Eisermann K, Masoodi KZ, Ai J, Wang D, Severance T, et al. N-terminal domain of the androgen receptor contains a region that can promote cytoplasmic localization. The Journal of steroid biochemistry and molecular biology 2014;139:16-24.

110. Attard G, Cooper CS, de Bono JS. Steroid hormone receptors in prostate cancer: a hard habit to break? Cancer cell 2009;16(6):458-62.

111. Marques RB, Dits NF, Erkens-Schulze S, van Weerden WM, Jenster G. Bypass mechanisms of the androgen receptor pathway in therapy-resistant prostate cancer cell models. PloS one 2010;5(10):e13500.

112. Harris WP, Mostaghel EA, Nelson PS, Montgomery B. Androgen deprivation therapy: progress in understanding mechanisms of resistance and optimizing androgen depletion. Nature clinical practice Urology 2009;6(2):76-85.

113. Scher HI, Sawyers CL. Biology of progressive, castration-resistant prostate cancer: directed therapies targeting the androgen-receptor signaling axis.

Journal of clinical oncology : official journal of the American Society of Clinical Oncology 2005;23(32):8253-61.

114. Koivisto P, Kononen J, Palmberg C, Tammela T, Hyytinen E, Isola J, et al. Androgen receptor gene amplification: a possible molecular mechanism for androgen deprivation therapy failure in prostate cancer. Cancer research 1997;57(2):314-9.

115. Visakorpi T, Hyytinen E, Koivisto P, Tanner M, Keinanen R, Palmberg C, et al. In vivo amplification of the androgen receptor gene and progression of human prostate cancer. Nature genetics 1995;9(4):401-6.

116. Linja MJ, Savinainen KJ, Saramaki OR, Tammela TL, Vessella RL, Visakorpi T. Amplification and overexpression of androgen receptor gene in hormone-refractory prostate cancer. Cancer research 2001;61(9):3550-5.

117. Sharma A, Yeow WS, Ertel A, Coleman I, Clegg N, Thangavel C, et al. The retinoblastoma tumor suppressor controls androgen signaling and human prostate cancer progression. The Journal of clinical investigation 2010;120(12):4478-92.

118. Quigley CA, De Bellis A, Marschke KB, el-Awady MK, Wilson EM, French FS. Androgen receptor defects: historical, clinical, and molecular perspectives. Endocrine reviews 1995;16(3):271-321.

119. Taplin ME, Rajeshkumar B, Halabi S, Werner CP, Woda BA, Picus J, et al. Androgen receptor mutations in androgen-independent prostate cancer: Cancer and Leukemia Group B Study 9663. Journal of clinical oncology : official journal of the American Society of Clinical Oncology 2003;21(14):2673-8.

120. Taplin ME, Bubley GJ, Ko YJ, Small EJ, Upton M, Rajeshkumar B, et al. Selection for androgen receptor mutations in prostate cancers treated with androgen antagonist. Cancer research 1999;59(11):2511-5.

121. Bergerat JP, Ceraline J. Pleiotropic functional properties of androgen receptor mutants in prostate cancer. Human mutation 2009;30(2):145-57.

122. Gaddipati JP, McLeod DG, Heidenberg HB, Sesterhenn IA, Finger MJ, Moul JW, et al. Frequent detection of codon 877 mutation in the androgen receptor gene in advanced prostate cancers. Cancer research 1994;54(11):2861-4.

123. Koivisto P, Kolmer M, Visakorpi T, Kallioniemi OP. Androgen receptor gene and hormonal therapy failure of prostate cancer. The American journal of pathology 1998;152(1):1-9.

124. Culig Z, Hobisch A, Cronauer MV, Cato AC, Hittmair A, Radmayr C, et al. Mutant androgen receptor detected in an advanced-stage prostatic carcinoma is activated by adrenal androgens and progesterone. Molecular endocrinology (Baltimore, Md) 1993;7(12):1541-50.

125. Zhao XY, Malloy PJ, Krishnan AV, Swami S, Navone NM, Peehl DM, et al. Glucocorticoids can promote androgen-independent growth of prostate cancer cells through a mutated androgen receptor. Nature medicine 2000;6(6):703-6.

126. Gottlieb B, Beitel LK, Nadarajah A, Paliouras M, Trifiro M. The androgen receptor gene mutations database: 2012 update. Human mutation 2012;33(5):887-94.

127. Chan SC, Dehm SM. Constitutive Activity of the Androgen Receptor. Advances in pharmacology (San Diego, Calif) 2014;70:327-66.

128. Heemers HV, Tindall DJ. Androgen receptor (AR) coregulators: a diversity of functions converging on and regulating the AR transcriptional complex. Endocrine reviews 2007;28(7):778-808.

129. Xu J, Wu RC, O'Malley BW. Normal and cancer-related functions of the p160 steroid receptor co-activator (SRC) family. Nature reviews Cancer 2009;9(9):615-30.

130. Wang Q, Zhou JL, Wang H, Ju Q, Ding Z, Zhou XL, et al. Inhibition effect of cypermethrin mediated by co-regulators SRC-1 and SMRT in interleukin-6-induced androgen receptor activation. Chemosphere 2016;158:24-9.

131. Chung AC, Zhou S, Liao L, Tien JC, Greenberg NM, Xu J. Genetic ablation of the amplified-in-breast cancer 1 inhibits spontaneous prostate cancer progression in mice. Cancer research 2007;67(12):5965-75.

132. Debes JD, Schmidt LJ, Huang H, Tindall DJ. p300 mediates androgen-independent transactivation of the androgen receptor by interleukin 6. Cancer research 2002;62(20):5632-6.

133. Chandrasekar T, Yang JC, Gao AC, Evans CP. Mechanisms of resistance in castration-resistant prostate cancer (CRPC). Translational Andrology and Urology 2015;4(3):365-80.

134. Wang Q, Li W, Liu XS, Carroll JS, Janne OA, Keeton EK, et al. A hierarchical network of transcription factors governs androgen receptor-dependent prostate cancer growth. Molecular cell 2007;27(3):380-92.

135. Augello MA, Hickey TE, Knudsen KE. FOXA1: master of steroid receptor function in cancer. The EMBO Journal 2011;30(19):3885-94.

136. Bohm M, Locke WJ, Sutherland RL, Kench JG, Henshall SM. A role for GATA-2 in transition to an aggressive phenotype in prostate cancer through modulation of key androgen-regulated genes. Oncogene 2009;28(43):3847-56.

137. Wang Q, Li W, Zhang Y, Yuan X, Xu K, Yu J, et al. Androgen receptor regulates a distinct transcription program in androgen-independent prostate cancer. Cell 2009;138(2):245-56.

138. Watson PA, Chen YF, Balbas MD, Wongvipat J, Socci ND, Viale A, et al. Constitutively active androgen receptor splice variants expressed in castration-

resistant prostate cancer require full-length androgen receptor. Proceedings of the National Academy of Sciences of the United States of America 2010;107(39):16759-65.

139. Zhang X, Morrissey C, Sun S, Ketchandji M, Nelson PS, True LD, et al. Androgen receptor variants occur frequently in castration resistant prostate cancer metastases. PloS one 2011;6(11):e27970.

140. Hornberg E, Ylitalo EB, Crnalic S, Antti H, Stattin P, Widmark A, et al. Expression of androgen receptor splice variants in prostate cancer bone metastases is associated with castration-resistance and short survival. PloS one 2011;6(4):e19059.

141. Li Y, Alsagabi M, Fan D, Bova GS, Tewfik AH, Dehm SM. Intragenic rearrangement and altered RNA splicing of the androgen receptor in a cell-based model of prostate cancer progression. Cancer research 2011;71(6):2108-17.

142. Welti J, Rodrigues DN, Sharp A, Sun S, Lorente D, Riisnaes R, et al. Analytical Validation and Clinical Qualification of a New Immunohistochemical Assay for Androgen Receptor Splice Variant-7 Protein Expression in Metastatic Castration-resistant Prostate Cancer. European urology 2016.

143. Guo Z, Yang X, Sun F, Jiang R, Linn DE, Chen H, et al. A novel androgen receptor splice variant is up-regulated during prostate cancer progression and promotes androgen depletion-resistant growth. Cancer research 2009;69(6):2305-13.

144. Mostaghel EA, Marck BT, Plymate SR, Vessella RL, Balk S, Matsumoto AM, et al. Resistance to CYP17A1 inhibition with abiraterone in castration-resistant prostate cancer: induction of steroidogenesis and androgen receptor splice variants. Clinical cancer research : an official journal of the American Association for Cancer Research 2011;17(18):5913-25.

145. Maughan BL, Antonarakis ES. Clinical Relevance of Androgen Receptor Splice Variants in Castration-Resistant Prostate Cancer. Current treatment options in oncology 2015;16(12):57.

146. van der Steen T, Tindall DJ, Huang H. Posttranslational Modification of the Androgen Receptor in Prostate Cancer. International Journal of Molecular Sciences 2013;14(7):14833-59.

147. Culig Z, Hobisch A, Cronauer MV, Radmayr C, Trapman J, Hittmair A, et al. Androgen receptor activation in prostatic tumor cell lines by insulin-like growth factor-I, keratinocyte growth factor, and epidermal growth factor. Cancer research 1994;54(20):5474-8.

148. Lamont KR, Tindall DJ. Minireview: Alternative activation pathways for the androgen receptor in prostate cancer. Molecular endocrinology (Baltimore, Md) 2011;25(6):897-907.

149. Craft N, Shostak Y, Carey M, Sawyers CL. A mechanism for hormone-independent prostate cancer through modulation of androgen receptor signaling by the HER-2/neu tyrosine kinase. Nature medicine 1999;5(3):280-5.

150. Nazareth LV, Weigel NL. Activation of the human androgen receptor through a protein kinase A signaling pathway. The Journal of biological chemistry 1996;271(33):19900-7.

151. Mahajan NP, Liu Y, Majumder S, Warren MR, Parker CE, Mohler JL, et al. Activated Cdc42-associated kinase Ack1 promotes prostate cancer progression via androgen receptor tyrosine phosphorylation. Proceedings of the National Academy of Sciences of the United States of America 2007;104(20):8438-43.

152. Holzbeierlein J, Lal P, LaTulippe E, Smith A, Satagopan J, Zhang L, et al. Gene expression analysis of human prostate carcinoma during hormonal therapy identifies androgen-responsive genes and mechanisms of therapy resistance. The American journal of pathology 2004;164(1):217-27.

153. Yuan X, Balk SP. Mechanisms mediating androgen receptor reactivation after castration. Urologic oncology 2009;27(1):36-41.

154. Cai C, He HH, Chen S, Coleman I, Wang H, Fang Z, et al. Androgen receptor gene expression in prostate cancer is directly suppressed by the androgen receptor through recruitment of lysine-specific demethylase 1. Cancer cell 2011;20(4):457-71.

155. Taylor BS, Schultz N, Hieronymus H, Gopalan A, Xiao Y, Carver BS, et al. Integrative genomic profiling of human prostate cancer. Cancer cell 2010;18(1):11-22.

156. Rameh LE, Cantley LC. The role of phosphoinositide 3-kinase lipid products in cell function. The Journal of biological chemistry 1999;274(13):8347-50.

157. Shaw RJ, Cantley LC. Ras, PI(3)K and mTOR signalling controls tumour cell growth. Nature 2006;441(7092):424-30.

158. Majumder PK, Sellers WR. Akt-regulated pathways in prostate cancer. Oncogene 2005;24(50):7465-74.

159. Mulholland DJ, Tran LM, Li Y, Cai H, Morim A, Wang S, et al. Cell autonomous role of PTEN in regulating castration-resistant prostate cancer growth. Cancer cell 2011;19(6):792-804.

160. Templeton AJ, Dutoit V, Cathomas R, Rothermundt C, Bartschi D, Droge C, et al. Phase 2 trial of single-agent everolimus in chemotherapy-naive patients with castration-resistant prostate cancer (SAKK 08/08). European urology 2013;64(1):150-8.

161. Carver BS, Chapinski C, Wongvipat J, Hieronymus H, Chen Y, Chandarlapaty S, et al. Reciprocal feedback regulation of PI3K and androgen receptor signaling in PTEN-deficient prostate cancer. Cancer cell 2011;19(5):575-86.

162. Thomas C, Lamoureux F, Crafter C, Davies BR, Beraldi E, Fazli L, et al. Synergistic targeting of PI3K/AKT pathway and androgen receptor axis significantly delays castration-resistant prostate cancer progression in vivo. Molecular cancer therapeutics 2013;12(11):2342-55.

163. Kuwano M, Uchiumi T, Hayakawa H, Ono M, Wada M, Izumi H, et al. The basic and clinical implications of ABC transporters, Y-box-binding protein-1 (YB-1) and angiogenesis-related factors in human malignancies. Cancer science 2003;94(1):9-14.

164. Gimenez-Bonafe P, Fedoruk MN, Whitmore TG, Akbari M, Ralph JL, Ettinger S, et al. YB-1 is upregulated during prostate cancer tumor progression and increases P-glycoprotein activity. The Prostate 2004;59(3):337-49.

165. Shiota M, Takeuchi A, Song Y, Yokomizo A, Kashiwagi E, Uchiumi T, et al. Y-box binding protein-1 promotes castration-resistant prostate cancer growth via androgen receptor expression. Endocrine-related cancer 2011;18(4):505-17.

166. Stratford AL, Fry CJ, Desilets C, Davies AH, Cho YY, Li Y, et al. Y-box binding protein-1 serine 102 is a downstream target of p90 ribosomal S6 kinase in basal-like breast cancer cells. Breast Cancer Research : BCR 2008;10(6):R99-R99.

167. Clark DE, Errington TM, Smith JA, Frierson HF, Jr., Weber MJ, Lannigan DA. The serine/threonine protein kinase, p90 ribosomal S6 kinase, is an important regulator of prostate cancer cell proliferation. Cancer research 2005;65(8):3108-16.

168. Shiota M, Yokomizo A, Takeuchi A, Itsumi M, Imada K, Kashiwagi E, et al. Inhibition of RSK/YB-1 signaling enhances the anti-cancer effect of enzalutamide in prostate cancer. The Prostate 2014;74(9):959-69.

169. Feldman BJ, Feldman D. The development of androgen-independent prostate cancer. Nature reviews Cancer 2001;1(1):34-45.

170. Anvari K, Seilanian Toussi M, Kalantari M, Naseri S, Karimi Shahri M, Ahmadnia H, et al. Expression of Bcl-2 and Bax in advanced or metastatic prostate carcinoma. Urology journal 2012;9(1):381-8.

171. Colombel M, Symmans F, Gil S, O'Toole KM, Chopin D, Benson M, et al. Detection of the apoptosis-suppressing oncoprotein bc1-2 in hormone-refractory human prostate cancers. The American journal of pathology 1993;143(2):390-400.

172. Moltzahn F, Thalmann GN. Cancer stem cells in prostate cancer. Translational Andrology and Urology 2013;2(3):242-53.

173. Li P, Yang R, Gao W-Q. Contributions of epithelial-mesenchymal transition and cancer stem cells to the development of castration resistance of prostate cancer. Molecular Cancer 2014;13:55-55.

174. Sun Y, Wang BE, Leong KG, Yue P, Li L, Jhunjhunwala S, et al. Androgen deprivation causes epithelial-mesenchymal transition in the prostate: implications for androgen-deprivation therapy. Cancer research 2012;72(2):527-36.

175. Isaacs JT. The biology of hormone refractory prostate cancer. Why does it develop? The Urologic clinics of North America 1999;26(2):263-73.

176. Lang SH, Frame FM, Collins AT. Prostate cancer stem cells. The Journal of pathology 2009;217(2):299-306.

177. Liu T, Xu F, Du X, Lai D, Liu T, Zhao Y, et al. Establishment and characterization of multi-drug resistant, prostate carcinoma-initiating stem-like cells from human prostate cancer cell lines 22RV1. Molecular and cellular biochemistry 2010;340(1-2):265-73.

178. Bui M, Reiter RE. Stem cell genes in androgen-independent prostate cancer. Cancer metastasis reviews 1998;17(4):391-9.

179. Discacciati A, Orsini N, Wolk A. Body mass index and incidence of localized and advanced prostate cancer--a dose-response meta-analysis of prospective studies. Annals of oncology : official journal of the European Society for Medical Oncology / ESMO 2012;23(7):1665-71.

180. Aucoin M, Cooley K, Knee C, Fritz H, Balneaves LG, Breau R, et al. Fish-Derived Omega-3 Fatty Acids and Prostate Cancer: A Systematic Review. Integrative cancer therapies 2016.

181. Apte SA, Cavazos DA, Whelan KA, Degraffenried LA. A low dietary ratio of omega-6 to omega-3 Fatty acids may delay progression of prostate cancer. Nutrition and cancer 2013;65(4):556-62.

182. Di Sebastiano KM, Mourtzakis M. The role of dietary fat throughout the prostate cancer trajectory. Nutrients 2014;6(12):6095-109.

183. Cavazos DA, Price RS, Apte SS, deGraffenried LA. Docosahexaenoic acid selectively induces human prostate cancer cell sensitivity to oxidative stress through modulation of NF-kappaB. The Prostate 2011;71(13):1420-8.

184. Ettinger SL, Sobel R, Whitmore TG, Akbari M, Bradley DR, Gleave ME, et al. Dysregulation of sterol response element-binding proteins and downstream effectors in prostate cancer during progression to androgen independence. Cancer research 2004;64(6):2212-21.

185. Migita T, Ruiz S, Fornari A, Fiorentino M, Priolo C, Zadra G, et al. Fatty acid synthase: a metabolic enzyme and candidate oncogene in prostate cancer. Journal of the National Cancer Institute 2009;101(7):519-32.

186. Myers JS, von Lersner AK, Sang QX. Proteomic Upregulation of Fatty Acid Synthase and Fatty Acid Binding Protein 5 and Identification of Cancer- and Race-Specific Pathway Associations in Human Prostate Cancer Tissues. Journal of Cancer 2016;7(11):1452-64.

187. Shah S, Carriveau WJ, Li J, Campbell SL, Kopinski PK, Lim HW, et al. Targeting ACLY sensitizes castration-resistant prostate cancer cells to AR antagonism by impinging on an ACLY-AMPK-AR feedback mechanism. Oncotarget 2016.

188. Wen S, Niu Y, Lee SO, Yeh S, Shang Z, Gao H, et al. Targeting fatty acid synthase with ASC-J9 suppresses proliferation and invasion of prostate cancer cells. Molecular carcinogenesis 2016.

189. Morgan EA, Forootan SS, Adamson J, Foster CS, Fujii H, Igarashi M, et al. Expression of cutaneous fatty acid-binding protein (C-FABP) in prostate cancer: potential prognostic marker and target for tumourigenicity-suppression. International journal of oncology 2008;32(4):767-75.

190. Adamson J, Morgan EA, Beesley C, Mei Y, Foster CS, Fujii H, et al. High-level expression of cutaneous fatty acid-binding protein in prostatic carcinomas and its effect on tumorigenicity. Oncogene 2003;22(18):2739-49.

191. Jing C, Beesley C, Foster CS, Chen H, Rudland PS, West DC, et al. Human cutaneous fatty acid-binding protein induces metastasis by up-regulating the expression of vascular endothelial growth factor gene in rat Rama 37 model cells. Cancer Res 2001;61(11):4357-64.

192. Bao Z, Malki MI, Forootan SS, Adamson J, Forootan FS, Chen D, et al. A Novel Cutaneous Fatty Acid–Binding Protein-Related Signaling Pathway Leading to Malignant Progression in Prostate Cancer Cells. Genes & Cancer 2013;4(7-8):297-314.

193. Chabowski A, Gorski J, Luiken JJ, Glatz JF, Bonen A. Evidence for concerted action of FAT/CD36 and FABPpm to increase fatty acid transport across the plasma membrane. Prostaglandins, leukotrienes, and essential fatty acids 2007;77(5-6):345-53.

194. Glatz JF, Luiken JJ, Bonen A. Membrane fatty acid transporters as regulators of lipid metabolism: implications for metabolic disease. Physiological reviews 2010;90(1):367-417.

195. Spitsberg VL, Matitashvili E, Gorewit RC. Association and coexpression of fatty-acid-binding protein and glycoprotein CD36 in the bovine mammary gland. European journal of biochemistry 1995;230(3):872-8.

196. Schroeder F, Petrescu AD, Huang H, Atshaves BP, McIntosh AL, Martin GG, et al. Role of fatty acid binding proteins and long chain fatty acids in modulating nuclear receptors and gene transcription. Lipids 2008;43(1):1-17.

197. Tan N-S, Shaw NS, Vinckenbosch N, Liu P, Yasmin R, Desvergne B, et al. Selective Cooperation between Fatty Acid Binding Proteins and Peroxisome Proliferator-Activated Receptors in Regulating Transcription. Molecular and cellular biology 2002;22(14):5114-27.

198. Wolfrum C, Borrmann CM, Borchers T, Spener F. Fatty acids and hypolipidemic drugs regulate peroxisome proliferator-activated receptors

alpha - and gamma-mediated gene expression via liver fatty acid binding protein: a signaling path to the nucleus. Proceedings of the National Academy of Sciences of the United States of America 2001;98(5):2323-8.

199. McArthur MJ, Atshaves BP, Frolov A, Foxworth WD, Kier AB, Schroeder F. Cellular uptake and intracellular trafficking of long chain fatty acids. Journal of lipid research 1999;40(8):1371-83.

200. Ishimura S, Furuhashi M, Watanabe Y, Hoshina K, Fuseya T, Mita T, et al. Circulating Levels of Fatty Acid-Binding Protein Family and Metabolic Phenotype in the General Population. PloS one 2013;8(11):e81318.

201. Ockner RK, Manning JA, Poppenhausen RB, Ho WK. A binding protein for fatty acids in cytosol of intestinal mucosa, liver, myocardium, and other tissues. Science (New York, NY) 1972;177(4043):56-8.

202. Smathers RL, Petersen DR. The human fatty acid-binding protein family: evolutionary divergences and functions. Human genomics 2011;5(3):170-91.

203. Haunerland NH, Spener F. Fatty acid-binding proteins--insights from genetic manipulations. Progress in lipid research 2004;43(4):328-49.

204. Crovetto CA, Córdoba OL. Structural and biochemical characterization and evolutionary relationships of the fatty acid-binding protein 10 (Fabp10) of hake (Merluccius hubbsi). Fish Physiology and Biochemistry 2016;42(1):149-65.

205. Chmurzynska A. The multigene family of fatty acid-binding proteins (FABPs): function, structure and polymorphism. Journal of applied genetics 2006;47(1):39-48.

206. Furuhashi M, Hotamisligil GS. Fatty acid-binding proteins: role in metabolic diseases and potential as drug targets. Nature reviews Drug discovery 2008;7(6):489-503.

207. Balendiran GK, Schnutgen F, Scapin G, Borchers T, Xhong N, Lim K, et al. Crystal structure and thermodynamic analysis of human brain fatty acid-binding protein. The Journal of biological chemistry 2000;275(35):27045-54.

208. Schachtrup C, Emmler T, Bleck B, Sandqvist A, Spener F. Functional analysis of peroxisome-proliferator-responsive element motifs in genes of fatty acid-binding proteins. The Biochemical journal 2004;382(Pt 1):239-45.

209. Tan NS, Shaw NS, Vinckenbosch N, Liu P, Yasmin R, Desvergne B, et al. Selective cooperation between fatty acid binding proteins and peroxisome proliferator-activated receptors in regulating transcription. Molecular and cellular biology 2002;22(14):5114-27.

210. Alshareeda AT, Rakha EA, Nolan CC, Ellis IO, Green AR. Fatty acid binding protein 7 expression and its sub-cellular localization in breast cancer. Breast cancer research and treatment 2012;134(2):519-29.

211. Forootan FS, Forootan SS, Malki MI, Chen D, Li G, Lin K, et al. The expression of C-FABP and PPARgamma and their prognostic significance in prostate cancer. International journal of oncology 2014;44(1):265-75.

212. Madsen P, Rasmussen HH, Leffers H, Honore B, Celis JE. Molecular cloning and expression of a novel keratinocyte protein (psoriasis-associated fatty acid-binding protein [PA-FABP]) that is highly up-regulated in psoriatic skin and that shares similarity to fatty acid-binding proteins. J Invest Dermatol 1992;99(3):299-305.

213. Masouye I, Saurat JH, Siegenthaler G. Epidermal fatty-acid-binding protein in psoriasis, basal and squamous cell carcinomas: an immunohistological study. Dermatology (Basel, Switzerland) 1996;192(3):208-13.

214. Dunnington DJ, Hughes CM, Monaghan P, Rudland PS. Phenotypic instability of rat mammary tumor epithelial cells. Journal of the National Cancer Institute 1983;71(6):1227-40.

215. Jing C, Beesley C, Foster CS, Rudland PS, Fujii H, Ono T, et al. Identification of the messenger RNA for human cutaneous fatty acid-binding protein as a metastasis inducer. Cancer Res 2000;60(9):2390-8.

216. Forootan SS, Bao ZZ, Forootan FS, Kamalian L, Zhang Y, Bee A, et al. Atelocollagen-delivered siRNA targeting the FABP5 gene as an experimental therapy for prostate cancer in mouse xenografts. International journal of oncology 2010;36(1):69-76.

217. Forootan FS, Forootan SS, Gou X, Yang J, Liu B, Chen D, et al. Fatty acid activated PPARgamma promotes tumorigenicity of prostate cancer cells by up regulating VEGF via PPAR responsive elements of the promoter. Oncotarget 2016;7(8):9322-39.

218. Nakamura M, Chi YM, Yan WM, Nakasugi Y, Yoshizawa T, Irino N, et al. Strong antinociceptive effect of incarvillateine, a novel monoterpene alkaloid from Incarvillea sinensis. Journal of natural products 1999;62(9):1293-4.

219. Wang ML, Yu G, Yi SP, Zhang FY, Wang ZT, Huang B, et al. Antinociceptive effects of incarvillateine, a monoterpene alkaloid from Incarvillea sinensis, and possible involvement of the adenosine system. Scientific reports 2015;5:16107.

220. Furuhashi M, Tuncman G, Gorgun CZ, Makowski L, Atsumi G, Vaillancourt E, et al. Treatment of diabetes and atherosclerosis by inhibiting fatty-acid-binding protein aP2. Nature 2007;447(7147):959-65.

221. Lehmann F, Haile S, Axen E, Medina C, Uppenberg J, Svensson S, et al. Discovery of inhibitors of human adipocyte fatty acid-binding protein, a potential type 2 diabetes target. Bioorganic & medicinal chemistry letters 2004;14(17):4445-8.

222. Liu X, Huang X, Lin W, Wang D, Diao Y, Li H, et al. New aromatic substituted pyrazoles as selective inhibitors of human adipocyte fatty acid-binding protein. Bioorganic & medicinal chemistry letters 2011;21(10):2949-52.

223. Berger WT, Ralph BP, Kaczocha M, Sun J, Balius TE, Rizzo RC, et al. Targeting fatty acid binding protein (FABP) anandamide transporters - a novel strategy for development of anti-inflammatory and anti-nociceptive drugs. PloS one 2012;7(12):e50968.

224. Kaczocha M, Rebecchi MJ, Ralph BP, Teng Y-HG, Berger WT, Galbavy W, et al. Inhibition of Fatty Acid Binding Proteins Elevates Brain Anandamide Levels and Produces Analgesia. PloS one 2014;9(4):e94200.

225. Thanos PK, Clavin BH, Hamilton J, O'Rourke JR, Maher T, Koumas C, et al. Examination of the Addictive and Behavioral Properties of Fatty Acid-Binding Protein Inhibitor SBFI26. Frontiers in psychiatry 2016;7:54.

226. Hohoff C, Borchers T, Rustow B, Spener F, van Tilbeurgh H. Expression, purification, and crystal structure determination of recombinant human epidermal-type fatty acid binding protein. Biochemistry 1999;38(38):12229-39.

227. Levine AJ, Oren M. The first 30 years of p53: growing ever more complex. Nature reviews Cancer 2009;9(10):749-58.

228. Wilton DC. A continuous fluorescence displacement assay for the measurement of phospholipase A2 and other lipases that release long-chain fatty acids. Biochemical Journal 1990;266(2):435-39.

229. Vorum H, Madsen P, Svendsen I, Cells JE, Honore B. Expression of recombinant psoriasis-associated fatty acid binding protein in Escherichia coli: gel electrophoretic characterization, analysis of binding properties and comparison with human serum albumin. Electrophoresis 1998;19(10):1793-802.

230. Thumser AE, Wilton DC. The binding of cholesterol and bile salts to recombinant rat liver fatty acid-binding protein. The Biochemical journal 1996;320 (Pt 3):729-33.

231. Koehl P, Delarue M. Polar and nonpolar atomic environments in the protein core: implications for folding and binding. Proteins 1994;20(3):264-78.

232. Rey-Burusco M F, Ibáñez-Shimabukuro M, Gabrielsen M, Franchini Gisela R, Roe Andrew J, Griffiths K, et al. Diversity in the structures and ligand-binding sites of nematode fatty acid and retinol-binding proteins revealed by Na-FAR-1 from Necator americanus. Biochemical Journal 2015;471(Pt 3):403-14.

233. Currie E, Schulze A, Zechner R, Walther TC, Farese RV. Cellular Fatty Acid Metabolism and Cancer. Cell metabolism 2013;18(2):153-61.

234. Pascual G, Avgustinova A, Mejetta S, Martín M, Castellanos A, Attolini CS-O, et al. Targeting metastasis-initiating cells through the fatty acid receptor CD36. Nature 2016;advance online publication.

235. Bao Z, Malki MI, Forootan SS, Adamson J, Forootan FS, Chen D, et al. A novel cutaneous Fatty Acid-binding protein-related signaling pathway leading to malignant progression in prostate cancer cells. Genes Cancer 2013;4(7-8):297-314.

236. Hulme EC, Trevethick MA. Ligand binding assays at equilibrium: validation and interpretation. British Journal of Pharmacology 2010;161(6):1219-37.

237. Satone H, Akahoshi E, Nakamura A, Lee JM, Honda M, Shimasaki Y, et al. Expression and functional characterization of recombinant tributyltin-binding protein type 2. The Journal of toxicological sciences 2013;38(6):885-90.

238. Lobel D, Marchese S, Krieger J, Pelosi P, Breer H. Subtypes of odorant-binding proteins--heterologous expression and ligand binding. European journal of biochemistry 1998;254(2):318-24.

239. Patil R, Laguerre A, Wielens J, Headey SJ, Williams ML, Hughes ML, et al. Characterization of two distinct modes of drug binding to human intestinal fatty acid binding protein. ACS chemical biology 2014;9(11):2526-34.

240. Zimmerman AW, van Moerkerk HT, Veerkamp JH. Ligand specificity and conformational stability of human fatty acid-binding proteins. The international journal of biochemistry & cell biology 2001;33(9):865-76.

241. Chuang S, Velkov T, Horne J, Porter CJ, Scanlon MJ. Characterization of the drug binding specificity of rat liver fatty acid binding protein. Journal of medicinal chemistry 2008;51(13):3755-64.

242. Velkov T, Horne J, Laguerre A, Jones E, Scanlon MJ, Porter CJ. Examination of the role of intestinal fatty acid-binding protein in drug absorption using a parallel artificial membrane permeability assay. Chemistry & biology 2007;14(4):453-65.

243. DeSantis MC, Kim JH, Song H, Klasse PJ, Cheng W. Quantitative Correlation between Infectivity and Gp120 Density on HIV-1 Virions Revealed by Optical Trapping Virometry. The Journal of biological chemistry 2016;291(25):13088-97.

244. Pavese J, Ogden IM, Bergan RC. An orthotopic murine model of human prostate cancer metastasis. Journal of visualized experiments : JoVE 2013(79):e50873.

245. Zeng XJ, Bi XC, Dai QS, Han ZD, Zhong WD. Effects of PPAR-gamma on the proliferation and glycolysis metabolism of prostate cancer cells. National journal of andrology 2012;18(8):692-6.

246. Mueller E, Smith M, Sarraf P, Kroll T, Aiyer A, Kaufman DS, et al. Effects of ligand activation of peroxisome proliferator-activated receptor gamma in

human prostate cancer. Proceedings of the National Academy of Sciences of the United States of America 2000;97(20):10990-5.

247. Janik P, Briand P, Hartmann NR. The effect of estrone-progesterone treatment on cell proliferation kinetics of hormone-dependent GR mouse mammary tumors. Cancer research 1975;35(12):3698-704.

248. Thumser AE, Storch J. Characterization of a BODIPY-labeled fluorescent fatty acid analogue. Binding to fatty acid-binding proteins, intracellular localization, and metabolism. Molecular and cellular biochemistry 2007;299(1):67-73.

249. Segawa Y, Yoshimura R, Hase T, Nakatani T, Wada S, Kawahito Y, et al. Expression of peroxisome proliferator-activated receptor (PPAR) in human prostate cancer. The Prostate 2002;51(2):108-16.

250. Subbarayan V, Sabichi AL, Kim J, Llansa N, Logothetis CJ, Lippman SM, et al. Differential peroxisome proliferator-activated receptor-gamma isoform expression and agonist effects in normal and malignant prostate cells. Cancer epidemiology, biomarkers & prevention : a publication of the American Association for Cancer Research, cosponsored by the American Society of Preventive Oncology 2004;13(11 Pt 1):1710-6.

251. Apostoli AJ, Roche JM, Schneider MM, SenGupta SK, Di Lena MA, Rubino RE, et al. Opposing roles for mammary epithelial-specific PPARγ signaling and activation during breast tumour progression. Molecular Cancer 2015;14:85.

252. Nickkho-Amiry M, McVey R, Holland C. Peroxisome proliferator-activated receptors modulate proliferation and angiogenesis in human endometrial carcinoma. Molecular cancer research : MCR 2012;10(3):441-53.

253. Butler R, Mitchell SH, Tindall DJ, Young CY. Nonapoptotic cell death associated with S-phase arrest of prostate cancer cells via the peroxisome proliferator-activated receptor gamma ligand, 15-deoxy-delta12,14-prostaglandin J2. Cell growth & differentiation : the molecular biology journal of the American Association for Cancer Research 2000;11(1):49-61.

254. Forootan SS HS, Aachi V, Foster CS, Ke Y. Molecular Mechanisms Involved in the Transition of Prostate Cancer Cells from Androgen Dependant to Castration Resistant State. Journal of Andrology & Gynaecology 2014;2(2).

255. Karantanos T, Corn PG, Thompson TC. Prostate cancer progression after androgen deprivation therapy: mechanisms of castrate resistance and novel therapeutic approaches. Oncogene 2013;32(49):5501-11.

256. Katzenwadel A, Wolf P. Androgen deprivation of prostate cancer: Leading to a therapeutic dead end. Cancer letters 2015;367(1):12-7.

257. Li CC, Hou YC, Yeh CL, Yeh SL. Effects of eicosapentaenoic acid and docosahexaenoic acid on prostate cancer cell migration and invasion induced by tumor-associated macrophages. PloS one 2014;9(6):e99630.

258. Ridley AJ, Schwartz MA, Burridge K, Firtel RA, Ginsberg MH, Borisy G, et al. Cell migration: integrating signals from front to back. Science (New York, NY) 2003;302(5651):1704-9.

259. Clark AG, Vignjevic DM. Modes of cancer cell invasion and the role of the microenvironment. Current opinion in cell biology 2015;36:13-22.

260. Jiang WG, Sanders AJ, Katoh M, Ungefroren H, Gieseler F, Prince M, et al. Tissue invasion and metastasis: Molecular, biological and clinical perspectives. Seminars in cancer biology 2015;35 Suppl:S244-75.

261. Rohrig F, Schulze A. The multifaceted roles of fatty acid synthesis in cancer. Nature reviews Cancer 2016;16(11):732-49.

262. Kahn BB, Flier JS. Obesity and insulin resistance. Journal of Clinical Investigation 2000;106(4):473-81.

263. Seargent JM, Yates EA, Gill JH. GW9662, a potent antagonist of PPARγ, inhibits growth of breast tumour cells and promotes the anticancer effects of the PPARγ agonist rosiglitazone, independently of PPARγ activation. British Journal of Pharmacology 2004;143(8):933-37.

264. Weng JR, Chen CY, Pinzone JJ, Ringel MD, Chen CS. Beyond peroxisome proliferator-activated receptor gamma signaling: the multi-facets of the antitumor effect of thiazolidinediones. Endocrine-related cancer 2006;13(2):401-13.

265. Mansure JJ, Nassim R, Kassouf W. Peroxisome proliferator-activated receptor gamma in bladder cancer: a promising therapeutic target. Cancer biology & therapy 2009;8(7):6-15.

266. Bolden A, Bernard L, Jones D, Akinyeke T, Stewart LV. The PPAR Gamma Agonist Troglitazone Regulates Erk 1/2 Phosphorylation via a PPARgamma-Independent, MEK-Dependent Pathway in Human Prostate Cancer Cells. PPAR research 2012;2012:929052.

267. Kubota T, Koshizuka K, Williamson EA, Asou H, Said JW, Holden S, et al. Ligand for peroxisome proliferator-activated receptor gamma (troglitazone) has potent antitumor effect against human prostate cancer both in vitro and in vivo. Cancer research 1998;58(15):3344-52.

268. Gouni-Berthold I, Berthold HK, Weber AA, Ko Y, Seul C, Vetter H, et al. Troglitazone and rosiglitazone induce apoptosis of vascular smooth muscle cells through an extracellular signal-regulated kinase-independent pathway. Naunyn-Schmiedeberg's archives of pharmacology 2001;363(2):215-21.

269. Papageorgiou E, Pitulis N, Msaouel P, Lembessis P, Koutsilieris M. The non-genomic crosstalk between PPAR-gamma ligands and ERK1/2 in cancer cell lines. Expert opinion on therapeutic targets 2007;11(8):1071-85.

270. Houseknecht KL, Cole BM, Steele PJ. Peroxisome proliferator-activated receptor gamma (PPARgamma) and its ligands: a review. Domestic animal endocrinology 2002;22(1):1-23.

271. Murakami K, Tobe K, Ide T, Mochizuki T, Ohashi M, Akanuma Y, et al. A novel insulin sensitizer acts as a coligand for peroxisome proliferator-activated receptor-alpha (PPAR-alpha) and PPAR-gamma: effect of PPAR-alpha activation on abnormal lipid metabolism in liver of Zucker fatty rats. Diabetes 1998;47(12):1841-7.

272. Wang M, Wise SC, Leff T, Su TZ. Troglitazone, an antidiabetic agent, inhibits cholesterol biosynthesis through a mechanism independent of peroxisome proliferator-activated receptor-gamma. Diabetes 1999;48(2):254-60.

273. Wang X, Sun Y, Wong J, Conklin DS. PPARgamma maintains ERBB2-positive breast cancer stem cells. Oncogene 2013;32(49):5512-21.

274. Lin S-J, Yang D-R, Wang N, Jiang M, Miyamoto H, Li G, et al. TR4 nuclear receptor enhances prostate cancer initiation via altering the stem cell population and EMT signals in the PPARG-deleted prostate cells. Oncoscience 2015;2(2):142-50.

275. Vara D, Morell C, Rodriguez-Henche N, Diaz-Laviada I. Involvement of PPARgamma in the antitumoral action of cannabinoids on hepatocellular carcinoma. Cell death & disease 2013;4:e618.

276. Ahmad I, Mui E, Galbraith L, Patel R, Tan EH, Salji M, et al. Sleeping Beauty screen reveals Pparg activation in metastatic prostate cancer. Proceedings of the National Academy of Sciences of the United States of America 2016;113(29):8290-5.

277. Nakano R, Kurosaki E, Yoshida S, Yokono M, Shimaya A, Maruyama T, et al. Antagonism of peroxisome proliferator-activated receptor gamma prevents high-fat diet-induced obesity *in vivo*. Biochemical pharmacology 2006;72(1):42-52.

278. Yuan H, Kopelovich L, Yin Y, Lu J, Glazer RI. Drug-targeted inhibition of peroxisome proliferator-activated receptor-gamma enhances the chemopreventive effect of anti-estrogen therapy. Oncotarget 2012;3(3):345-56.

279. Ferrer FA, Miller LJ, Andrawis RI, Kurtzman SH, Albertsen PC, Laudone VP, et al. Vascular endothelial growth factor (VEGF) expression in human prostate cancer: in situ and in vitro expression of VEGF by human prostate cancer cells. The Journal of urology 1997;157(6):2329-33.

280. Ambrosio MR, Di Serio C, Danza G, Rocca BJ, Ginori A, Prudovsky I, et al. Carbonic anhydrase IX is a marker of hypoxia and correlates with higher Gleason scores and ISUP grading in prostate cancer. Diagnostic pathology 2016;11(1):45.

281. Danza G, Di Serio C, Ambrosio MR, Sturli N, Lonetto G, Rosati F, et al. Notch3 is activated by chronic hypoxia and contributes to the progression of human prostate cancer. International journal of cancer Journal international du cancer 2013;133(11):2577-86.

282. Eisermann K, Broderick CJ, Bazarov A, Moazam MM, Fraizer GC. Androgen up-regulates vascular endothelial growth factor expression in prostate cancer cells via an Sp1 binding site. Mol Cancer 2013;12:7.

283. Kluetz PG, Figg WD, Dahut WL. Angiogenesis Inhibitors in the treatment of Prostate Cancer. Expert opinion on pharmacotherapy 2010;11(2):233-47.

284. Gordon MS, Cunningham D. Managing patients treated with bevacizumab combination therapy. Oncology 2005;69 Suppl 3:25-33.

285. Kamba T, McDonald DM. Mechanisms of adverse effects of anti-VEGF therapy for cancer. British journal of cancer 2007;96(12):1788-95.

286. Hurwitz H, Saini S. Bevacizumab in the treatment of metastatic colorectal cancer: safety profile and management of adverse events. Seminars in oncology 2006;33(5 Suppl 10):S26-34.

287. Chapin BF, McGuire SE, Aparicio A. Is treatment of the primary tumor in metastatic prostate cancer justified? European urology 2014;65(6):1067-8.

288. Chambers AF, Groom AC, MacDonald IC. Metastasis: Dissemination and growth of cancer cells in metastatic sites. Nature reviews Cancer 2002;2(8):563-72.

289. Morgan SC, Parker CC. Local treatment of metastatic cancer--killing the seed or disturbing the soil? Nature reviews Clinical oncology 2011;8(8):504-6.

290. Liu Y, Zuckier LS, Ghesani NV. Dominant uptake of fatty acid over glucose by prostate cells: a potential new diagnostic and therapeutic approach. Anticancer research 2010;30(2):369-74.

291. Liao J, Sportsman R, Harris J, Stahl A. Real-time quantification of fatty acid uptake using a novel fluorescence assay. Journal of lipid research 2005;46(3):597-602.

292. Kawaguchi K, Senga S, Kubota C, Kawamura Y, Ke Y, Fujii H. High expression of Fatty Acid-Binding Protein 5 promotes cell growth and metastatic potential of colorectal cancer cells. FEBS open bio 2016;6(3):190-9.

293. Itoh T, Fairall L, Amin K, Inaba Y, Szanto A, Balint BL, et al. Structural basis for the activation of PPARgamma by oxidized fatty acids. Nature structural & molecular biology 2008;15(9):924-31.

294. Kliewer SA, Umesono K, Noonan DJ, Heyman RA, Evans RM. Convergence of 9-cis retinoic acid and peroxisome proliferator signalling pathways through heterodimer formation of their receptors. Nature 1992;358(6389):771-4.

295. Hostetler HA, McIntosh AL, Atshaves BP, Storey SM, Payne HR, Kier AB, et al. L-FABP directly interacts with PPARalpha in cultured primary hepatocytes. Journal of lipid research 2009;50(8):1663-75.

Appendixes

A. Reagents

Reagents	Supplier

A.1 Reagents for general molecular biology

Absolute ethanol	BDH, England, UK
Agarose	Genflow, Fradley, UK
Ampicillin	Invitrogen, CA, USA
BL21 *E. coli* bacteria	Invitrogen, CA, USA
DH5α *E. coli* bacteria	Invitrogen, CA, USA
DNA marker III	Roche, England, UK
DNA marker XIV	Roche, England, UK
E. coli BL21 cells	InvivoGen, USA
E. coli DH5α cells	InvivoGen, USA
Glucose	Sigma, USA
Glycerol	Sigma, USA
IPTG (Isopropylthiogalactoside)	Sigma, USA
Isopropanol	BDH, England, UK
LB agar	Sigma, USA
LB broth	Sigma, USA

Reagents	Supplier
Ligation enzyme buffer	New England BioLabs
Magnesium chloride	Sigma, USA
Magnesium sulphate	Sigma, USA
MOPS	Sigma, USA
pBluescript II SK vector	InvivoGen, USA
Potassium acetate	Sigma, USA
Potassium chloride	Sigma, USA
pQE-32 vector	InvivoGen, USA
QIAGEN Ni-NTA Fast Start Kit	QIAGEN, CA, USA
QIAGEN Plasmid mini-preparation kit	QIAGEN, CA, USA
Restriction enzyme buffers	New England BioLabs
Restriction enzymes	New England BioLabs
Safe View (Nucleic Acid Stain)	NBS Biological, Cambridgeshire, UK
SDS	Sigma, USA
T4 DNA ligase	New England BioLabs
Tryptone	Sigma, USA
Wizard DNA Clean-Up System	Promega, WI, USA
Yeast extract	Fisher scientific, Loughborough, UK

Reagents	Supplier

A.2 Reagents for Western blot

Ammonium persulfate (APS)	Sigma, USA
Bradford reagent	Sigma, USA
Bromophenol blue	Sigma, USA
CelLytic-M	Sigma, USA
Commassie brilliant blue	Bio-Rad GmbH, Munchen, Germany
ECL detection kit	GE Healthcare, Buckinghamshire, UK
Glycine	Melford, UK
Kodak Developer	Sigma, USA
Kodak film	GE Healthcare, Buckinghamshire, UK
Kodak Fixer	Sigma, USA
Methanol	Fisher scientific, Loughborough, UK
Next Gel 12.5%	Amresco, OH, USA
Ponceau solution	Sigma, USA
PVDF membrane	Millipore, USA
TEMED	Sigma, USA
Tris base ultrapure	Melford, UK
Tween-20	Sigma, USA

Reagents	Supplier
β-mercaptoethanol	Sigma, USA

A.3 Reagents for fluorescence displacement assay

DAUDA	Cayman, USA
Lipidex-1000 (Hydroxyalkoxypropyl-Dextran)	Sigma, USA

A.4 Reagents for cell culture

DMSO	Sigma, Germany
Fetal calf serum (FBS)	Biosera, East Sussex, UK
FuGENE HD transfection reagent	Promega, USA
Hygromycin	InvivoGen, CA, USA
L-Glutamine	Lonza, Belgium
Opti-MEM I medium	Gibco, Invitrogen, Paisley, UK
Penicillin/Streptomycin	Lonza, Belgium
pGL4.50 [*luc2*/CMV/Hygro] vector	Promega, USA
Phosphate buffered saline (tablet)	Gibco, Invitrogen, Paisley, UK
Potassium D-luciferin	Promega, USA
RPMI 1640	Gibco, Invitrogen, Paisley, UK
Sodium pyruvate	Sigma, USA
Trypsin	Gibco, Invitrogen, Paisley, UK
Trypsin/EDTA solution	Gibco, Invitrogen, Paisley, UK

Reagents	Supplier
Versene	Gibco, Invitrogen, Paisley, UK

A.5 Reagents for cell proliferation assay

MTT	Sigma, USA
DMSO	Sigma, Germany

A.6 Reagent for soft agar assay

Low melting point agarose	Genflow, Fradley, UK
MTT	Sigma, USA

A.7 Reagents for cell invasion assay

Crystal violet	Sigma, USA

A.8 Reagents for tumorigenicity and metastasis *in vivo*

Isofluorane	Hoechst, German
Novalgin	Hoechst, Germany
Potassium D-luciferin	Promega, USA

A.9 Reagents for histology

Acetone	Sigma, USA
Ethanol (IMS)	GENTA, Tockwith, UK
Formaldehyde	Sigma, USA
Haematoxylin	Sigma, USA
Xylene	GENTA, Tockwith, UK

Reagents	Supplier

A.10 Reagents for fatty acid uptake assay

BODIPY 558/568C_{12}	Invitrogen, USA

B. Buffers

B.1 Molecular Biology

LB medium

LB broth 20g

dH_2O 1 Lit

Autoclaved

LB agar

LB agar 35g

dH_2O 1 Lit

Autoclaved

RF1 buffer (pH 5.8)

KCl 7.456g (100mM)

MgCl2.4H_2O 9.9g (50mM)

CaCl2 1.5g (10mM)

K-acetate 2.94g (30mM)

Glycerol (v/v) 150ml (15%)

dH_2O up to 1 Lit

Adjust the pH and sterilized by filtration

RF2 buffer (pH 6.8)

MOPS 2.1g (10mM)

CaCl2 11g (75mM)

KCl 0.745g (10mM)

Glycerol (v/v) 150ml (15%)

dH_2O up to 1 Lit

Adjust the pH and sterilized by autoclave

Glucose 20%

Glucose 20g

dH_2O 10ml

Sterilized by filtration

Magnesium salt solution (2M)

MgSO4 2.465g (1M)

MgCl2 2.033g (1M)

dH_2O 10ml

Sterilized by filtration

SOB medium (pH 7)

NaCl 0.5g

Tryptone 20g

Yeast extracts 5g

KCl 0.186g

dH_2O up to 1 Lit

Adjust the pH and sterilized by autoclave

SOC medium

SOB medium 4.850ml

Mg2+ salt solution (2M) 50µl

Glucose 20% 150µl

Stock medium for bacteria

Glycerol 5ml

LB medium 4ml

Bacteria culture 3ml

10× TBE stock solution

Boric acid 55g (890mM)

Tris base 108g (890mM)

EDTA 0.5M, pH 8 40ml (20mM)

dH_2O up to 1 Lit

Adjust the pH and sterilized by autoclave

100mM IPTG

IPTG 238mg

Sterile distilled H_2O 10ml

Filter sterilized

6×DNA loading buffer

Bromophenol blue 0.5% 0.5ml

Xylene cyanol FF 0.5ml

Glycerol in sterile dH_2O (60%) 1ml

B.2 Western Blot

1M Tris (pH 6.8)

Tris base 12.1g

dH_2O 100ml

pH adjusted with HCl

10% (w/v) APS solution

Ammonium persulfate 100mg

dH_2O 1ml

10% (w/v) SDS solution

Sodium Dodecyl Sulfate 10g

dH_2O 100ml

5× SDS-PAGE sample loading buffer

1M Tris-HCl (pH 6.8) 1.25ml

Bromophenol blue 0.5% (w/v) 2.5ml

Glycerol 40% (v/v) 15ml

SDS 10% 5ml

β-mercaptoethanol 1.25ml

2× SDS-PAGE sample loading buffer

1M Tris-HCl (pH 6.8) 2.5ml

Bromophenol blue 0.5% (w/v) 0.8ml

Glycerol 40% (v/v) 4ml

SDS 10% 2ml

dH_2O 4.7ml

Transfer buffer (pH 8.3)

Glycine 14.4g (192mM)

Tris base 3.03g (25mM)

Methanol 20% (v/v)

dH_2O up to 1Lit

pH adjusted with HCl

10× TBS buffer (pH 7.6)

Sodium chloride 87.66g (1500mM)

Tris base 60.58g (500mM)

dH_2O up to 1 Lit

pH adjusted with HCl

Autoclaved

1×TBS-Tween 1%

10× TBS buffer 100ml

Tween 20 1ml

dH_2O up to 1 Lit

TBS-T-milk 5%

Dried milk 5g

1×TBS-T 100ml

B.3 Fluorescence displacement DAUDA assay

Delipidated solution

Lipidex-1000 10g

Tris HCL(10Mm) pH 7.5

B.4 Cell Culture

Routine cell culture medium

RPMI medium 1640 500ml

Fetal calf serum 10% (v/v)

Penicillin-Streptomycin (5000 U/ml) 5ml

L-Glutamine (20mM) 5ml

Sodium pyruvate (100mM) 5ml

Selective medium

Routine medium with Hygromycin (200µg/mL)

Culture medium for evaluation the fatty acid uptake

PBS 500ml

FCS 5% (v/v)

BODIPY 2 µM

Culture medium for identification of stably luciferase expressing PC3-M

Routine cell culture medium

D-luciferin150µg/mL

Freezing medium

Routine cell culture medium 92.5% (v/v)

DMSO 7.5% (v/v)

Trypsin/EDTA solution (T/E) (2.5%)

1× Versene 100ml

Trypsin 2.5ml

MTT solution (5mg/ml)

MTT 50mg

PBS 10ml

PBS

PBS one tablet

dH_2O 500ml

Autoclaved

C. Equipments

AccuWeigh, WA, USA

Portable Lab Scale

Bandelin, Germany

Sonicator

BD Microlance 3, Ireland

Needle

Syringes

BD Biosciences, USA

BD BioCoatTM Growth Factor Reduced (GFR) Matrigel TM Invasion Chamber

BD Plastics, Sunderland, UK

Syringes

Beckman coulter, UK

Microcentrifuge

Beckman coulter, USA

EPICS XL flow Cytometer

Becton Dikinson, USA

Falcon 2059 tube

Berthold detection system, Germany

Sirius Luminometer

Bio-Rad, Hemel, UK

Gel electrophoresis rig

Mini-protein 3 cell system

BioTek, USA

Multiskan MS (plate reader)

Borolabs, Basingstoke, UK

CO2 incubator Model TC2323

Jenway, Genova, UK

Spectrophotometer

Flowgen, Nottingham, UK

Gel drier

Generier bio-one, UK

Tissue culture pipettes (5-50 ml)

Universal tube

Grant Instruments, UK

H_2O bath

GMI, MJ Research, MN, USA

Thermal cycler (Peltier Thermal Cycler PTC-200)

Heraeus Holding GmbH, Germany

Labofuge 400R (centrifuge)

Labtech International, Ringmer, UK

NanoDrop spectrophotometer

Leica, Germany

Superior Adhesive slide

Leitz Labovert, Luton, UK

Light microscope

Microm, Oxford, UK

Microtome HM355

Merck Millipore, UK

Immobilon, Transfer membrane

Merck Millipore, UK

D-Tube dialyzer

Nalgene, UK

Cryobox DNA

New Brunswick Scientific, USA

CO2 Shaking incubator

Nunc, Denmark

Cell culture filter cap flasks

Cell culture plates

Cryogenic vial

Oxford Optronix, Oxford, UK

GelCount

Perkin Elmer, USA

IVIS imaging system

QIAGEN, Crawley, UK

Qiagen tip

QIA Shredder spin column

Shandon, UK

Sequenza slide rack

Coverslip (20×40mm)

SLS Ltd., Nottingham, UK

Haemocytometer

Magnificent stirrer

Starlab, Milton Keynes, UK

Microtubes

Pipette tips

Surgipath, UK

Microslide

Tissue cassette

Swann-Morton, Sheffeild, UK

Carbon steel surgical blades

Techne, England, UK

Hot plate (Ori-Block 08-3)

Thermo Electron Corporation, Waltham, USA

Varioskan Flash Spectral Scanning Multimode Reader

Thermo Scientific, USA

Shandon Citadel 1000 tissue processor

Whatman, England, UK

Whatman filter paper

Weber scientific International, NJ, USA

Haemocytometer slide